Solubility Products of Chloride and Sulfate Green Rust During Transformation to Magnetite

by

Neil MacPherson

A thesis submitted in partial fulfillment of the requirements for the degree of

Master of Science

Department of Earth and Atmospheric Sciences
University of Alberta

© Neil MacPherson, 2020

Abstract

Green rust (GR) is a group of mixed Fe^{II} and Fe^{III} hydroxide minerals and is an important phase in both modern and ancient geochemical systems. For this reason, establishing the thermodynamic properties of GR is vital to understanding and modelling its role in natural systems. In this study, batch solubility experiments were conducted on fully characterized GR(Cl) and GR(SO_4) to determine their solubility products (K_{sp}). While the solubility products calculated here are not true solubility products because GR is a metastable phase that transforms into magnetite over the course of days, the kinetics of this transformation is slow enough to make the K_{sp} values useful in predicting aqueous iron concentrations. Triplicate solubility experiments of GR(Cl) and GR(SO_4) were performed in pure water and simulated seawater (0.56 M ionic strength) at three intervals of GR aging: 0, 2, and 7 days. X-ray diffraction (XRD) and Mössbauer spectroscopy analyses evidenced a progressive transformation of GR into magnetite with time. The solubility experiments yielded an average K_{sp} for the three GR age intervals. Variation between the average K_{sp} as a function of GR age were statistically insignificant, thus the resulting average K_{sp} for each GR age were averaged to produce a grand mean log K_{sp} for GR(Cl) and GR(SO_4) in pure water and simulated seawater. The grand mean log $K_{sp}(Cl)$ in pure water and 0.56 M IS water is calculated to be -75.07 ± 1.39 and -76.22 ± 0.42, respectively. The grand mean log $K_{sp}(SO_4)$ in pure water and 0.56 M IS water are -119.72 ± 1.03 and -126.60 ± 1.07, respectively. Chemical speciation modelling of the concomitant dissolution of GR and magnetite showed that solution Fe concentrations were almost entirely controlled by GR dissolution. This is a key finding in predicting the role of GR in geochemical systems, as many existing models assume that magnetite controls dissolved iron concentrations rather than GR.

Acknowledgments

I would like to express my utmost gratitude to my supervisor Dr. Daniel Alessi, whom will always be a role model to me. Thank you for guiding me throughout the course of my graduate studies and for the chance to be a member of your lab group. I also wish to thank Dr. Leslie Jamie Robbins and Dr. Kurt Konhauser for their assistance regarding my research. Furthermore, I would like to thank all my fellow colleagues of the Environmental Geochemistry Lab and the Geobiology Lab for supporting me through several aspects of my experimental research and for greatly enriching my graduate experience.

Table of Contents

List of Figures

List of Tables

Introduction

Green rust, herein referred to as "GR", is a group of mixed valent Fe hydroxide minerals (O'Loughlin et al., 2003) that are composed of alternating layers of Fe(II)-Fe(III) hydroxides and hydrated-anion filled interlayers (Figure 1). Because the structure of GR is comprised of positively charged brucite-like layers and hydrated charge balancing anions in the interlayers, GR is categorized into a group in minerals known as layered double hydroxides (Evans and Slade, 2005). There are multiple varieties of GR, which are defined by the type of anion occupying the interlayer space. GR that consists of the spherical or planar anions of Cl^- or CO_3^{2-} are often termed GR1, whereas those consisting of the tetrahedral interlayer anion of SO_4^{2-} are deemed GR2 (Bernal et al., 1959). GR1 and GR2 are identified by their differing X-ray diffraction (XRD) spectra. GR is thermodynamically metastable and has been observed to transform into other Fe-bearing solid phases, such as goethite, maghemite, lepidocrocite, ferrihydrite, and particularly magnetite (O'Loughin et al., 2003; Halevy et al., 2017; Genin et al., 1998; Tamaura et al., 1984; Ona-Nguema et al., 2002; Li et al., 2017). Refait et al. (2003) showed that under most conditions, magnetite is thermodynamically more stable than GR(SO_4). As a result, GR will abiotically transform into magnetite, the thermodynamically stable phase at ambient temperature and pressure. However, it may be more kinetically favorable for a system to precipitate metastable GR rather than thermodynamically stable magnetite. Observations by Steefel and Van Capellen (1990) indicate that metastable phases form first, followed by progressively more stable phases, because a system preferentially forms the phase with the highest precipitation rate first, thus reducing oversaturation the fastest.

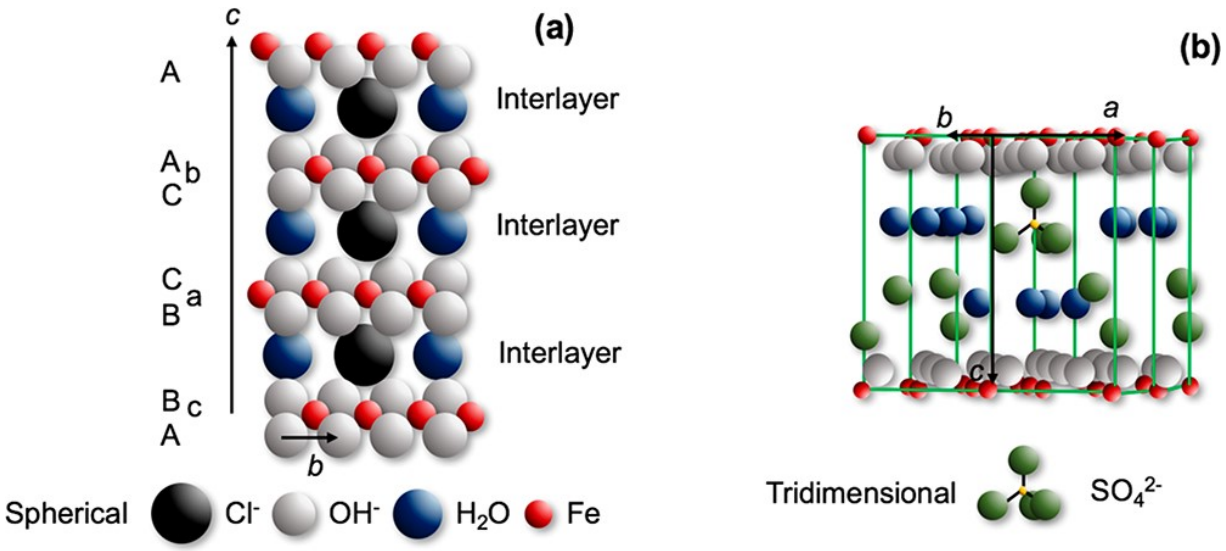

Figure 1. *Generalized crystal structures of: a) GR(Cl) and b) GR(SO_4). Adapted from Usman et al., 2018.*

GR is easily oxidized in the presence of atmospheric oxygen, and for this reason is both challenging to work with in the laboratory and is difficult to observe in natural environments. However, GR has been observed in nature, most notably as a significant component of hydromorphic soils, giving these soils their characteristic bluish-green color (Trolard et al., 1997; Genin et al., 1998; Abdelmoula et al., 1998; Bourrie et al., 1999; Feder et al., 2005). Christiansen et al. (2009) developed a method to obtain GR samples with minimal to no oxidation, which was subsequently used to identify GR in multiple groundwater samples. GR forms in suboxic environments from neutral to alkaline pH conditions (O'Loughlin et al., 2003). It can form abiotically when Fe^{2+} reacts with Fe(III) oxyhydroxides (Tamura et al., 1984) or from the oxidation of Fe(II) hydroxides (McGill et al., 1976). GR has also been observed to form via biotic pathways, such as microbially mediated Fe(III) reduction (Zegeye et al., 2005; Kukkadapu et al., 2003; Fredrickson et al., 2001; Ona-Nguema et al., 2002), microbially mediated Fe(II) oxidation (Pantke et al., 2011), and biocorrosion of marine steel (Pineau et al., 2008; Refait et al., 1997; Refait et al., 1998; Genin et al., 1998; Refait et al., 2003). In the laboratory, GR is typically synthesized via two

methods: controlled oxidation of a ferrous iron solution or co-precipitation from a solution containing both ferrous and ferric iron.

Mixed valence Fe minerals are among the most reactive iron compounds found in the subsurface. Due to highly reactive surfaces and large effective surface areas, GR is a significant reductant in environmental systems. The reduction of contaminants can often lead to less toxic and/or less mobile chemical species than their parent compound. By influencing a chemical compound's toxicity and mobility, GR can control the fate of inorganic and organic contaminants in soils, sediments, and groundwater. It has been shown in many studies that GR can react with a great variety of environmentally relevant compounds, such as chromate, selenate, arsenate, antimony, hexavalent uranium, technetium, nitrate, nitrite, carbon tetrachloride, chlorinated ethylenes and halogenated methanes (Bond and Fendorf, 2003; Elsner et al., 2004; Erbs et al., 1999; Hansen et al., 1994; Hansen et al., 1996; Jönsson and Sherman, 2008; Lee and Batchelor, 2002; Legrand et al., 2004; Loyaux-Lawniczak et al., 1999; Loyaux-Lawniczak et al., 2000; Maithreepala and Doong, 2005; Mitsuonbu et al., 2008; Mitsuonbu et al., 2009; Myneni et al., 1997; O'Loughlin and Burris, 2004; O'Loughlin et al., 2003; Pepper et al., 2003; Randall et al., 2001; Refait et al., 2000; Skovbjerg et al., 2006). Yet while GR is an important phase in environmental systems, the majority of groundwater reactive transport models do not factor in the possible presence of GR (Christiansen et al., 2009).

Apart from modern environments, GR is of interest regarding the generation of Precambrian banded iron formations (BIFs) in Earth's ancient oceans. Generally, it is believed that BIFs were formed by initial deposition of Fe(III) oxyhydroxides, which then transformed into the magnetite and hematite that are observed in BIFs today (Konhauser et al., 2017; Robbins et al.,

2019). However, research performed by Halevy et al. (2017) and Li et al. (2017) suggests that GR may have been a precursor precipitate to magnetite in Algoma-type BIFs. Their studies displayed that GR can precipitate under simulated seawater conditions and, with time, transforms into nanosized magnetite particles. Further supporting this hypothesis, GR has also been observed in Lake Matano, Indonesia, which is proposed to be a geochemical analogue to the Archean oceans (Zegeye et al., 2012). The uptake of dissolved Ni in Lake Matano greatly increased during the formation of GR, giving rise to the question of how GR may have impacted trace element cycling and nutrient availability in the Archaen oceans. Zegeye et al. (2012) suggested that by regulating dissolved Ni – an essential metal co-factor in methanogens – GR may have indirectly limited rates of methanogenesis. Because methane is a major sink for atmospheric oxygen, restrained methanogenesis rates may have been a significant factor in the lead up to the great oxidation event (Konhauser et al., 2009).

As discussed above, GR is an important phase in modern environmental systems and may have played a more prominent role in ancient systems than previously believed. Therefore, constraining GR's solubility product and thermodynamic properties is key to understanding and modelling its role in natural systems. For example, the solubility product can be used to determine the potential formation of GR when only solution composition data is available (Davesne et al., 2010). Determining solubility products and thermodynamic parameters is also key to understanding the availability of GR as a subsurface reductant and sorbent, which could have major implications on how remediation strategies, contaminant transport models, and risk assessment models are developed. Additionally, these values can further our understanding of the potential presence of GR in Precambrian water columns and may be critical information in reconstructing the geochemical conditions of Earth's ancient oceans. More specifically, these

values may reveal if GR played a role as a precursor precipitate to magnetite in Algoma-type BIFs and its impact on trace element cycling.

Some solubility products (K_{sp}) and thermodynamic parameters have been reported for the chloride, carbonate, and sulfate varieties of GR. Generally, GR has a range of compositions due to varying Fe^{II}/Fe^{III} ratios, different interlayer anions, and varying amounts of structural water which is likely the main cause of variation in reported K_{sp} values. Therefore, select studies have standardized their reported thermodynamic parameters to anhydrous GR. Of these studies, the majority investigate the solubility and/or the standard Gibbs free energy of formation of GR(SO_4). Thermodynamic parameters for GR(Cl) (Refait and Génin., 1993) and GR(CO_3) (Drissi et al., 1995) have only been reported by a single manuscript each, and only one enthalpy of formation has been reported for any GR, by Mazeina et al. (2008) for GR(SO_4). Despite their basic importance to thermodynamic calculations, to date no entropy of formations (S^o) for any GR have been reported, although Mazeina et al. (2008) did estimate the range of GR(SO_4) S^o by utilizing their calculated enthalpy of formation and literature values of Gibbs free energies of formation.

The objective of this study is to determine the solubility products (K_{sp}) of chloride and sulfate GR by conducting batch solubility experiments. Because GR is a metastable phase that ultimately transforms to magnetite, these solubility products are not true solubility products because the dissolution reaction can never reach perfect equilibrium. Thus, these experiments describe how the K_{sp} changes as a function of GR transformation into magnetite. Despite this complication, the K_{sp} values are useful in applied, real-world conditions where GR is present with other iron phases and is inevitably transforming into more stable iron phases. Here, we report the

solubility products of fully characterized GR, which may ultimately be used in various forms geochemical speciation modeling.

Table 1. *Existing thermodynamic parameters and solubility products for GR(Cl), GR(CO_3), and GR(SO_4), the formula from which they are derived, and the studies which they originate from.*

Formula	Author	$\Delta_f G^O$ (kJ/mol)	$\Delta_f H^O$ (kJ/mol)	$\log(K_{sp})$
$3Fe^{II}(OH)_2Fe^{III}(OH)_2Cl$	Refait and Génin (1993)	-2132 ± 2[a]		
$Fe^{II}_4Fe^{III}_2(OH)_{12}CO_3•2H_2O$	Drissi et al. (1995)	-4043 ± 1[a]		
$Fe^{II}_4Fe^{III}_2(OH)_{12}SO_4•3H_2O$	Hansen et al. (1994)	-4380 ± 4		-124.6 ± 0.7
$Fe^{II}_4Fe^{III}_2(OH)_{12}SO_4$		-3669 ± 4		-112.8 ± 4.3[b]
$4Fe^{II}(OH)_2•2Fe^{III}OOH•Fe^{II}SO_4$	Refait and Genin (1994)	-3783 ± 1[a]		
$Fe^{II}_4Fe^{III}_2(OH)_{12}SO_4•2H_2O$	Genin et al. (1996)	-4245 ± 10		
$Fe^{II}_4Fe^{III}_2(OH)_{12}SO_4$		-3770 ± 10		
$Fe^{II}_4Fe^{III}_2(OH)_{12}SO_4$	Refait et al. (1999)	-3790 ± 10		-134.0 ± 5.9[b]
$Fe^{II}_4Fe^{III}_2(OH)_{12}SO_4$	Ayala-Luis et al. (2008)	-3819 ± 6		-139.2 ± 4.8
$Fe^{II}_{1-x}Fe^{III}_x(OH)_{2+x-2y}(SO_4)_y•nH_2O$	Mazeina et al. (2008)		-1036 to -1079	
$NaFe^{II}_6Fe^{III}_3(OH)_{18}(SO_4)_2$	Davesne et al. (2010)	-6366 ± 18		-210.5 ± 3.2

[a] Values converted from cal mol^{-1} to kJ mol^{-1}
[b] Values calculated by Ayala-Luis et al. (2008)

Methods

2.1 Anaerobic Experiments

A vinyl anaerobic chamber (Coy Laboratory Products, Grass Lake, Michigan) was used to maintain an anoxic atmosphere of 2.5-3.5% $H_{2(g)}$ balanced with $N_{2(g)}$, conditions required for GR precipitation, subsequent solubility measurements, and sample handling. A hydrogen/oxygen monitor (Coy CAM-12) was used to measure oxygen (ppm) and hydrogen (%) levels. Oxygen was scrubbed out of the atmosphere via a circulation and palladium catalyst system (Coy).

2.2 Preparation of Anoxic Water

Ultrapure water was boiled in a 2 L glass media bottle for one hour to remove dissolved $O_{2(g)}$. After being briefly allowed to cool, the media bottle was sealed with an open-topped cap and PFTE faced septum. A 12-inch needle was inserted through the septum, which was used to vigorously bubble the water with $N_{2(g)}$ for 1 hour to remove residual oxygen. A small needle was inserted through the septum to allow gas to vent to the atmosphere. The needles were removed and the anoxic ultrapure water was transferred to the anaerobic chamber. Once inside, the cap was loosened so to allow the water to equilibrate with the anaerobic atmosphere and to deoxygenate further for a minimum of 24 hours. Only anoxic ultrapure water was used in the following synthesis and solubility experiments.

2.3.1 Synthesis of GR(Cl)

Chloride GR was synthesized within the anaerobic chamber via precipitation according to the methods of Refait et al. (1998). This entailed creating a solution with a final NaOH concentration of 1 M, a Fe(II)/Fe(III) ratio of 3, and a $\{[FeCl_2]+[FeCl_3]\}/[NaOH]$ ratio of 0.6. These parameters were used to calculate the required quantities of ferrous chloride tetrahydrate, $FeCl_2 \cdot 4H_2O$, and ferric chloride hexahydrate, $FeCl_3 \cdot 6H_2O$, which were each fully dissolved in 50 mL of anoxic ultrapure water. A magnetic stir bar was used to enhance dissolution rates. Following complete dissolution, a 50 mL solution of 2 M NaOH was added while swirling with the stir bar. A dark bluish-green precipitate quickly formed.

2.3.2 Synthesis of GR(SO_4)

Sulphate GR was synthesized in an anaerobic chamber via precipitation according to Géhin et al. (2002). Ferrous sulphate heptahydrate, $FeSO_4 \cdot 7H_2O$, and ferric sulphate pentahydrate, $Fe_2(SO_4)_3 \cdot 5H_2O$, were each fully dissolved in 100 mL of anoxic ultrapure pure water. Magnetic stir bars were used to ensure complete and rapid dissolution. Quantities of the above ingredients were calculated such that an iron ratio of [Fe(II)]/[Fe(III)] = 3 and {[Fe(II)]+[Fe(III)]} = 0.2 M were met. Following, a 100 mL solution of 0.3 M NaOH was added, such that [OH^-]/{[Fe(II)]+[Fe(III)]} = 1.5. A dark bluish-green solid was observed to quickly precipitate.

2.4 Mineral Washing

Freshly precipitated GR solution was transferred to a 500 mL centrifuge bottle. The 500 mL centrifuge tube containing GR was capped with a gasketed air-tight lid, transferred out of the anaerobic chamber, and centrifuged for 10 minutes at 10,000 g. Then, it was transferred back into the anaerobic chamber and the supernatant was decanted. Approximately 50 mL of anoxic ultrapure water was added to re-suspend and disaggregate the mineral, which was done by capping, vortexing, and vigorously shaking the centrifuge tube within the anaerobic chamber. Following, it was washed and centrifuged three additional times using the procedure described above. Following the fourth centrifugation, it was transferred back to the anaerobic chamber and the final supernatant decanted. Using a scoopula, the GR was transferred from the centrifuge tube to a 200 mL serum bottle. The GR containing serum bottle was filled with 150 mL of anoxic ultrapure water, stoppered, and vortexed to re-suspend and disaggregate the mineral. Finally, the stopper was crimped and the resulting suspension is hereafter referred to as GR stock slurry.

Over multiple pre-determined time intervals, the GR stock slurry was hand-shaken and homogenized GR was then extracted and deposited into 1.5 mL freezer tubes. These freezer tubes were stored in a -80°C freezer for various future analyses, at which point the exact date and time was recorded.

2.5 Batch Solubility Experiments

For both GR(Cl) and GR(SO_4), solubility experiments were conducted in triplicate at both low and high salinities in order to simulate freshwater and saltwater environments. To do so, six 100 mL media bottles were filled with 100 mL of ultrapure water. Next, $NaCl_{(s)}$ was added to three of the six serum bottles to form 0.56 M NaCl solutions, replicating modern seawater ionic strength. The media bottles were sealed with open-topped caps and PFTE faced septa, which could be removed for inserting electrodes and obtaining samples.

Using a syringe and needle, 3 mL of the GR stock slurry was extracted and injected into each media bottle. The exact time and date of each injection was recorded, marking the beginning of the GR dissolution reaction.

The following actions were performed during each sampling interval:

1) Using a pH probe and chloride combination electrode (specific to GR(Cl)), the pH and conductivity (as mV) of each solubility experiment was measured, as well as the time and date of measurement.
2) Without disturbing the settled GR, approximately 1.5 mL of supernatant was extracted from the media bottle and were filtered through 0.2 μm filters into 1.5 mL Eppendorf (epi) tubes.

3) These tubes were subsequently centrifuged at 12,000 rpm for 6 minutes by a high-speed microcentrifuge (Fisherbrand) to separate any remaining GR particles from solution by collecting it into a pellet.
4) Approximately 1 mL of supernatant was extracted from each epi tube. These were deposited into another 1.5 mL epi tube pre-filled with 0.5 mL of 1 M HCl, for later ferrozine analysis of Fe, and into a 1.5 mL epi tube pre-filled with 0.5 mL of 1 M HNO_3, for later ICP-MS analysis of metals. The exact times and dates at which the samples were deposited into acid were recorded.

Following the method above, six solubility experiments for both GR(SO_4) and GR(Cl) were conducted at three predetermined time intervals of stock GR age: immediately following synthesis, 2 days, and 7 days.

2.6 Ferrozine Assay

Concentrations of dissolved ferrous and ferric iron were determined using a spectrophotometric approach (Stookey, 1970; Viollier et al., 2000). Dissolved Fe^{2+} reacts with ferrozine to form a complex which turns the solution purple. Using a UV-Vis spectrophotometer measuring absorbance at 562 nm, this complex can be quantified. By determining total Fe via using hydroxylamine hydrochloride (HAHCl) to reduce Fe, Fe(III) quantities were calculated as the difference between total Fe and Fe(II).

To determine the [Fe^{2+}] of a sample, the following were added to a 1 mL cuvette: 0.4 mL of 1 M HCl, 0.1 mL of sample, and 0.5 mL of 0.1% ferrozine in 50% ammonium acetate. Following, the cuvette was incubated in the dark for 5 minutes, and was then measured for

absorbance using a UV-Vis set to a wavelength of 562 nm. To determine the total Fe, 0.4 mL of 10% HAHCl in 1 M HCl and 0.1 mL of sample were mixed in a cuvette. The cuvette was then incubated in the dark for 30 minutes, after which 0.5 mL of 0.1% ferrozine in 50% ammonium acetate was added, and the resulting solution then measured for absorbance using a UV-Vis set to 562 nm. Two calibration curves, one for Fe(II) and a second for total Fe, were generated using standards made from diluting a 1000 ppm ICP-MS grade Fe standard solution composed of 0.10% Fe, 3.61% HNO_3, and 96.29% H_2O.

2.7 ICP-MS Analysis

The total sulfur in samples from the GR(SO_4) batch solubility experiments was analyzed in the Environmental Geochemistry Lab (University of Alberta) with an inductively coupled plasma – double mass spectrometer (ICP-MS/MS; Agilent Technologies 8800) in the O_2 reaction/collision cell mode. Each sample collected from the batch solubility experiments was diluted with 0.5 mL of 1 M HNO_3, as described in section *2.5*. In preparation for analysis, the samples were further diluted at a ratio of 0.5 mL of sample to 4.5 mL of 3% nitric acid. A 1000 ppm sulfur ICP reference solution was used to prepare sulfur standards in 3% nitric acid in order to construct a calibration curve, which was later used to determine the total sulfur concentrations in the samples. The 1000 ppm sulfur ICP standard was composed of 0.41% $(NH_4)_2SO_4$ and 99.59% H_2O.

2.8 Chloride Ion Selective Electrode

Chloride concentrations were measured using an Accumet Chloride Combination Electrode. A 1000 ppm chloride ICP standard was used to prepare chloride standards for

calibration. The 1000 ppm chloride standard was composed of 0.1% NaCl and 99.9% H_2O. A calibration curve was constructed on a semi-log scale before each set of measurements.

2.9 Mössbauer Spectroscopy

Mössbauer spectroscopy was completed by the Geomicrobiology Group of the University of Tübingen. Mineral suspensions were prepared by filtration in an anoxic glovebox (100% N_2) and kept anoxic until they were transferred to the instrument and loaded inside a closed-cycle exchange gas cryostat (Janis Cryogenics). Measurements were collected at 140 K with a constant acceleration drive system (WissEL) in transmission mode with a ^{57}Co/Rh source and calibrated against a 7 µm thick α-^{57}Fe foil measured at room temperature. All spectra were analyzed using Recoil (University of Ottawa) by applying the Voigt Based Fitting (VBF) routine (Rancourt and Ping, 1991). The half width at half maximum (HWHM) was fixed to a value of 0.138 mm/s for all samples.

2.10 Bulk X-Ray Diffraction

A Rigaku Geigeflex Powder Diffractometer (Rigaku Ultima IV) equipped with a graphite monochromator, cobalt tube, and scintillation detector was used to conduct Bulk X-Ray Diffraction (XRD) analyses. Small quantities of wet GR paste were mounted on zero background plates and immediately analyzed to minimize oxidation. JADE 9.1 software and the ICDD and ICSD diffraction pattern databases were used to conduct diffraction pattern matching.

Results & Discussion

The XRD spectra for both GR(Cl) and GR(SO_4) (Figures 2 & 3) exhibit strong GR and magnetite peaks. Additionally, the Mössbauer spectra (Figure 4 & 5) all consist of twin doublets that are characteristic of GR, and twin sextets that are characteristic of magnetite. The XRD spectra for GR(Cl) displays a small peak at approximately 55 degrees, which may correspond to the mineral lepidocrocite; however, no such mineral was detected by the Mössbauer results, nor were there other XRD peaks characteristic of lepidocrocite. The Mössbauer and XRD spectra both indicate a progressive transformation of GR into magnetite. The magnetite peaks in the XRD spectra notably become more prominent with GR age, indicating that GR is transforming into magnetite with time. The Mössbauer results confirm this trend by quantifying the fraction of magnetite present in the ageing GR samples. The 0 d, 2 d, and 7 d old samples corresponded to respective magnetite compositions of 22.5%, 25.0%, and 31.2% for GR(Cl) and 0.0%, 17.3%, and 24.4%. for GR(SO_4). Unlike the 0 d GR(Cl) sample, the XRD and Mössbauer spectra for 0 d GR(SO_4) sample do not display any evidence of magnetite present, indicating that this sample was initially composed of nearly pure GR(SO_4). Many studies have observed the transformation of GR to magnetite in anoxic systems. Through the use of SEM, TEM, EDS, and SAED, Li et al. (2017) documented the dissolution of hexagonal GR(SO_4) platelets followed by the crystallization of hollow spheroidal aggregates composed of magnetite nanocrystals. Sumoondur et al. (2008) studied the abiotic formation of magnetite via GR(SO_4) transformation using field emission gun scanning electron microscopy (FEG-SEM). They too observed an initial crystallization of hexagonal GR(SO_4) particles which subsequently appeared to decay as magnetite nanoparticles growth transpired, thereby indicating that a dissolution-precipitation mechanism facilitates the transformation of GR(SO_4) to magnetite.

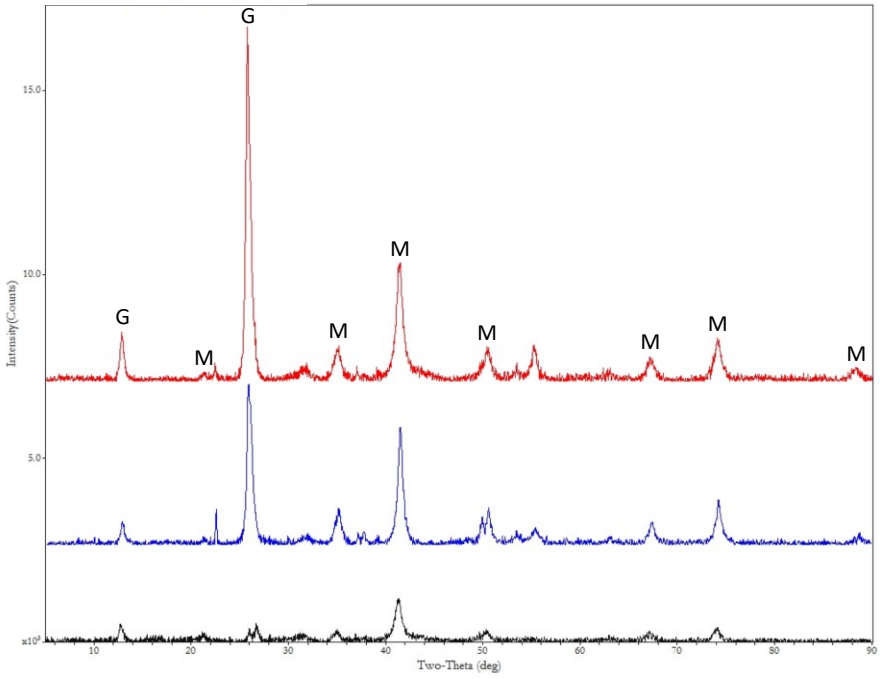

Figure 2. *XRD overlays show a qualitative increase in magnetite peaks with time. M – magnetite, G – GR(Cl). The spectra are coloured as a function of sample age. Black - 3.73 h, blue - 50.12 h, red - 168.45 h.*

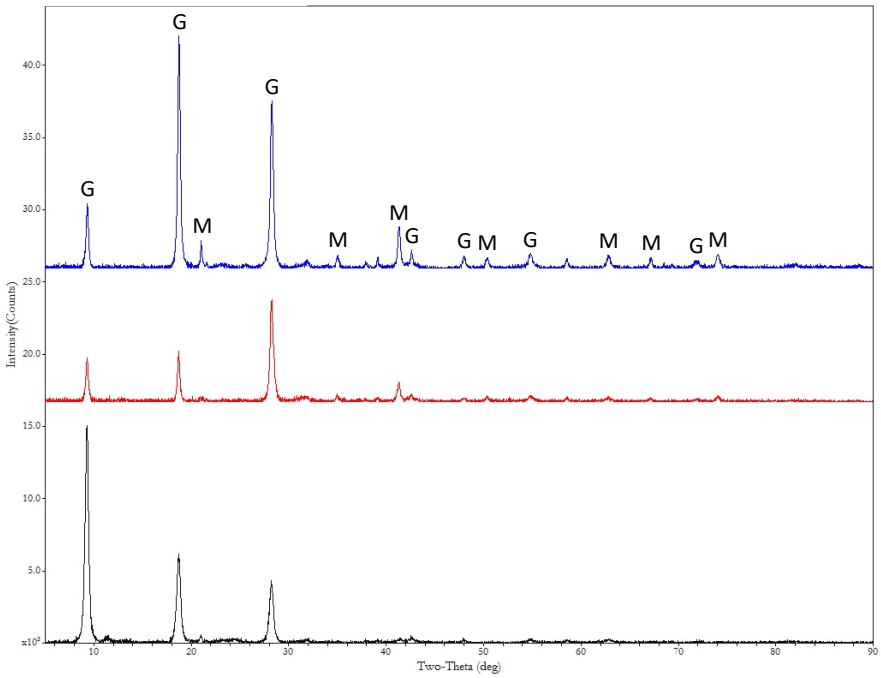

Figure 3. *XRD overlays show a qualitative increase in magnetite peaks with time. M – magnetite, G – GR(SO_4). The spectra are coloured as a function of sample age. Black = 3.80 h, red = 50.18 h, blue = 168.52 h.*

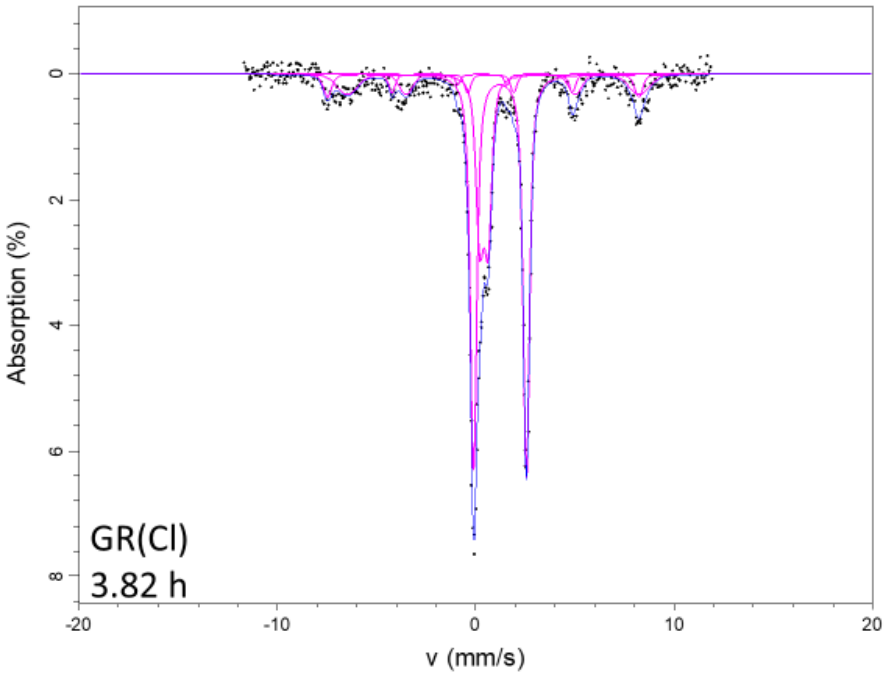
Absorption (%)
0
2
4
6
8
GR(Cl)
3.82 h
-20
-10
0
10
20
v (mm/s)

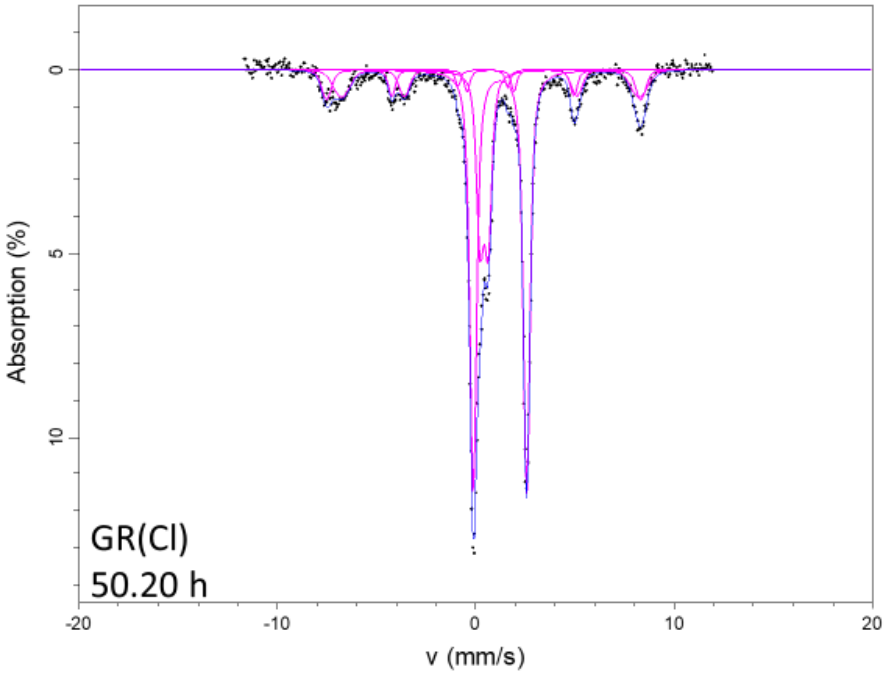
Absorption (%)
0
5
10
GR(Cl)
50.20 h
-20
-10
0
10
20
v (mm/s)

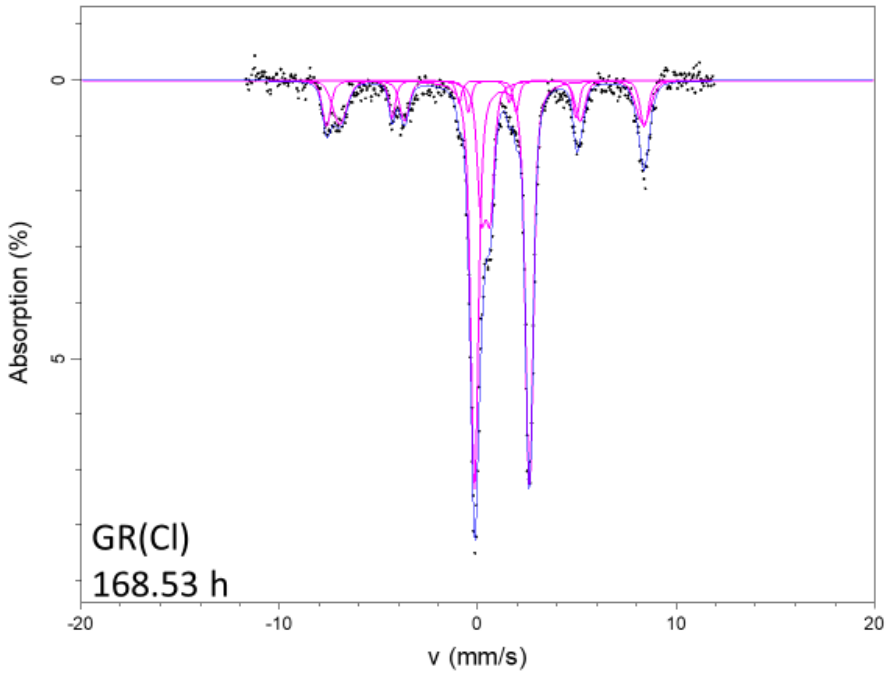

Figure 4. *Mössbauer spectra measured at 140 K of GR(Cl).*

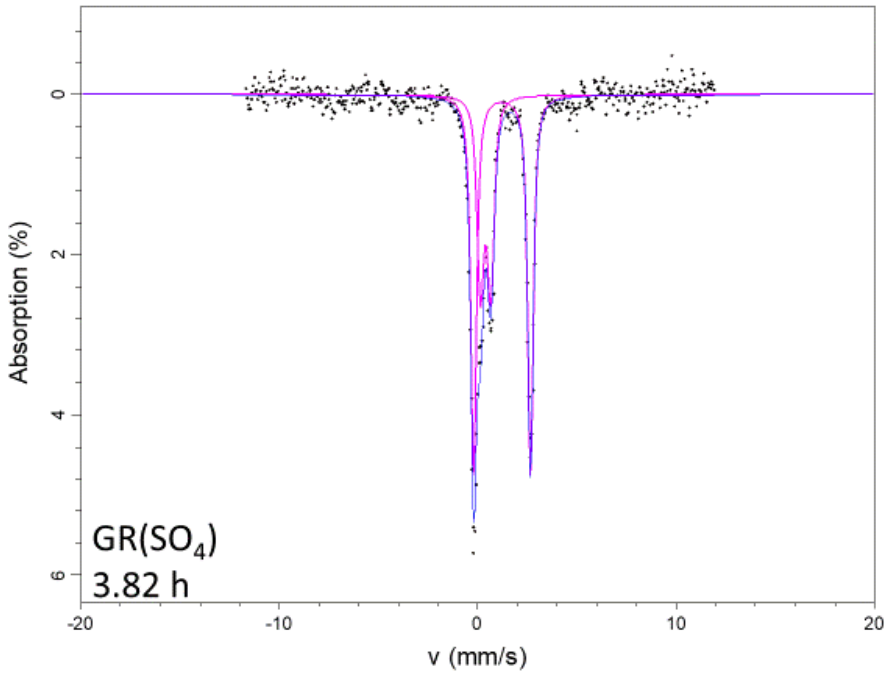
Absorption (%)
0
2
4
6
GR(SO4)
3.82 h
-20
-10
0
10
20
v (mm/s)

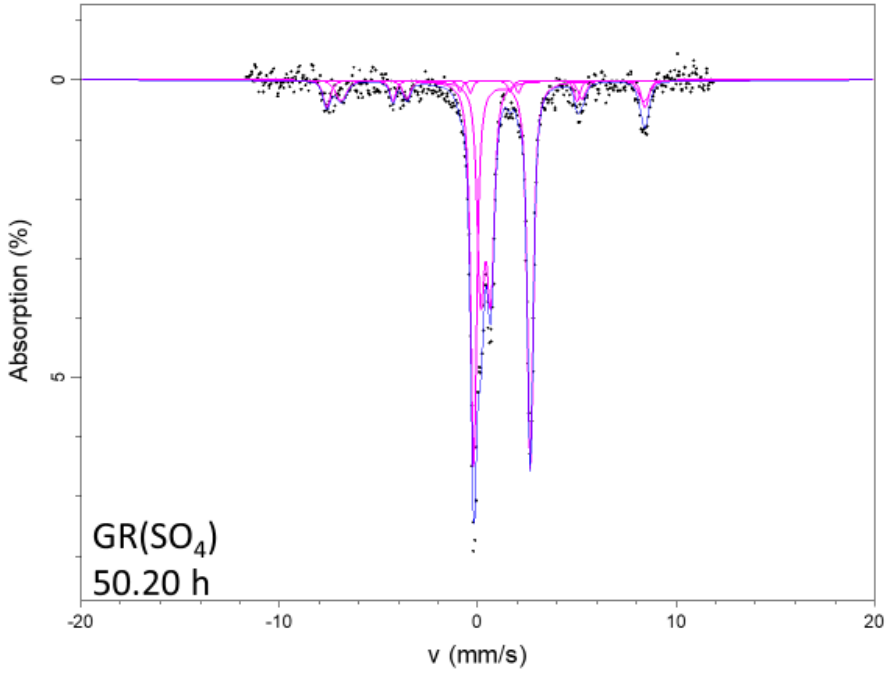
Absorption (%)
0
5
GR(SO4)
50.20 h
-20
-10
0
10
20
v (mm/s)

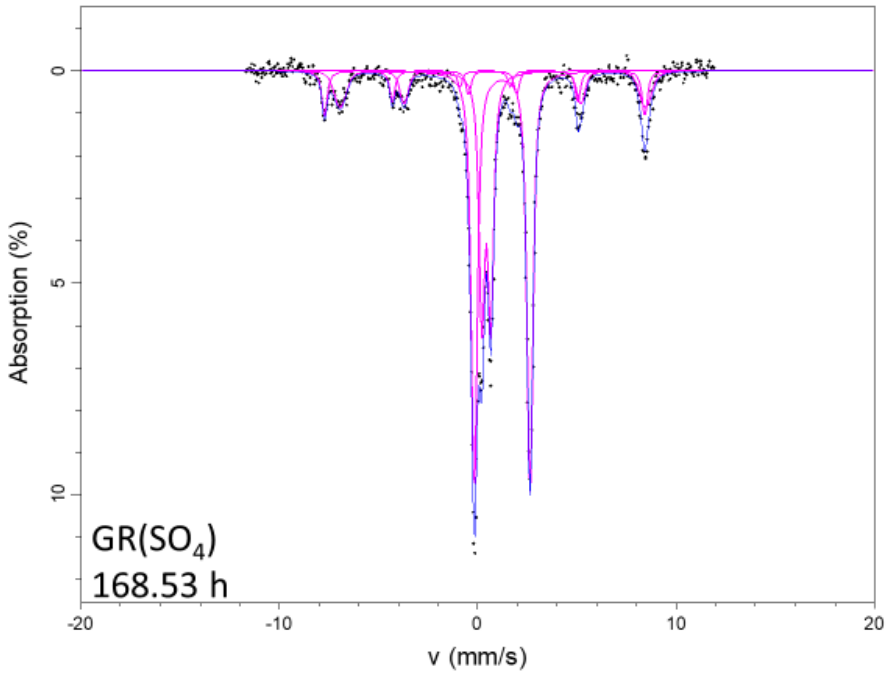

Figure 5. *Mössbauer spectra measured at 140 K of GR(SO_4).*

Table 2. *Hyperfine parameters and results of the fitting spectra.* *δ – center shift, ΔE_Q – quadrupole splitting, ε – quadrupole shift (for sextets only), B_{hf} – hyperfine magnetic field, R.A. – relative abundance of the mineral phase at the given temperature, ± signifies the error in the relative abundance, χ^2 indicates the goodness of fit, Fe(II)/Fe(III) denotes the ratio of Fe(II) to Fe(III), and the Fraction (%) specifies the fraction of GR versus magnetite.*

Sample ID	Age (h)	Site	Phase	δ (mm s^{-1})	ΔE_Q (mm s^{-1})	ε (mm s^{-1})	B_{hf} (T)	R. A. (%)	±	χ^2	Fe(II)/ Fe(III)	Fraction (%)
GR(Cl) – 0 d	3.82	QSD 1	GR (Fe(II))	1.22	2.67	-	-	53.7	2.2	0.63	0.69	77.5
		QSD 2	GR (Fe(III))	0.41	0.43	-	-	23.8	1.2			
		HFD 1	Magnetite	0.35	-	0.02	48.7	7.6	1.9		0.50	22.5
		HFD 2	Magnetite	0.82	-	0.07	45.7	14.9	2.8			
GR(Cl) – 2 d	50.20	QSD 1	GR (Fe(II))	1.22	2.70	-	-	53.4	1.2	0.88	0.71	75.0
		QSD 2	GR (Fe(III))	0.43	0.42	-	-	21.6	6.3			
		HFD 1	Magnetite	0.38	-	0.02	49.1	10.4	1.3		0.41	25.0
		HFD 2	Magnetite	0.74	-	0	46.5	14.6	1.5			
GR(Cl) – 7 d	168.53	QSD 1	GR (Fe(II))	1.22	2.77	-	-	52.4	1.5	0.73	0.76	68.8
		QSD 2	GR (Fe(III))	0.41	0.45	-	-	16.4	0.8			
		HFD 1	Magnetite	0.36	-	0.03	49.7	12.5	1.5		0.43	31.2
		HFD 2	Magnetite	0.72	-	-0.02	47.5	18.7	1.8			
$GR(SO_4)$ – 0 d	3.82	QSD 1	GR (Fe(II))	1.23	2.87	-	-	62.8	1.1	0.81	0.63	100
		QSD 2	GR (Fe(III))	0.40	0.52	-	-	37.2	1.1			
$GR(SO_4)$ – 2 d	50.20	QSD 1	GR (Fe(II))	1.22	2.85	-	-	51.2	1.7	0.66	0.62	82.7
		QSD 2	GR (Fe(III))	0.40	0.50	-	-	31.5	1.2			
		HFD 1	Magnetite	0.39	-	0.02	49.7	8.3	1.8		0.35	17.3
		HFD 2	Magnetite	0.80	-	-0.04	47.3	9.0	2.2			
$GR(SO_4)$ – 7 d	168.53	QSD 1	GR (Fe(II))	1.23	2.81	-	-	48.8	1.0	0.76	0.64	75.6
		QSD 2	GR (Fe(III))	0.43	0.45	-	-	26.8	0.7			
		HFD 1	Magnetite	0.36	-	-0.01	50.1	9.7	1.0		0.43	24.4
		HFD 2	Magnetite	0.75	-	0.01	47.7	14.7	1.3			

GR solubility experiments were conducted in both pure water and 0.56 M ionic strength water. As the 0 d and 2 d old GR(Cl) samples dissolved, the pH and concentrations of GR(Cl)'s constituent ions were measured. These parameters reached an apparent equilibrium within approximately 50 hours and 190 hours in ultrapure water and 0.56 M water, respectively. In solubility experiments using 7 d old GR(Cl), apparent equilibrium was reached after approximately 30 hours and 190 hours in ultrapure and 0.56 M water, respectively. The $GR(SO_4)$ pure water solubility experiments all took approximately 190 hours to reach an apparent equilibrium, regardless of the age of the GR used. Under simulated seawater ionic strength conditions, solubility experiments using 0 d $GR(SO_4)$ took approximately 90 hours to reach apparent equilibrium, whereas for those using 2 d and 7 d old $GR(SO_4)$, it took approximately 120 hours.

Measured Fe^{3+} concentrations in the solubility experiments vary considerably in comparison to concentration trends of other ions (Figures 6 & 7), due to low aqueous concentrations below the detection limits of the ferrozine method. However, there is an identifiable increasing trend in Fe^{3+} concentrations. Measured Fe^{3+} concentrations generally fell between 2 μM to 200 μM. The fact that Fe^{3+} concentrations are so low is due to the insolubility of ferric iron, which possibly have precipitated as ferric iron oxyhydroxides phases, such as ferrihydrite.

Table 3. *Mean apparent equilibrium concentrations of the ions released in solution throughout the GR(Cl) solubility experiments. The mean of each parameter was determined using the last 4 data points of the solubility experiments.*

GR(Cl)	Mean pH	Mean [Cl^-] mM	Mean [Fe^{2+}] mM	Mean [Fe^{3+}] mM	Mean Ionic Strength mM
0 d – Pure Water					
Triplicate 1	7.62	2.19E-03	8.19E-04	1.16E-04	3.05E-03
Triplicate 2	7.80	2.24E-03	8.85E-04	8.10E-05	3.25E-03
Triplicate 3	8.22	2.21E-03	9.44E-04	1.62E-04	3.72E-03
2 d - Pure Water					
Triplicate 1	8.19	2.64E-03	1.10E-03	1.14E-04	3.85E-03
Triplicate 2	8.19	2.72E-03	1.11E-03	1.04E-04	4.05E-03
Triplicate 3	8.19	2.86E-03	1.20E-03	1.01E-04	4.29E-03
7 d - Pure Water					
Triplicate 1	8.02	2.45E-03	9.78E-04	8.81E-05	3.58E-03
Triplicate 2	8.08	2.54E-03	1.01E-03	9.39E-05	3.71E-03
Triplicate 3	8.13	2.72E-03	1.12E-03	1.10E-04	4.10E-03
0 d - 0.56 M Ionic Strength					
Triplicate 1	8.65	5.56E-01	2.66E-04	1.20E-05	5.57E-01
Triplicate 2	8.65	5.57E-01	2.84E-04	2.33E-05	5.58E-01
Triplicate 3	8.66	5.57E-01	2.71E-04	3.45E-05	5.58E-01
2 d - 0.56 M Ionic Strength					
Triplicate 1	8.47	5.57E-01	4.95E-04	5.98E-05	5.58E-01
Triplicate 2	8.46	5.56E-01	5.20E-04	2.09E-05	5.57E-01
Triplicate 3	8.47	5.57E-01	4.66E-04	2.29E-05	5.58E-01
7 d - 0.56 M Ionic Strength					
Triplicate 1	8.39	5.56E-01	7.04E-04	2.50E-05	5.58E-01
Triplicate 2	8.41	5.56E-01	7.36E-04	2.47E-04	5.58E-01
Triplicate 3	8.42	5.55E-01	6.76E-04	4.01E-05	5.57E-01

Table 4. *Mean apparent equilibrium concentrations of the ions released in solution throughout the GR(SO_4) solubility experiments. The mean of each parameter was determined using the last 4 data points of the solubility experiments.*

GR(SO_4)	Mean pH	Mean [SO_4^{2-}] mM	Mean [Fe^{2+}] mM	Mean [Fe^{3+}] mM	Mean Ionic Strength mM
0 d - Pure Water					
Triplicate 1	8.59	3.80E-04	4.60E-01	1.67E-05	1.34E-03
Triplicate 2	8.60	3.44E-04	2.74E-04	8.31E-06	1.23E-03
Triplicate 3	8.54	3.54E-04	3.06E-04	1.33E-05	1.38E-03
2 d - Pure Water					
Triplicate 1	8.32	5.07E-04	4.20E-04	1.27E-05	1.42E-03
Triplicate 2	8.27	4.76E-04	4.52E-04	3.04E-06	1.79E-03
Triplicate 3	8.39	5.02E-04	4.30E-04	3.80E-05	2.04E-03
7 d - Pure Water					
Triplicate 1	8.31	6.09E-04	5.43E-04	1.05E-05	2.15E-03
Triplicate 2	8.18	6.27E-04	5.22E-04	3.27E-05	2.45E-03
Triplicate 3	8.18	6.13E-04	5.00E-04	5.28E-05	2.40E-03
0 d - 0.56 M Ionic Strength					
Triplicate 1	8.49	4.14E-04	1.96E-04	2.15E-05	5.59E-01
Triplicate 2	8.47	4.16E-04	2.07E-04	1.71E-05	5.58E-01
Triplicate 3	8.44	3.99E-04	2.23E-04	2.57E-05	5.58E-01
2 d - 0.56 M Ionic Strength					
Triplicate 1	8.48	5.39E-04	2.74E-04	3.08E-05	5.58E-01
Triplicate 2	8.50	5.44E-04	2.81E-04	1.38E-05	5.59E-01
Triplicate 3	8.52	5.61E-04	2.82E-04	1.45E-05	5.60E-01
7 d - 0.56 M Ionic Strength					
Triplicate 1	8.32	7.43E-04	3.52E-04	3.20E-05	5.59E-01
Triplicate 2	8.35	7.48E-04	3.55E-04	2.52E-05	5.57E-01
Triplicate 3	8.32	6.79E-04	3.37E-04	3.04E-05	5.60E-01

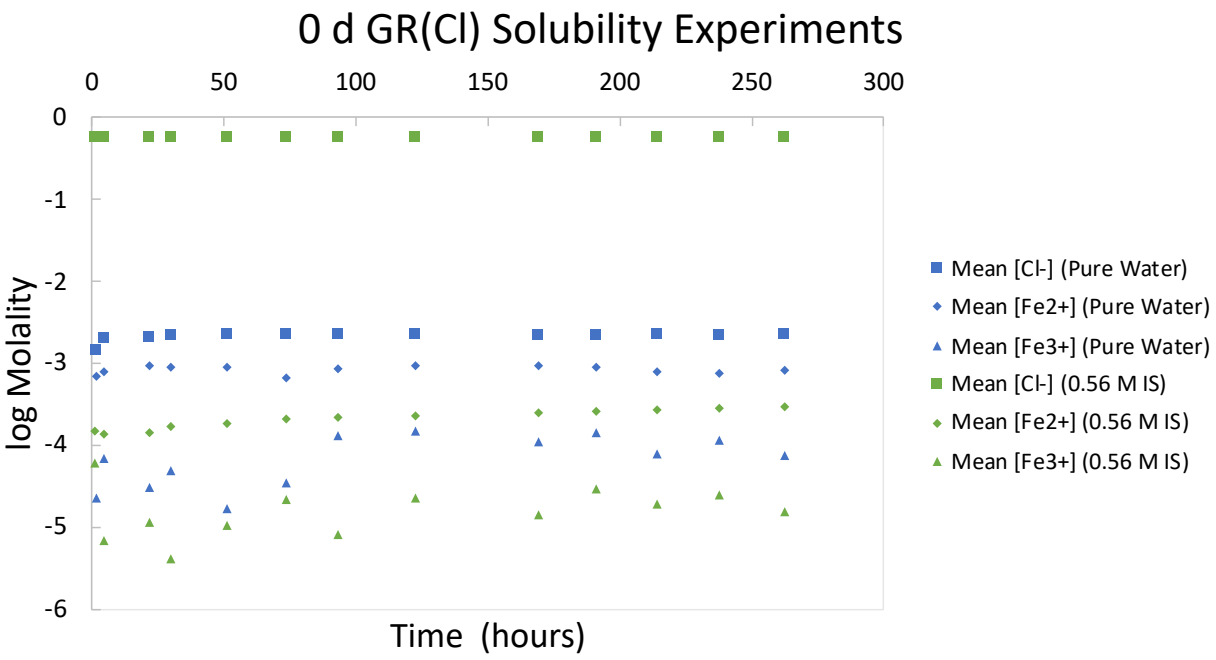
0 d GR(Cl) Solubility Experiments
0
50
100
150
200
250
300
0
-1
-2
-3
-4
-5
-6
log Molality
Time (hours)
Mean [Cl-] (Pure Water)
Mean [Fe2+] (Pure Water)
Mean [Fe3+] (Pure Water)
Mean [Cl-] (0.56 M IS)
Mean [Fe2+] (0.56 M IS)
Mean [Fe3+] (0.56 M IS)

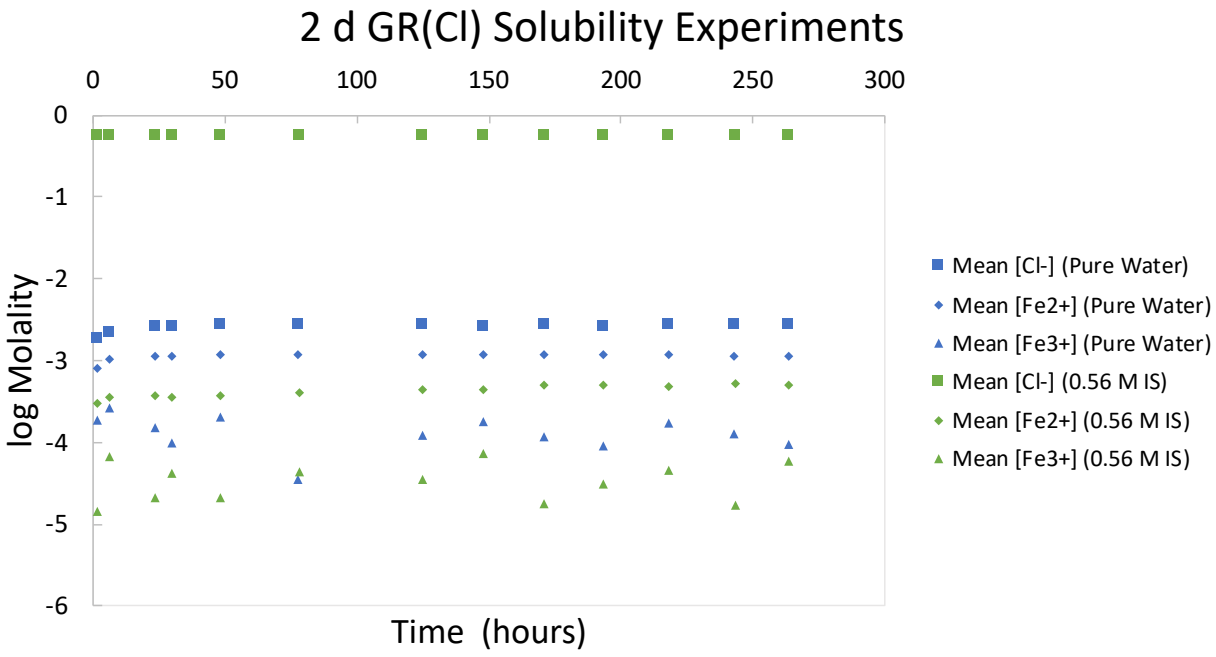
2 d GR(Cl) Solubility Experiments
0
50
100
150
200
250
300
0
-1
-2
-3
-4
-5
-6
log Molality
Time (hours)
Mean [Cl-] (Pure Water)
Mean [Fe2+] (Pure Water)
Mean [Fe3+] (Pure Water)
Mean [Cl-] (0.56 M IS)
Mean [Fe2+] (0.56 M IS)
Mean [Fe3+] (0.56 M IS)

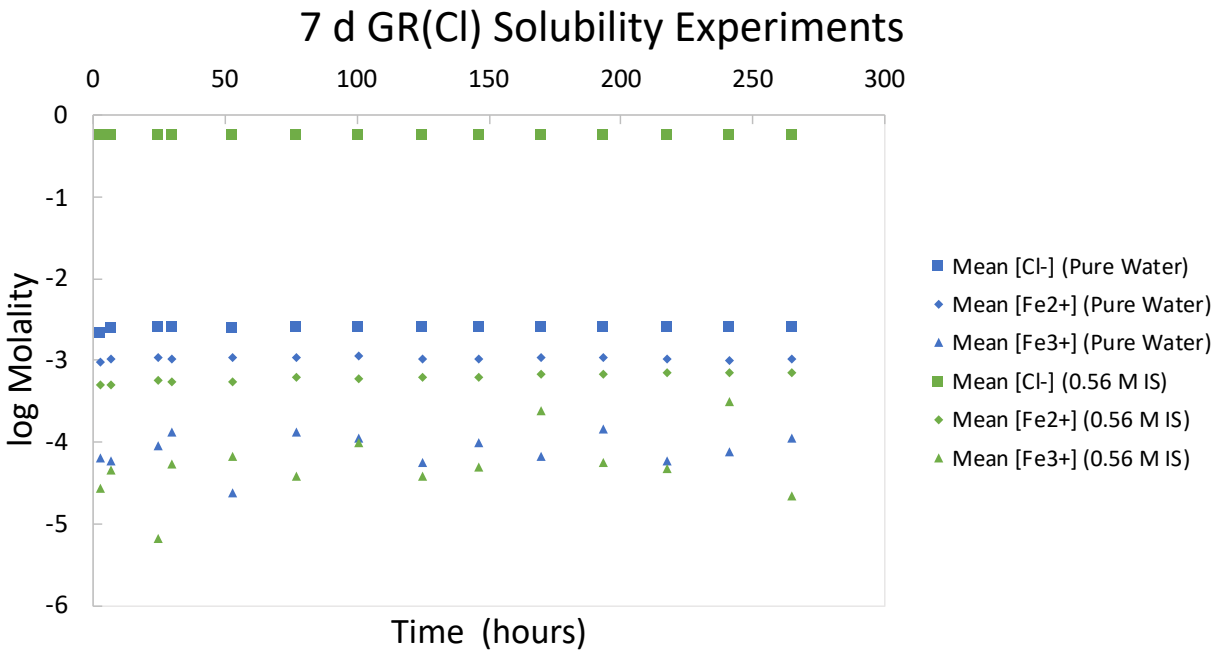

Figure 6. *The mean logarithmic triplicate concentrations of the constituent ions throughout the GR(Cl) solubility experiments as a function of age.*

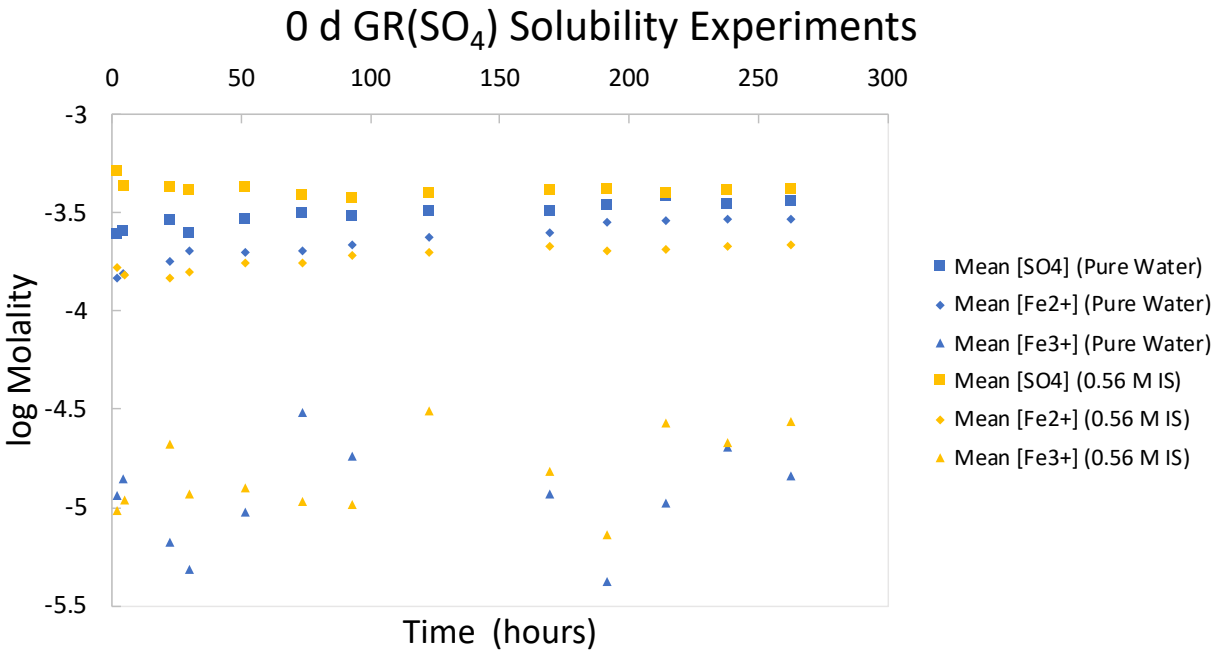
0 d GR(SO4) Solubility Experiments
0
50
100
150
200
250
300
-3
-3.5
-4
-4.5
-5
-5.5
log Molality
Time (hours)
Mean [SO4] (Pure Water)
Mean [Fe2+] (Pure Water)
Mean [Fe3+] (Pure Water)
Mean [SO4] (0.56 M IS)
Mean [Fe2+] (0.56 M IS)
Mean [Fe3+] (0.56 M IS)

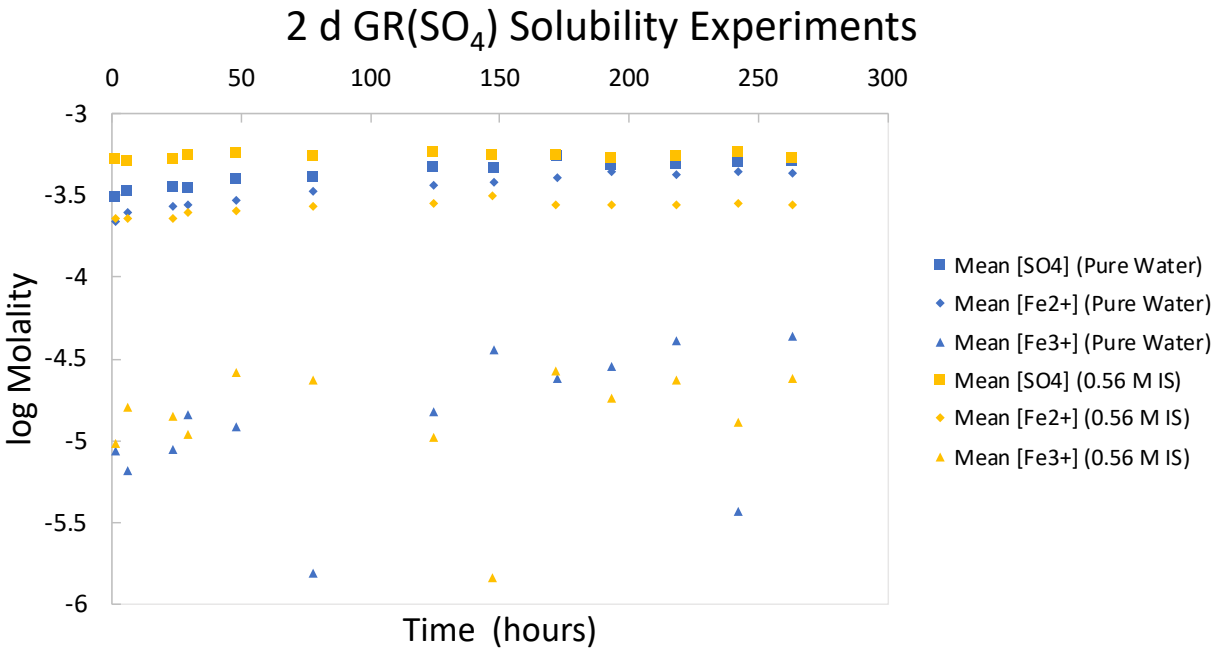
2 d GR(SO4) Solubility Experiments
0
50
100
150
200
250
300
-3
-3.5
-4
-4.5
-5
-5.5
-6
log Molality
Time (hours)
Mean [SO4] (Pure Water)
Mean [Fe2+] (Pure Water)
Mean [Fe3+] (Pure Water)
Mean [SO4] (0.56 M IS)
Mean [Fe2+] (0.56 M IS)
Mean [Fe3+] (0.56 M IS)

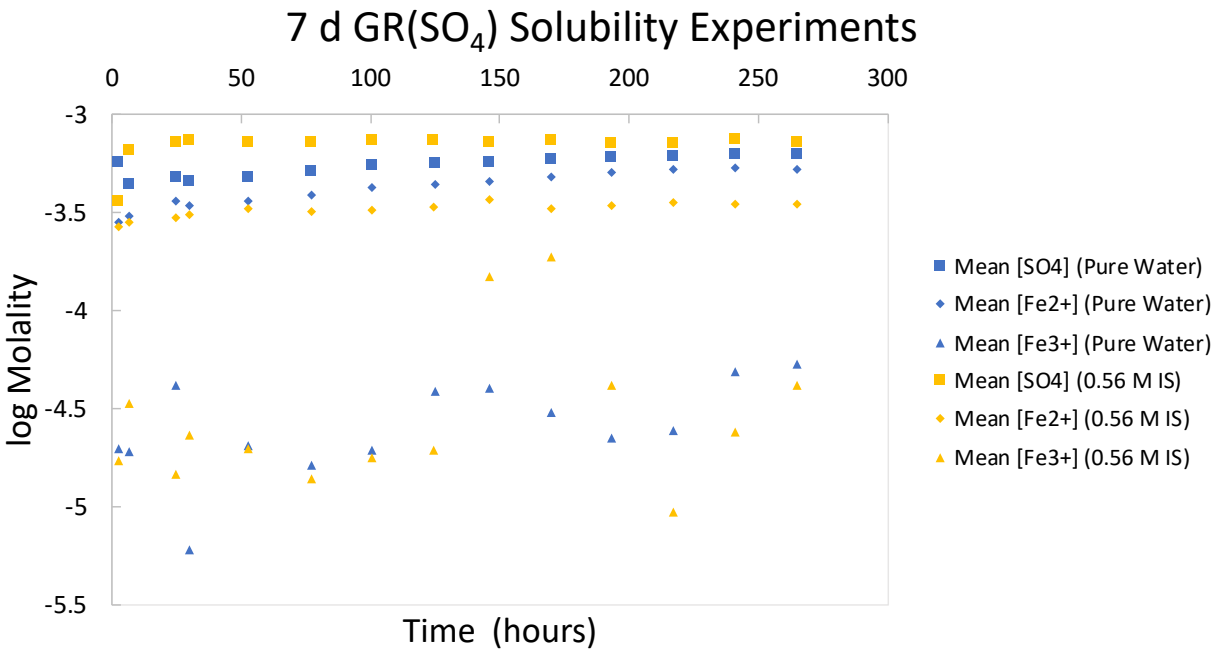

Figure 7. *The mean logarithmic triplicate concentrations of the constituent ions throughout the GR(SO_4) solubility experiments as a function of age.*

The average equilibrium concentrations of ionic species and pH values were determined using the last 4 time points from each solubility experiment, excluding [Fe^{3+}] data that were below detection limits. These time points were selected because the concentrations had plateaued, indicating that apparent equilibrium had been achieved. The average solution ionic strength was calculated based on the ionic strength (I) of the last four sets of data points for each solubility experiment, according to:

$$I = \frac{1}{2}\sum_{i=1}^{n} m_i z_i^2 \quad (1)$$

where m_i is the molal concentration and z_i is the formal charge of the relevant ion.

Next, the activity coefficients (γ_i) for each ion in solution were calculated. The extended Debye-Hückel equation was used to calculate γ_i for the ions of the pure water experiments:

$$\log(\gamma_i) = \frac{-Az_i^2\sqrt{I}}{1 + B\alpha_i^0\sqrt{I}} \quad (2)$$

where A and B are constants and α_i^0 represents ion specific constants that were obtained from Drever (1997). The α_i^0 value for OH^- was sourced from Kielland (1937).

The Truesdell-Jones equation was used to calculate γ_i for the ions of the 0.56 M IS experiments, which is reliable up to an ionic strength of approximately 2 mol/kg (Parkhurst 1990):

$$\log(\gamma_i) = -Az_i^2\left(\frac{\sqrt{I}}{1 + B\alpha_i^0\sqrt{I}}\right) + b_i I \quad (3)$$

where A and B are constants (Drever 1997), and α_i^0 and b_i are ion-specific constants. The α_i^0 and b_i values for Fe^{3+} were sourced from Truesdell and Jones (1974) and the α_i^0 and b_i values for all other ions are from Parkhurst (1990).

Once calculated, the ion-specific activity coefficients were applied to the concentration of each ion to determine their thermodynamic activities (α_i):

$$\alpha_i = \gamma_i m_i \quad (4)$$

Not all Fe(II) will exist as $Fe^{2+}_{(aq)}$, nor Fe(III) as $Fe^{3+}_{(aq)}$, Cl as $Cl^-_{(aq)}$, and S as $SO_4^{2-}_{(aq)}$; rather, these chemical components exist as a variety of different chemical species in solution, including, but not limited to, $Fe^{2+}_{(aq)}$, $Fe^{3+}_{(aq)}$, $Cl^-_{(aq)}$ and $SO_4^{2-}_{(aq)}$. To account for this, PHREEQC (version 3.4.0; MINTEQ 2016 database) was used to model the speciation of ions for each solubility experiment, using the previously calculated activities. In the resulting models, the fractions of $Fe^{2+}_{(aq)}$, $Fe^{3+}_{(aq)}$, $Cl^-_{(aq)}$ and $SO_4^{2-}_{(aq)}$ species were determined. These fractions were then applied to the experimental activities of $Fe^{2+}_{(aq)}$, $Fe^{3+}_{(aq)}$, $Cl^-_{(aq)}$ and $SO_4^{2-}_{(aq)}$, yielding new and appropriate thermodynamic activities to be used in solubility product equations (eq. 7 & 8).

The dissolution reactions that occur for the GR(Cl) and GR(SO_4) in solubility experiments are:

$$[Fe(II)_3Fe(III)(OH)_8][Cl \bullet\ nH_2O]_{(s)} \leftrightarrow 3Fe^{2+} + Fe^{3+} + 8OH^- + Cl^- + nH_2O \quad (5)$$

$$[Fe(II)_4Fe(III)_2(OH)_{12}][SO_4 \bullet\ nH_2O]_{(s)} \leftrightarrow 4Fe^{2+} + 2Fe^{3+} + 12OH^- + SO_4^{2-} + nH_2O \quad (6)$$

The corresponding apparent solubility product equations, derived from the above equations, are therefore:

$$K_{sp}(Cl) = \frac{\alpha^3_{Fe^{2+}} \times \alpha_{Fe^{3+}} \times \alpha^8_{OH^-} \times \alpha_{Cl^-} \times \alpha^n_{H_2O}}{a_{[Fe(II)_3Fe(III)(OH)_8][Cl \bullet\ nH_2O]_{(s)}}} \quad (7)$$

$$K_{sp}(SO_4) = \frac{\alpha^4_{Fe^{2+}} \times \alpha^2_{Fe^{3+}} \times \alpha^{12}_{OH^-} \times \alpha_{SO_4{}^{2-}} \times \alpha^n_{H_2O}}{a_{[Fe(II)_4Fe(III)_2(OH)_{12}][SO_4 \bullet\ nH_2O]_{(s)}}} \quad (8)$$

Where the thermodynamic activities of the minerals and H_2O are assumed to be 1.

With little variation in K_{sp} between solubility experiments as a function of GR age, the resulting grand mean log $K_{sp}(Cl)$ values (Table 5.) across all GR ages in pure water and 0.56 M IS water were calculated to be -75.07 ± 1.39 and -76.22 ± 0.42, respectively. The resulting grand mean log $K_{sp}(SO_4)$ values (Table 6) across all GR ages in pure water and 0.56 M IS water are -119.72 ± 1.03 and -126.60 ± 1.07, respectively.

Table 5. *The log K_{sp} determined in all GR(Cl) solubility experiments. The mean of the triplicate results for each age interval was determined. The means of each age interval were averaged to yield the grand mean log K_{sp} for GR(Cl) under low IS and 0.56 M IS conditions.*

GR(Cl)	log (K_{sp})			Grand Mean
Pure Water	0 d	2 d	7 d	
Triplicate 1	-76.32 ± 3.75	-74.58 ± 0.18	-75.58 ± 0.80	
Triplicate 2	-75.46 ± 3.95	-74.61 ± 0.90	-75.17 ± 0.97	
Triplicate 3	-74.51 ± 0.40	-74.51 ± 0.42	-74.84 ± 1.12	
Mean	-75.43 ± 2.70	-74.57 ± 0.50	-75.20 ± 0.96	-75.07 ± 1.39
0.56 M IS				
Triplicate 1	-76.79 ± 0.29	-76.03 ± 0.26	-76.27 ± 0.14	
Triplicate 2	-76.42 ± 0.31	-76.48 ± 0.60	-75.17 ± 0.60	
Triplicate 3	-76.26 ± 0.21	-76.54 ± 0.63	-75.99 ± 0.72	
Mean	-76.49 ± 0.27	-76.35 ± 0.50	-75.81 ± 0.49	-76.22 ± 0.42

Table 6. *The log K_{sp} determined in all GR(SO_4) solubility experiments. The mean of the triplicate results for each age interval was determined. The means of each age interval were averaged to yield the grand mean log K_{sp} for GR(SO_4) under low IS and 0.56 M IS conditions.*

GR(SO_4)	log (K_{sp})			Grand Mean
Pure Water	0 d	2 d	7 d	
Triplicate 1	-119.30 ± 2.17	-120.03 ± 0.86	-119.97 ± 0.27	
Triplicate 2	-119.88 ± 1.48	-120.63 ± 1.02	-119.74 ± 0.81	
Triplicate 3	-119.61 ± 0.91	-118.89 ± 1.24	-119.41 ± 0.55	
Mean	-119.56 ± 1.52	-119.85 ± 1.04	-119.70 ± 0.54	-119.72 ± 1.03
0.56 M IS				
Triplicate 1	-127.07 ± 0.95	-126.11 ± 0.78	-126.28 ± 0.67	
Triplicate 2	-127.21 ± 0.67	-126.66 ± 1.30	-126.30 ± 0.55	
Triplicate 3	-126.85 ± 1.19	-126.52 ± 1.07	-126.41 ± 2.45	
Mean	-127.04 ± 0.94	-126.43 ± 1.05	-126.33 ± 1.23	-126.60 ± 1.07

Theoretically, the resulting K_{sp} should be the same between pure water and simulated seawater ionic strength. This is true regarding the grand mean log $K_{sp}(Cl)$ values, as the grand mean log $K_{sp}(Cl)$ value determined in 0.56 M IS water falls within error of the grand mean log $K_{sp}(Cl)$ value determined in pure water. However, this is not the case for GR(SO_4). The grand

mean log $K_{sp}(SO_4)$ values differ by 6.88 orders of magnitude and do not fall within error of each other, which could be caused by various sources. Statistically, the largest source of error for both the GR(Cl) and GR(SO_4) solubility experiments are the Fe^{3+} concentrations, which is likely due to the analytical resolution of the ferrozine methodology struggling to measure the Fe^{3+} at such low concentrations. However, the measured Fe^{2+} and Fe^{3+} concentrations in the GR(SO_4) solubility experiments were approximately an order of magnitude less, thus generating additional uncertainty, than those found in the GR(Cl) solubility experiments. The K_{sp} calculations further magnify the error in $K_{sp}(SO_4)$ when compared to $K_{sp}(Cl)$. This is because the Fe^{2+}, Fe^{3+}, and OH^- activities used to calculate $K_{sp}(SO_4)$ (eq. 8) are raised to the power of 4, 2, and 12 respectively, as opposed to 3, 1, and 8 in the $K_{sp}(Cl)$ equation (eq. 7). Additionally, it is likely that in the GR(SO_4) solubility experiments performed in 0.56 IS water, the formation of additional mineral phases may have been facilitated due to anion exchange between aqueous Cl^- and SO_4^{2-} in the mineral phase. It has been shown that many other LDH minerals have a high capacity for anion exchange (Miyata, 1983; Bish, 1980). Nonetheless, the grand mean log $K_{sp}(SO_4)$ of -119.72 ± 1.03 (pure water) and -126.60 ± 1.07 (0.56 M IS) are well within the range of other reported literature log $K_{sp}(SO_4)$ values (Table 1.). Considering the wide gamut of reported literature log $K_{sp}(SO_4)$ values that span a range of nearly 100 orders of magnitude and the difficulty of working with oxidation-sensitive metastable phases, we believe that our pure water and 0.56 M IS grand mean log $K'_{sp}(SO_4)$ results, which differ by 6.88 orders of magnitude, are fairly reasonable.

Generally, there is little difference in the apparent equilibrium concentrations of the ions released in solution across the 0 to 7 d old GR solubility experiments. On the other hand, the difference in apparent equilibrium concentrations between pure water and simulated seawater ionic

strength conditions are stark. The high ionic strength in the simulated seawater solubility experiments resulted in significantly lower Fe concentrations and higher pH readings, which is expected. This difference is even more apparent in the resulting thermodynamic activities, because ionic strength is a major factor in controlling activity coefficient values.

Previously reported K_{sp} and $\Delta_f G°$ values for GR(Cl) and GR(SO_4) are compiled in Table 1. The K_{sp} determined in this study cannot be directly compared to the K_{sp} values determined in other studies because magnetite existed alongside GR throughout our solubility experiments. The inconsistencies amongst reported GR thermodynamic values found in literature may have occurred due to various factors. For example, varying synthesis methods, most commonly precipitation or controlled oxidation, may have given rise to different phases alongside GR, or even different crystal structures of GR (Ayala-Luis et al., 2008). As Ayala-Luis et al. (2008) point out, following synthesis, GR undergoes various treatments across different studies. For instance, Mazeina et al. (2008) determined the $\Delta_f H°$ of GR(SO_4) and their experiments were carried out without washing the precipitate; thus, their results may actually apply to a mixture of phases rather than pure GR(SO_4). Although their XRD data does show the presence of GR, they notably fail to provide the complete XRD data which would reveal if any other phases were present. In many other studies, including this one, the precipitate was removed from the synthesis solution and washed before further experiments were carried out. Another large source of uncertainty in K_{sp}, specifically those indirectly calculated through the determination of $\Delta_f G°$, is the degree of hydration of the GR in question. In those cases, the true value of $\Delta_f G°$ is dependent upon the number of water molecules in the interlayer space of the structure of GR. However, an absolute number for this value has yet to be resolved (Génin et al., 1996; Refait et al., 1999; Simon et al.,

2003; Ayala-Luis et al., 2008). Finally, GR is unstable at near-surface conditions. Being a ferrous iron-bearing metastable phase, GR may undergo oxidation and/or transformation into other iron phases. Considering this, the time required to wash (if done at all) and conduct solubility or calorimetric experiments on GR, and the fact that GR itself is inherently an ill-defined phase, it is difficult to envision that many of the GR phases studied in Table 1 are truly pure.

In the determination of solubility products, a solubility experiment-based approach maintains various advantages when compared to calorimetric methods. To properly determine the solubility product of GR using calorimetry, the GR phase would have to be at its standard state – that is, it exists in its pure and structurally ordered form at a specific temperature and pressure. Considering the effort required to perform calorimetry without oxidation and abiotic transformation, reasonably achieving standard state for calorimetric purposes would be immensely challenging. Additionally, performing drop calorimetry requires a solid phase. In our experience, anoxically drying a GR slurry into a solid, using $N_{2(g)}$, not only dehydrates the phase, but seemed to increase the rate of magnetite crystallization, thereby inhibiting a pure-solid GR phase from existing. Furthermore, a knowledge of the exact stoichiometry of the GR is required to execute the necessary thermodynamic calculations to determine a solubility product. Conversely, our solubility experiments take into account the inevitable fact that GR will transform into magnetite. The solubility experiments can easily be contained within a small anaerobic chamber, making oxidation avoidance more straightforward. Additionally, drying GR is not required as the phase is kept in an aqueous environment throughout the solubility experiments and determining the degree of GR hydration is unwarranted as the activity of the H_2O is assumed to be 1 (eq. 7 & 8).

As discussed earlier, these solubility products, K_{sp}, are not a true solubility products because GR is a metastable phase and transforms into magnetite, and thus the dissolution reaction can never truly reach equilibrium until all of the GR transforms to magnetite. Therefore, the concentrations of the measured ions in the solubility experiments (Figures 6 & 7) reach an apparent equilibrium. However, a major finding of this study is that the K_{sp} does not significantly change as GR aged and transformed into magnetite. To investigate if GR or magnetite controls dissolved iron concentrations, three geochemical models were created using PHREEQC software (Parkhurst & Apello, 1999); two models of the pure water dissolution of GR(SO_4) and GR(Cl) using K_{sp} values from Ayala-Luis et al. (2008) and Refait and Génin (1993), respectively, and of the pure water dissolution of magnetite using the program's MINTEQ database. The Fe^{2+} molal concentrations from the models of GR dissolution, 5.362 x 10^{-7} M for GR(SO_4) and 5.380 x 10^{-6} M for GR(Cl), matched far more closely to the apparent equilibrium concentrations of Fe^{2+} observed in this study, than that of the magnetite model: $[Fe^{2+}] = 9.207 \times 10^{-13}$ M. Average apparent equilibrium concentrations of Fe^{2+} were observed to be 1.036 x 10^{-3} M for 7d old pure water GR(Cl) and 5.215 x 10^{-4} M for 7d old pure water GR(SO_4). In essence, the equilibrium Fe^{2+} concentrations of the magnetite dissolution model did not resemble the apparent equilibrium concentrations of Fe^{2+} observed in the 7d old pure water solubility experiments, which contain GR with evident magnetite fractions, as shown by the XRD (Figure 2 & 3) and Mössbauer results (Figure 4 & 5). Instead, the apparent equilibrium concentrations of Fe^{2+} in the 7d old pure water solubility experiments more closely resembled the equilibrium Fe^{2+} concentrations of the GR(Cl) and GR(SO_4) dissolution models. This suggests that in a solution containing GR and magnetite, GR exerts greater control over dissolved iron concentrations, independent of the GR:magnetite ratios in our experiments. Furthermore, that GR exerts far more control on the aqueous ion

concentrations than does magnetite, indicates that our K_{sp} values are close to the true K_{sp} values for GR(Cl) and GR(SO4). This finding resonates with the work completed by Génin et al. (1998), whom demonstrated that GR(OH^-) controls the activity of Fe^{2+} in the B and C horizons of a hydromorphic soil. The magnetite PHREEQC model also results in an equilibrium pH of 7, whereas the other models show an equilibrium pH of 8.9 for GR(Cl) and 7.9 for GR(SO_4). The apparent equilibrium pH values observed in our solubility experiments were much closer to the pH levels calculated in the GR PHREEQC models than those of the magnetite models, suggesting that GR also exerts greater control of solution pH than magnetite.

These results may have broad implications to how geochemical models involving GR are constructed, as many are incorrectly premised on magnetite controlling dissolved iron concentrations. Research conducted by Halevy et al. (2017) and Li et al. (2017) suggests that GR does precipitate under seawater conditions, suggesting that GR may have existed in Precambrian oceans. Our observations show that GR exerts control over aqueous iron concentrations, even in the presence of magnetite. Therefore, models aiming to reconstruct the geochemical conditions of early Earth should consider GR as a potential phase in the water column, which may significantly influence iron cycling in Earth's early oceans, even if there are lesser quantities of GR than magnetite. This study may be particularly useful regarding modelling trace element cycling and nutrient availability in natural systems where GR is present. Zegeye et al. (2012) observed that the uptake of Ni in Lake Matano, Indonesia – an analogue to the Archean oceans – significantly increased with the formation of GR. This is suggestive that GR may have had some control over trace element cycling and nutrient availability in the Archean oceans, and as a result, may have indirectly impacted large-scale geochemical phenomena. For example, if GR controlled dissolved

Ni in Archean oceans, an essential metal co-factor in methanogenic microbes, GR may have also exerted some control on the rate of methanogenesis (Zegeye et al., 2012). Methane is a major sink for atmospheric oxygen; thus, by constraining rates of methanogenesis through controlling dissolved Ni availability (Konhauser et al., 2009), GR may have played a significant role in the rise of the great oxidation event. Additionally, our research may provide insights into understanding the deposition of BIFs. Studies by Halevy et al. (2017) and Li et al. (2017) indicate that GR may have been a precursor precipitate to magnetite in Algoma-type BIFs, as their research showed that GR can precipitate under simulated seawater conditions and can subsequently transform into nanosized magnetite particles. We quantitatively measured the progressive transformation of GR to magnetite at seawater conditions, providing an initial understanding of the kinetics of GR-magnetite transformation (Figure 8). This may provide some insight regarding the plausibility of GR as a precursor precipitate to magnetite in BIFs.

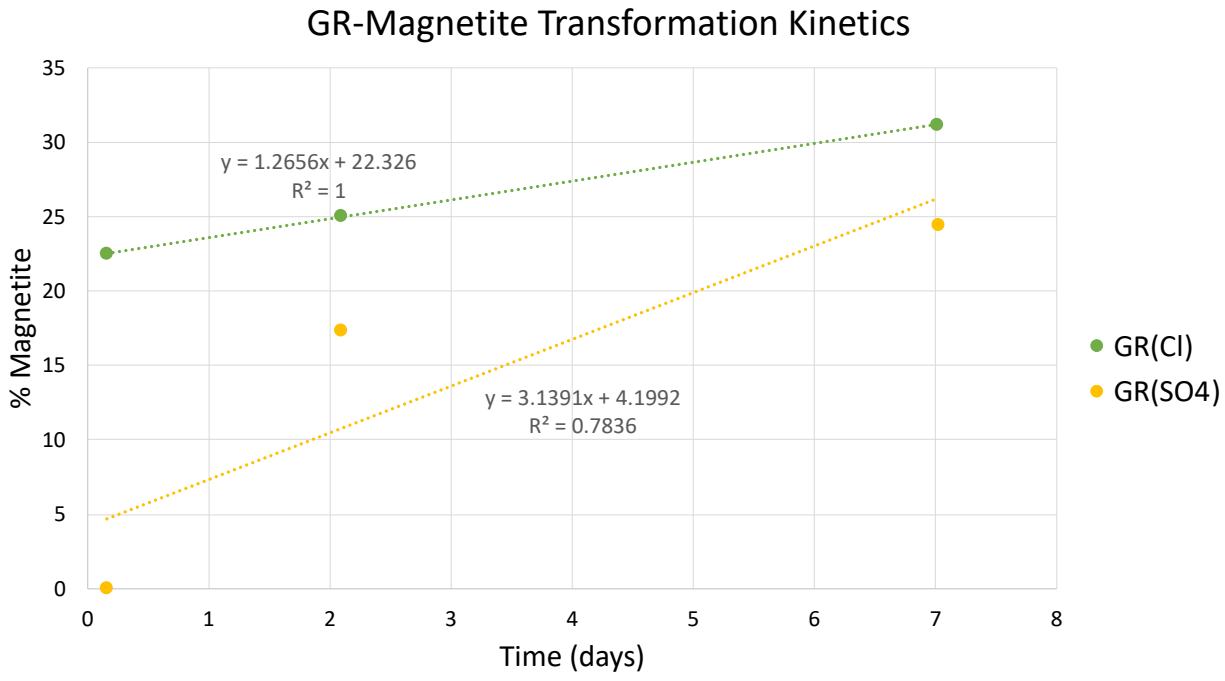

Figure 8. *The kinetics of GR transformation into magnetite determined via Mössbauer spectroscopy. At 0 d, 2 d, and 7 d time intervals, the % magnetite corresponded to 22.5%, 25.0%, and 31.2% for GR(Cl) and 0.0%, 17.3%, and 31.2% for GR(SO_4).*

Geochemical models of modern environmental systems should also carefully consider GR as a potential phase, as GR has been identified in both soil and groundwater (Trolard et al., 1997; Genin et al., 1998; Abdelmoula et al., 1998; Bourrie et al., 1999; Feder et al., 2005; Christiansen et al., 2009). Our research indicates that GR exerts control over iron concentrations, even in the presence of magnetite, yet the majority of groundwater reactive transport models do not factor in the possible presence of GR (Christiansen et al., 2009). GR has reactive and large effective surface areas, and has been observed to act as a sorbent and/or reductant for a variety of environmentally relevant compounds. The thermodynamic parameters determined in this study will contribute to our abilities to understand and model the availability of GR as a subsurface sorbent and reductant. The incorporation of GR into geochemical models could have major implications on how remediation strategies, contaminant transport models, and risk assessment models are developed.

Conclusions & Future Direction

Batch solubility experiments were conducted on GR(Cl) and GR(SO_4) within an anaerobic chamber to determine their solubility products (K_{sp}). These solubility products are not true solubility products because GR is a metastable phase that eventually transforms into magnetite, thus the dissolution reactions can never truly reach equilibrium; however, they are useful in accurately predicting the aqueous concentrations of iron in natural systems that contain GR. Triplicate solubility experiments of GR(Cl) and GR(SO_4) were carried out in three intervals of GR aging: 0, 2, and 7 days. The concentrations of GR constituent ions were determined using ferrozine, ICP-MS, and chloride ion selective electrode analyses. Over multiple pre-determined time

intervals, GR samples were analyzed by bulk X-Ray diffraction and Mössbauer spectroscopy in order to characterize the GR and its transformation into magnetite.

Through the use of XRD and Mössbauer spectroscopy, the presence of GR and magnetite were positively identified in the GR stock slurry samples. The XRD spectra qualitatively displayed magnetite peaks becoming increasingly prominent with time. Consistent with this, the Mössbauer spectra quantified the fractions of GR and magnetite in each sample. It was found that with age, the fraction of GR decreased whereas the fraction of magnetite increased. The XRD spectra for GR(Cl) displays a small peak at approximately 55 degrees, which may correspond to the mineral lepidocrocite; however, no such mineral was detected by the Mössbauer analysis, nor were there other XRD peaks characteristic of lepidocrocite. The peak may possibly represent the presence of a third unidentified phase or could be due to instrumental error. The source of the peak remains unknown.

Triplicate batch solubility experiments of GR(Cl) and GR(SO_4) were conducted at three different age intervals of 0, 2, and 7 days. It was observed that as GR dissolved, the concentrations of its constituent ions increased and plateaued. The last four data points along the concentration plateau were selected for the use of calculating the K_{sp}, as the plateau indicates that the GR dissolution had reached an apparent equilibrium. The average concentrations of the constituent ions, as well as the average solution ionic strength (I), were determined using the last four data points. Using the extended Debye-Hückel equation (equation 2) and the Trusdell-Jones equation (equation 3), the activity coefficients (γ_i) for each ion in solution were determined. Using these activity coefficients together with the measured concentrations, the thermodynamic activities (α_i) of the ions were calculated. Finally, PHREEQC software was used to model the speciation of ions

for each solubility experiment in order to determine which fraction of the total constituent ions were the species specified in the GR dissolution equations. These fractions were applied to the experimentally determined thermodynamic activities, in which the products were subsequently used to determine the K_{sp} of GR(Cl) and GR(SO_4).

There was little variation in the calculated K_{sp} as a function of GR age. Thus, the determined K_{sp} for each experimental condition, which were the mean of triplicate experiments, were averaged to produce a grand mean log K_{sp}. The grand mean log $K_{sp}(Cl)$ in pure water and 0.56 M IS water is calculated to be -75.07 ± 1.39 and -76.22 ± 0.42, respectively. The grand mean log $K_{sp}(Cl)$ value determined in 0.56 M IS water falls within error of the grand mean log $K_{sp}(Cl)$ determined in pure water. The grand mean log $K_{sp}(SO_4)$ in pure water and 0.56 M IS water are -119.72 ± 1.03 and -126.60 ± 1.07, respectively. These grand mean log $K_{sp}(SO_4)$ values differ by 6.88 orders of magnitude and do not fall within error of each other. This could be due to a combination of factors. The activity coefficients were determined using the extended Debye-Hückel equation (equation 2) regarding the pure water conditions, and the Trusdell-Jones equation (equation 3) under the simulated seawater conditions. The measured Fe^{3+} concentrations are the largest source of error in both the GR(Cl) and GR(SO_4) solubility experiments due to the analytical resolution limitations of the ferrozine methodology, however, the measured Fe^{2+} and Fe^{3+} concentrations in the GR(SO_4) solubility experiments were less than those found in the GR(Cl) solubility experiments by approximately one order of magnitude. Due to differences between equations 7 and 8, error in the $K_{sp}(SO_4)$ calculations are magnified more so than error in the $K_{sp}(Cl)$ calculations. Nonetheless, we believe these results are reliable in light of the wide range of literature reported log $K_{sp}(SO_4)$ values and the complexity of working with metastable phases.

In addition to these solubility products, this research demonstrates that GR exerts control over aqueous iron concentrations, even in the presence of magnetite. This is a significant finding regarding understanding and modelling GR's role in natural systems, as many assume magnetite controls dissolved iron concentrations rather than GR. There is mounting scientific evidence that GR is a significant phase in modern environmental systems and that GR may have played a more significant role in ancient systems than previously believed.

Research has shown that GR can precipitate under simulated seawater conditions, thereby indicating that GR may have existed in Precambrian oceans (Halevy et al., 2017 and Li et al., 2017). The findings from our research reveals that GR exerts control over aqueous iron concentrations, even in the presence of magnetite. Accordingly, geochemical models attempting to reconstruct the geochemistry of early Earth should incorporate GR as a mineral phase in aqueous environments, even if it is proposed to be present as a relatively minor Fe-bearing phase by mass or concentration. It has been observed that the formation of GR increased the uptake of Ni in Lake Matano, Indonesia, a proposed analogue to the Archean oceans (Zegeye et al., 2012). Because Ni is an essential metal co-factor in methanogens, Zegeye et al. (2012) suggested that GR may have regulated rates of methanogenesis. By indirectly limiting the production of methane, a major sink for atmospheric oxygen, GR may have been a key factor in the development of the great oxidation event (Konhauser et al., 2009). By exerting control over trace element cycling and nutrient availability, it is conceivable that GR may have indirectly affected numerous large-scale geochemical events. Hence, GR-metal sorption experiments should be performed on a suite of biologically significant elements in order to investigate the impact of GR on dissolved metal availability. The outcomes of these experiments may have large implications on our understanding of ancient ocean chemistry and the evolution of the Earth's climate and atmosphere. GR may have

been a precursor precipitate to magnetite in Algoma-type BIFs, as suggested by Halevy et al. (2017) and Li et al. (2017). These two studies implied that GR can precipitate under simulated seawater conditions and transform into nanosized magnetite particles. By quantitatively measuring the GR rate of transformation into magnetite, our research provides insights regarding the possibility of GR acting as a precursor precipitate to magnetite in BIFs. Further complementary research should be conducted to investigate the plausibility of GR acting as a precursor precipitate to magnetite in BIFs. For example, studies examining GR-magnetite transformation rates as a function of temperature should be performed to investigate the effect of temperature upon GR transformation rates, thereby simulating GR particles descending through the temperature gradient of an oceanic water column. In conjunction, settling experiments with GR particles in simulated seawater should be performed to simulate the rate at which GR particles sink through the oceanic water column. Together with our research and these two future experiments, it may be determined if GR particles could possibly settle on the ocean floor and become a primary depositional phase in BIFs before transforming into magnetite.

GR has been identified in both soil and groundwater (Trolard et al., 1997; Genin et al., 1998; Abdelmoula et al., 1998; Bourrie et al., 1999; Feder et al., 2005; Christiansen et al., 2009), but it could be argued that the scientific community does not recognize GR as a common subsurface mineral phase. Christiansen et al. (2009) points out that the majority of groundwater reactive transport models do not factor in the possible presence of GR, which could be major oversights. GR is both challenging to work with in the laboratory and is difficult to observe in natural environments because GR often oxidizes rapidly in the presence of atmospheric oxygen. Christiansen et al. (2009) developed a method to obtain GR samples with minimal to no oxidation, which was subsequently used to identify GR in multiple groundwater samples. Additional studies

that characterize natural soil and aquifer systems should be conducted in order to investigate whether GR is truly a common phase in natural systems and to understand the types of environments in which GR is likely to occur. This may be challenging, however, as samples taken from the subsurface must be kept at anoxic conditions from the start sampling event to the end of the laboratory analyses. It is important to include GR in relevant geochemical models, as GR has reactive and large effective surface areas, and has been observed to act as a sorbent and/or reductant for a variety of environmentally relevant compounds. Furthermore, our research has shown that GR controls aqueous iron concentrations, even in the presence of magnetite. Ignoring the presence of GR in geochemical models could have profound implications with regards to a model's output accuracy and predicting the fate of contaminants. The thermodynamic parameters determined in this study will contribute to our abilities to understand and model the availability of GR as a subsurface sorbent and reductant. In addition to existing scientific knowledge, supplementary research should be conducted to examine GR's capacity to sorb and/or reduce environmentally relevant organic and inorganic contaminants. With growing interest in technologies involving magnetic retrieval of contaminants, research examining the fate of GR-sorbed contaminants during GR-magnetite transformation may yields viable remediation techniques and should be pursued. GR should be carefully considered as a potential phase within natural systems, as it could have major implications on how remediation strategies, contaminant transport models, and risk assessment models are developed.

References

Abdelmoula, M., Trolard, F., Bourrié, G., & Génin, J. -M.R. (1998). Evidence for the Fe(II)-Fe(III) Green Rust "Fougerite" Mineral Occurrence in a Hydromorphic Soil and Its Transformation with Depth. *Hyperfine Interactions*, 112(1), 235-238.

Ayala-Luis, K. B., Koch, C. B., & Hansen, H. C. B. (2008). The standard Gibbs energy of formation of Fe(II)Fe(III) hydroxide sulfate green rust. *Clays and Clay Minerals*, *56*(6), 633–644.

Bernal, J. D., Dasgupta, D. R., & Mackay, A. L. (1959). The Oxides and Hydroxides of Iron and Their Structural Inter-Relationships. *Clay Minerals*, *4*(21), 15–30.

Bish, D. L. (1980). Anion-exchange in takovite: Applications to other hydroxide minerals. *Bulletin De Minéralogie, 103*(2), 170-175.

Bond, D. L., & Fendorf, S. (2003). Kinetics and Structural Constraints of Chromate Reduction by Green Rusts. *Environmental Science & Technology*, *37*(12), 2750–2757.

Bourrié, G., Trolard, F., Jaffrezic, J.-M. R. G., Maître Véronique, & Abdelmoula, M. (1999). Iron control by equilibria between hydroxy-Green Rusts and solutions in hydromorphic soils. *Geochimica et Cosmochimica Acta*, *63*(19-20), 3417–3427.

Christiansen, B. C., Balic-Zunic, T., Dideriksen, K., & Stipp, S. (2009). Identification of Green Rust in Groundwater. *Environmental Science & Technology*, *43*(10), 3436–3441.

Davesne, E., Dideriksen, K., Christiansen, B., Sonne, M., Ayala-Luis, K., Koch, C. B., Hansen, H. C. B., Stipp, S. (2010). Free energy of formation for green rust sodium sulphate (NaFeII6FeIII3(OH)18(SO4)2(s)). *Geochimica Et Cosmochimica Acta*, *74*(22), 6451–6467.

Drever, J. I. (1997). *The geochemistry of natural waters: surface and groundwater environments*. Upper Saddle River, NJ: Prentice Hall.

Drissi, S., Refait, P., Abdelmoula, M., & Génin, J. (1995). The preparation and thermodynamic properties of Fe(II)□Fe(III) hydroxide-carbonate (green rust 1); Pourbaix diagram of iron in carbonate-containing aqueous media. *Corrosion Science*, *37*(12), 2025–2041.

Elsner, M., Schwarzenbach, R. P., & Haderlein, S. B. (2004). Reactivity of Fe(II)-Bearing Minerals toward Reductive Transformation of Organic Contaminants. *Environmental Science & Technology*, *38*(3), 799–807.

Erbs, M., Hansen, H. C. B., & Olsen, C. E. (1999). Reductive Dechlorination of Carbon Tetrachloride Using Iron(II) Iron(III) Hydroxide Sulfate (Green Rust). *Environmental Science & Technology*, *33*(2), 307–311.

Evans, D. G., & Slade, R. C. T. (n.d.). Structural Aspects of Layered Double Hydroxides. *Structure and Bonding*.

Feder, F., Trolard, F., Klingelhöfer, G., & Bourrié, G. (2005). In situ Mössbauer spectroscopy: Evidence for green rust (fougerite) in a gleysol and its mineralogical transformations with time and depth. *Geochimica Et Cosmochimica Acta*, *69*(18), 4463–4483.

Fredrickson, J. K., Zachara, J. M., Kukkadapu, R. K., Gorby, Y. A., Smith, S. C., & Brown, C. F. (2001). Biotransformation of Ni-Substituted Hydrous Ferric Oxide by an Fe(III)-Reducing Bacterium. *Environmental Science & Technology*, *35*(4), 703–712.

Géhin, A., Ruby, C., Abdelmoula, M., Benali, O., Ghanbaja, J., Refait, P., & Génin, J.-M. R. (2002). Synthesis of Fe(II-III) hydroxysulphate green rust by coprecipitation. *Solid State Sciences*, *4*(1), 61–66.

Génin, J.-M., Olowe, A., Refait, P., & Simon, L. (1996). On the stoichiometry and pourbaix diagram of Fe(II)-Fe(III) hydroxy-sulphate or sulphate-containing green rust 2: An electrochemical and Mössbauer spectroscopy study. *Corrosion Science*, *38*(10), 1751–1762.

Génin, J.-M. R., Bourrié, G., Trolard, F., Abdelmoula, M., Jaffrezic, A., Refait, P., Maitre, V., Humbert, H., Herbillon, A. (1998). Thermodynamic Equilibria in Aqueous Suspensions of Synthetic and Natural Fe(II)−Fe(III) Green Rusts: Occurrences of the Mineral in Hydromorphic Soils. *Environmental Science & Technology*, *32*(8), 1058–1068.

Halevy, I., Alesker, M., Schuster, E. M., Popovitz-Biro, R., & Feldman, Y. (2017). A key role for green rust in the Precambrian oceans and the genesis of iron formations. *Nature Geoscience*, *10*(2), 135–139.

Hansen, H. C. B., Borggaard, O. K., & Sørensen, J. (1994). Evaluation of the free energy of formation of Fe(II)-Fe(III) hydroxide-sulphate (green rust) and its reduction of nitrite. *Geochimica Et Cosmochimica Acta*, *58*(12), 2599–2608.

Hansen, H. C. B., Koch, C. B., Nancke-Krogh, H., Borggaard, O. K., & Sørensen, J. (1996). Abiotic Nitrate Reduction to Ammonium: Key Role of Green Rust. *Environmental Science & Technology*, *30*(6), 2053–2056.

Jönsson, J., & Sherman, D. M. (2008). Sorption of As(III) and As(V) to siderite, green rust (fougerite) and magnetite: Implications for arsenic release in anoxic groundwaters. *Chemical Geology*, *255*(1-2), 173–181.

Kielland, J. (1937). Individual Activity Coefficients of Ions in Aqueous Solutions. *Journal of the American Chemical Society*, *59*(9), 1675–1678.

Konhauser, K., Planavsky, N., Hardisty, D., Robbins, L., Warchola, T., Haugaard, R., Lalonde, S. V., Partin, C. A., Oonk, P.B.H., Tsikos, H., Lyons, T.W., Bekker, A., Johnson, C. (2017). Iron formations: A global record of Neoarchaean to Palaeoproterozoic environmental history. *Earth-Science Reviews*, *172*, 140–177.

Konhauser, K. O., Pecoits, E., Lalonde, S. V., Papineau, D., Nisbet, E. G., Barley, M. E., Arndt, N.T., Zahnle, K., Kamber, B. S. (2009). Oceanic nickel depletion and a methanogen famine before the Great Oxidation Event. *Nature*, *458*(7239), 750–753.

Kukkadapu, R. K., Zachara, J. M., Fredrickson, J. K., & Kennedy, D. W. (2004). Biotransformation of two-line silica-ferrihydrite by a dissimilatory Fe(III)-reducing bacterium: formation of carbonate green rust in the presence of phosphate. *Geochimica Et Cosmochimica Acta*, *68*(13), 2799–2814.

Lee, W., & Batchelor, B. (2002). Abiotic Reductive Dechlorination of Chlorinated Ethylenes by Iron-Bearing Soil Minerals. 2. Green Rust. *Environmental Science & Technology*, *36*(24), 5348–5354.

Legrand, L., Figuigui, A. E., Mercier, F., & Chausse, A. (2004). Reduction of Aqueous Chromate by Fe(II)/Fe(III) Carbonate Green Rust: Kinetic and Mechanistic Studies. *Environmental Science & Technology*, *38*(17), 4587–4595.

Li, Y.-L., Konhauser, K. O., & Zhai, M. (2017). The formation of magnetite in the early Archean oceans. *Earth and Planetary Science Letters*, *466*, 103–114.

Loyaux-Lawniczak, S., Refait, P., Lecomte, P., Ehrhardt, J.-J., & Génin, J.-M. R. (1999). The reduction of chromate ions by Fe(II) layered hydroxides. *Hydrology and Earth System Sciences*, *3*(4), 593–599.

Loyaux-Lawniczak, S., Refait, P., Ehrhardt, J.-J., Lecomte, P., & Génin, J.-M. R. (2000). Trapping of Cr by Formation of Ferrihydrite during the Reduction of Chromate Ions by Fe(II)−Fe(III) Hydroxysalt Green Rusts. *Environmental Science & Technology*, *34*(3), 438–443.

Maithreepala, R. A., & Doong, R.-A. (2005). Enhanced Dechlorination of Chlorinated Methanes and Ethenes by Chloride Green Rust in the Presence of Copper(II). *Environmental Science & Technology*, *39*(11), 4082–4090.

Mazeina, L., Navrotsky, A., & Dyar, D. (2008). Enthalpy of formation of sulfate green rusts. *Geochimica Et Cosmochimica Acta*, *72*(4), 1143–1153.

Mcgill, I. R., Mcenaney, B., & Smith, D. C. (1976). Crystal structure of green rust formed by corrosion of cast iron. *Nature*, *259*(5540), 200–201.

Mitsunobu, S., Takahashi, Y., & Sakai, Y. (2008). Abiotic reduction of antimony(V) by green rust (Fe4(II)Fe2(III)(OH)12SO4·3H2O). *Chemosphere*, *70*(5), 942–947.

Mitsunobu, S., Takahashi, Y., Sakai, Y., & Inumaru, K. (2009). Interaction of Synthetic Sulfate Green Rust with Antimony(V). *Environmental Science & Technology*, *43*(2), 318–323.

Miyata, S. (1983). Anion-Exchange Properties of Hydrotalcite-Like Compounds. *Clays and Clay Minerals, 31*(4), 305-311.

Myneni, S. C., Tokunaga, T. K., & Brown Jr., G. E. (1997). Abiotic Selenium Redox Transformations in the Presence of Fe(II,III) Oxides. *Science*, *278*(5340), 1106–1109.

O'Loughlin, E. J., Kelly, S. D., Cook, R. E., Csencsits, R., & Kemner, K. M. (2003). Reduction of Uranium(VI) by Mixed Iron(II)/Iron(III) Hydroxide (Green Rust): Formation of UO2 Nanoparticles. *Environmental Science & Technology*, *37*(4), 721–727.

O'Loughlin, E. J., Kemner, K. M., & Burris, D. R. (2003). Effects of AgI, AuIII, and CuII on the Reductive Dechlorination of Carbon Tetrachloride by Green Rust. *Environmental Science & Technology*, *37*(13), 2905–2912.

Ona-Nguema, G., Abdelmoula, M., Jorand, F., Benali, O., Block, J.-C., & Génin, J.-M. R. (2002). Iron(II,III) Hydroxycarbonate Green Rust Formation and Stabilization from Lepidocrocite Bioreduction. *Environmental Science & Technology*, *36*(1), 16–20.

O'Loughlin, E. J., Kelly, S. D., Kemner, K. M., Csencsits, R., & Cook, R. E. (2003). Reduction of AgI, AuIII, CuII, and HgII by FeII/FeIII hydroxysulfate green rust. *Chemosphere*, *53*(5), 437–446.

Pantke, C., Obst, M., Benzerara, K., Morin, G., Ona-Nguema, G., Dippon, U., & Kappler, A. (2012). Green Rust Formation during Fe(II) Oxidation by the Nitrate-Reducing Acidovorax sp. Strain BoFeN1. *Environmental Science & Technology*, *46*(3), 1439–1446.

Parkhurst, D. L. (1990). Ion-Association Models and Mean Activity Coefficients of Various Salts. *ACS Symposium Series Chemical Modeling of Aqueous Systems II*, 30–43.

Pepper, S. E., Bunker, D. J., Bryan, N. D., Livens, F. R., Charnock, J. M., Pattrick, R. A., & Collison, D. (2003). Treatment of radioactive wastes: An X-ray absorption spectroscopy study of the reaction of technetium with green rust. *Journal of Colloid and Interface Science*, *268*(2), 408–412.

Pineau, S., Sabot, R., Quillet, L., Jeannin, M., Caplat, C., Dupont-Morral, I., & Refait, P. (2008). Formation of the Fe(II–III) hydroxysulphate green rust during marine corrosion of steel associated to molecular detection of dissimilatory sulphite-reductase. *Corrosion Science*, *50*(4), 1099–1111.

Rancourt, D., & Ping, J. (1991). Voigt-based methods for arbitrary-shape static hyperfine parameter distributions in Mössbauer spectroscopy. *Nuclear Instruments and Methods in Physics Research Section B: Beam Interactions with Materials and Atoms*, *58*(1), 85–97.

Randall, S. R., Sherman, D. M., & Ragnarsdottir, K. (2001). Sorption of As(V) on green rust (Fe4(II)Fe2(III)(OH)12SO4 · 3H2O) and lepidocrocite (γ-FeOOH): Surface complexes from EXAFS spectroscopy. *Geochimica Et Cosmochimica Acta*, *65*(7), 1015–1023.

Refait, P., & Génin, J.-M. (1993). The oxidation of ferrous hydroxide in chloride-containing aqueous media and pourbaix diagrams of green rust one. *Corrosion Science*, *34*(5), 797–819.

Refait, P., & Génin, J.-M. (1994). The transformation of chloride-containing green rust one into sulphated green rust two by oxidation in mixed Cl− and SO42− aqueous media. *Corrosion Science*, *36*(1), 55–65.

Refait, P., Memet, J.-B., Bon, C., Sabot, R., & Génin, J.-M. (2003). Formation of the Fe(II)–Fe(III) hydroxysulphate green rust during marine corrosion of steel. *Corrosion Science*, *45*(4), 833–845.

Refait, P., Drissi, S., Pytkiewicz, J., & Génin, J.-M. (1997). The anionic species competition in iron aqueous corrosion: Role of various green rust compounds. *Corrosion Science*, *39*(9), 1699–1710.

Refait, P., Abdelmoula, M., & Génin, J.-M. (1998). Mechanisms of formation and structure of green rust one in aqueous corrosion of iron in the presence of chloride ions. *Corrosion Science*, *40*(9), 1547–1560.

Refait, P., Bon, C., Simon, L., Bourrié, G., Trolard, F., Bessière, J., & Génin, J.-M. R. (1999). Chemical Composition and Gibbs Standard Free Energy of Formation of Fe(II)-Fe(III) Hydroxysulphate Green Rust and Fe(II) Hydroxide. *Clay Minerals*, *34*(3), 499–510.

Refait, P., Simon, L., & Génin, J.-M. R. (2000). Reduction of SeO42-Anions and Anoxic Formation of Iron(II)−Iron(III) Hydroxy-Selenate Green Rust. *Environmental Science & Technology*, *34*(5), 819–825.

Robbins, L. J., Funk, S. P., Flynn, S. L., Warchola, T. J., Li, Z., Lalonde, S. V., Rostron, B. J., Smith, A. J. B., Beukes, N. J., de Kock, M. O., Heaman, L. M., Alessi, D. S., Konhauser, K. O. (2019). Hydrogeological constraints on the formation of Palaeoproterozoic banded iron formations. *Nature Geoscience*, *12*(7), 558–563.

Simon, L., Francois, M., Refait, P., Renaudin, G., Lelaurain, M., & Genin, J.-M. R. (2003). Structure of the Fe(II—III) Layered Double Hydroxysulfate Green Rust Two From Rietveld Analysis. *ChemInform*, *34*(31), 327-334.

Skovbjerg, L., Stipp, S., Utsunomiya, S., & Ewing, R. (2006). The mechanisms of reduction of hexavalent chromium by green rust sodium sulphate: Formation of Cr-goethite. *Geochimica Et Cosmochimica Acta*, *70*(14), 3582–3592.

Steefel, C. I., & Cappellen, P. V. (1990). A new kinetic approach to modeling water-rock interaction: The role of nucleation, precursors, and Ostwald ripening. *Geochimica Et Cosmochimica Acta, 54*(10), 2657-2677.

Stookey, L. L. (1970). Ferrozine---a new spectrophotometric reagent for iron. *Analytical Chemistry*, *42*(7), 779–781.

Sumoondur, A., Shaw, S., Ahmed, I. A., & Benning, L. G. (2008). Green rust as a precursor for magnetite: an in situ synchrotron based study. Mineralogical Magazine, 72(1), 201–204.

Tamaura, Y., Yoshida, T., & Katsura, T. (1984). The Synthesis of Green Rust II(FeIII1–FeII2) and Its Spontaneous Transformation into Fe3O4. *Bulletin of the Chemical Society of Japan*, *57*(9), 2411–2416.

Trolard, F., Génin, J.-M., Abdelmoula, M., Bourrié, G., Humbert, B., & Herbillon, A. (1997). Identification of a green rust mineral in a reductomorphic soil by Mossbauer and Raman spectroscopies. *Geochimica Et Cosmochimica Acta*, *61*(5), 1107–1111.

Truesdell, A. H., & Jones, B. F. (1973). *Wateq, a computer program for calculating chemical equilibria of natural waters*. Washington: U.S. Dept. of the Interior, Geological Survey.

Usman, M., Byrne, J. M., Chaudhary, A., Orsetti, S., Hanna, K., Ruby, C., Kappler, A., Haderlein, S. B. (2018). Magnetite and Green Rust: Synthesis, Properties, and Environmental Applications of Mixed-Valent Iron Minerals. *Chemical Reviews*, *118*(7), 3251–3304.

Viollier, E., Inglett, P., Hunter, K., Roychoudhury, A., & Cappellen, P. V. (2000). The ferrozine method revisited: Fe(II)/Fe(III) determination in natural waters. Applied Geochemistry, 15(6), 785–790.

Zegeye, A., Ona-Nguema, G., Carteret, C., Huguet, L., Abdelmoula, M., & Jorand, F. (2005). Formation of Hydroxysulphate Green Rust 2 as a Single Iron(II-III) Mineral in Microbial Culture. *Geomicrobiology Journal*, *22*(7-8), 389–399.

Zegeye, A., Bonneville, S., Benning, L. G., Sturm, A., Fowle, D. A., Jones, C., Canfield, D. E., Ruby, C., MacLean, L. C., Nomosatryo, S., Crowe, S. A., Poulton, S. W. (2012). Green rust formation controls nutrient availability in a ferruginous water column. *Geology*, *40*(7), 599–602.

Appendix A

Table A.1. *Summary of $GR(SO_4)$ batch solubility experiment data. Triplicates A, B, and C were performed in pure water. Triplicates D, E, and F were performed in simulated seawater. Samples 1-14 correspond to 0 d old $GR(SO_4)$; 15-28 to 2 d old $GR(SO_4)$; and 29-42 to 7 d old $GR(SO_4)$.*

Sample ID	Sample Age (h)	pH	SO_4^{2-} (M)	Fe^{2+} (M)	Fe^{3+} (M)	Ionic Strength (M)
SFA1	1.58	8.96	2.0683E-04	1.1820E-04	1.3646E-05	7.1603E-04
SFA2	4.47	8.83	2.8114E-04	1.3971E-04	1.9146E-05	9.3124E-04
SFA3	22.08	8.78	2.7382E-04	1.6556E-04	4.6960E-06	9.0292E-04
SFA4	30.08	8.83	2.3603E-04	2.0791E-04	-1.3871E-05	8.2885E-04
SFA5	51.27	8.69	3.1896E-04	1.9485E-04	3.5721E-06	1.0462E-03
SFA6	73.73	8.83	3.1141E-04	1.9812E-04	6.8046E-05	1.3286E-03
SFA7	93.10	8.72	3.5739E-04	2.0964E-04	3.2575E-06	1.1513E-03
SFA8	122.75	8.57	3.1287E-04	2.3184E-04	-7.6756E-06	1.0567E-03
SFA9	-	-	-	-	-	-
SFA10	169.48	8.68	3.4489E-04	2.5710E-04	1.1493E-05	1.2581E-03
SFA11	191.25	8.59	3.6448E-04	2.8242E-04	-4.1007E-05	1.1112E-03
SFA12	214.33	8.56	3.8403E-04	2.8727E-04	3.3230E-07	1.3459E-03
SFA13	238.00	8.59	3.7406E-04	2.8156E-04	3.1217E-05	1.4537E-03
SFA14	262.40	8.61	3.9931E-04	2.8890E-04	1.8594E-05	1.4621E-03
SFA15	1.45	8.74	3.1745E-04	2.2396E-04	1.0001E-05	1.1306E-03
SFA16	6.17	8.69	3.1487E-04	2.4983E-04	1.6232E-06	1.1391E-03
SFA17	23.15	8.68	3.6194E-04	2.7117E-04	-5.5521E-06	1.2436E-03
SFA18	29.52	8.68	3.5776E-04	2.5945E-04	1.4349E-05	1.3014E-03
SFA19	48.02	8.67	3.9989E-04	2.9216E-04	4.9317E-06	1.4086E-03
SFA20	77.75	8.52	4.1265E-04	3.3807E-04	-8.4773E-06	1.4650E-03
SFA21	-	-	-	-	-	-
SFA22	124.38	8.53	4.6587E-04	3.7037E-04	5.2259E-06	1.6977E-03
SFA23	147.45	8.47	4.7592E-04	3.7737E-04	3.2171E-05	1.8528E-03
SFA24	172.77	8.45	5.2921E-04	4.0071E-04	2.8078E-05	1.9876E-03
SFA25	193.10	8.36	4.8135E-04	4.1136E-04	1.8707E-05	1.8707E-03
SFA26	218.10	8.35	5.0165E-04	4.2345E-04	1.4508E-05	1.9166E-03
SFA27	242.33	8.31	4.7835E-04	4.2530E-04	4.8557E-06	1.8302E-03
SFA28	263.32	8.25	5.6616E-04	4.2034E-04	-4.2228E-04	7.3653E-05
SFA29	2.70	8.76	4.6347E-04	3.0783E-04	-5.7686E-05	1.2859E-03
SFA30	6.70	8.77	4.3153E-04	3.1396E-04	2.9347E-06	1.5071E-03
SFA31	24.40	8.72	5.0342E-04	3.5831E-04	-2.3572E-05	1.6200E-03
SFA32	29.87	8.64	4.4849E-04	3.3504E-04	2.6507E-06	1.5812E-03

SFA33	52.90	8.67	5.2045E-04	3.5341E-04	3.5701E-05	1.9107E-03
SFA34	77.00	8.62	4.9820E-04	4.0786E-04	-8.6875E-06	1.7751E-03
SFA35	100.35	8.56	5.5114E-04	4.4603E-04	-2.8201E-05	1.8692E-03
SFA36	124.62	8.49	5.5460E-04	4.5735E-04	2.8184E-05	2.1523E-03
SFA37	145.78	8.4	6.0621E-04	4.6015E-04	3.8424E-05	2.3069E-03
SFA38	169.75	8.43	6.1015E-04	4.8568E-04	1.5024E-05	2.2606E-03
SFA39	193.07	8.33	5.7952E-04	5.3187E-04	-3.1284E-05	2.0831E-03
SFA40	217.30	8.32	6.3368E-04	5.3913E-04	1.0475E-05	2.3938E-03
SFA41	240.75	8.28	6.2315E-04	5.5079E-04	-6.1685E-05	2.0713E-03
SFA42	264.70	8.32	6.0001E-04	5.4905E-04	1.0437E-05	2.3461E-03
SFB1	1.60	8.83	2.2192E-04	1.6423E-04	-3.2294E-06	7.6113E-04
SFB2	4.48	8.71	2.1321E-04	1.6281E-04	8.6237E-06	7.9342E-04
SFB3	22.08	8.62	3.3777E-04	1.7576E-04	1.6094E-06	1.0364E-03
SFB4	30.07	8.69	2.3799E-04	1.8123E-04	6.4871E-06	8.7008E-04
SFB5	51.27	8.6	2.6924E-04	1.9063E-04	1.3105E-05	9.8072E-04
SFB6	73.73	8.78	3.2071E-04	1.9498E-04	1.0630E-05	1.0822E-03
SFB7	93.10	8.79	2.3003E-04	2.0594E-04	-1.5206E-05	8.0661E-04
SFB8	122.73	8.61	3.2783E-04	2.3113E-04	-1.2575E-05	1.0634E-03
SFB9	-	-	-	-	-	-
SFB10	169.48	8.71	2.8256E-04	2.3726E-04	5.2908E-06	1.0660E-03
SFB11	191.25	8.68	3.1665E-04	2.8000E-04	-1.3545E-05	1.1347E-03
SFB12	214.33	8.64	4.1554E-04	2.5938E-04	1.4414E-05	1.4169E-03
SFB13	238.00	8.53	3.1426E-04	2.7992E-04	-7.3668E-06	1.1569E-03
SFB14	262.40	8.53	3.3038E-04	2.7693E-04	2.2029E-06	1.2262E-03
SFB15	1.43	8.61	2.9371E-04	2.1156E-04	5.9970E-06	1.0396E-03
SFB16	6.15	8.61	3.2538E-04	2.4052E-04	1.1659E-05	1.1863E-03
SFB17	23.13	8.62	3.5051E-04	2.4954E-04	8.8170E-06	1.2419E-03
SFB18	29.50	8.65	3.4985E-04	2.7603E-04	-3.9687E-05	1.0754E-03
SFB19	48.00	8.64	3.9977E-04	2.6529E-04	1.9463E-05	1.4199E-03
SFB20	77.73	8.45	3.9498E-04	3.1025E-04	1.5517E-07	1.4126E-03
SFB21	-	-	-	-	-	-
SFB22	124.37	8.48	4.9315E-04	3.6165E-04	1.0596E-06	1.7159E-03
SFB23	147.43	8.49	4.7558E-04	3.7466E-04	3.4104E-05	1.8555E-03
SFB24	170.75	8.42	6.0808E-04	4.1954E-04	9.9299E-07	2.0610E-03
SFB25	193.08	8.29	4.7639E-04	4.5724E-04	-3.3140E-05	1.7191E-03
SFB26	218.07	8.3	4.7648E-04	4.4564E-04	-9.5321E-06	1.8024E-03
SFB27	242.32	8.28	4.7427E-04	4.4651E-04	3.0358E-06	1.8562E-03
SFB28	263.30	8.22	4.7570E-04	4.5896E-04	1.3586E-05	1.9313E-03
SFB29	2.70	8.68	6.3799E-04	2.7635E-04	1.9935E-05	1.9208E-03
SFB30	6.70	8.71	4.1911E-04	3.0397E-04	6.7565E-06	1.4791E-03

SFB31	24.40	8.66	4.6680E-04	3.1589E-04	1.9698E-05	1.6563E-03
SFB32	29.87	8.6	4.8371E-04	3.4578E-04	8.0912E-06	1.6974E-03
SFB33	52.90	8.6	4.5945E-04	3.4590E-04	2.4911E-05	1.7248E-03
SFB34	77.00	8.51	5.3054E-04	3.6397E-04	1.0697E-05	1.8388E-03
SFB35	100.35	8.42	5.5146E-04	4.1603E-04	1.7805E-05	2.0164E-03
SFB36	124.78	8.34	5.7468E-04	4.3404E-04	2.0872E-05	2.1125E-03
SFB37	145.78	8.31	5.6265E-04	4.6859E-04	9.1805E-06	2.1048E-03
SFB38	169.75	8.31	5.9866E-04	5.0601E-04	1.2008E-05	2.2644E-03
SFB39	193.07	8.26	6.1946E-04	4.9498E-04	2.2387E-05	2.3305E-03
SFB40	217.30	8.18	6.0242E-04	5.2248E-04	2.3955E-05	2.3584E-03
SFB41	240.75	8.12	6.3556E-04	5.3856E-04	3.9837E-05	2.5282E-03
SFB42	264.70	8.14	6.4916E-04	5.3228E-04	4.4482E-05	2.5637E-03
SFC1	1.60	8.74	3.0610E-04	1.6152E-04	9.5190E-06	9.8083E-04
SFC2	4.50	8.7	2.6353E-04	1.6331E-04	1.4602E-05	9.2189E-04
SFC3	22.08	8.51	2.4590E-04	1.8993E-04	1.3840E-05	9.3557E-04
SFC4	30.07	8.56	2.7181E-04	2.1801E-04	3.1629E-06	9.9568E-04
SFC5	51.27	8.45	2.8783E-04	2.0747E-04	1.2012E-05	1.0461E-03
SFC6	73.73	8.65	3.1468E-04	2.0800E-04	1.2131E-05	1.1022E-03
SFC7	93.10	8.7	3.2370E-04	2.3466E-04	3.2962E-05	1.2676E-03
SFC8	122.73	8.59	3.2251E-04	2.4717E-04	-2.2390E-06	1.1312E-03
SFC9	-	-	-	-	-	-
SFC10	169.48	8.66	3.2482E-04	2.5808E-04	1.8222E-05	1.2501E-03
SFC11	191.23	8.56	3.4051E-04	2.7938E-04	4.1852E-06	1.2604E-03
SFC12	214.33	8.58	3.4716E-04	3.1384E-04	1.6790E-05	1.3995E-03
SFC13	237.98	8.54	3.6886E-04	3.1467E-04	9.7116E-06	1.4125E-03
SFC14	262.38	8.46	3.6104E-04	3.1798E-04	2.2438E-05	1.4605E-03
SFC15	1.63	8.54	3.1275E-04	2.1628E-04	1.0250E-05	1.1059E-03
SFC16	6.35	8.55	3.5828E-04	2.5550E-04	-4.2696E-06	1.2101E-03
SFC17	23.33	8.52	3.5827E-04	2.9049E-04	-2.2369E-05	1.1985E-03
SFC18	29.70	8.58	3.4626E-04	2.8900E-04	-1.5353E-05	1.2033E-03
SFC19	48.20	8.68	3.8010E-04	3.2268E-04	-1.9146E-05	1.3218E-03
SFC20	77.93	8.59	4.0596E-04	3.6177E-04	-1.3585E-05	1.4763E-03
SFC21	-	-	-	-	-	-
SFC22	124.55	8.57	4.6325E-04	3.7255E-04	3.9145E-05	1.8496E-03
SFC23	147.62	8.54	4.3731E-04	3.8291E-04	4.2840E-05	1.8349E-03
SFC24	172.95	8.49	4.8888E-04	3.9895E-04	4.3425E-05	1.9726E-03
SFC25	193.28	8.39	4.7264E-04	4.4416E-04	3.7973E-05	2.0057E-03
SFC26	218.27	8.41	4.8848E-04	4.1364E-04	6.6673E-05	2.1055E-03
SFC27	242.52	8.4	5.5051E-04	4.4016E-04	3.3127E-06	1.9975E-03
SFC28	263.50	8.34	4.9798E-04	4.2241E-04	4.3955E-05	2.0397E-03

SFC29	2.68	8.65	6.1507E-04	2.6957E-04	-4.4704E-06	1.7514E-03
SFC30	6.68	8.65	4.5787E-04	2.9027E-04	4.8030E-05	1.7147E-03
SFC31	24.38	8.64	4.6277E-04	4.0628E-04	6.4188E-05	2.0291E-03
SFC32	29.83	8.57	4.4442E-04	3.5143E-04	7.5551E-06	1.6276E-03
SFC33	52.88	8.63	4.6685E-04	3.7938E-04	1.6513E-06	1.7020E-03
SFC34	76.98	8.59	5.2290E-04	3.8383E-04	2.1936E-05	1.9141E-03
SFC35	100.33	8.48	5.5857E-04	4.2020E-04	2.1136E-05	2.0542E-03
SFC36	124.60	8.48	5.4795E-04	4.3381E-04	6.7713E-05	2.2697E-03
SFC37	145.77	8.39	5.4558E-04	4.3564E-04	7.4161E-05	2.2974E-03
SFC38	169.73	8.41	5.6809E-04	4.5958E-04	6.4140E-05	2.3453E-03
SFC39	193.05	8.22	6.0961E-04	4.8332E-04	-3.4551E-06	2.1711E-03
SFC40	217.30	8.15	6.0267E-04	5.0131E-04	3.8696E-05	2.3828E-03
SFC41	240.73	8.13	6.2111E-04	5.1057E-04	5.7753E-05	2.5239E-03
SFC42	264.68	8.2	6.1726E-04	5.0385E-04	6.2032E-05	2.5222E-03
SFD1	1.60	8.62	4.8714E-04	4.5367E-04	-2.8348E-04	5.5835E-01
SFD2	4.52	8.65	4.3257E-04	1.4837E-04	-8.0219E-07	5.5890E-01
SFD3	22.07	8.65	4.3264E-04	1.2093E-04	4.5311E-05	5.5905E-01
SFD4	30.07	8.51	4.1163E-04	1.5826E-04	1.6768E-05	5.5896E-01
SFD5	51.27	8.54	4.1260E-04	1.6874E-04	1.0719E-05	5.5895E-01
SFD6	73.73	8.74	4.0444E-04	1.5081E-04	1.9065E-05	5.5894E-01
SFD7	93.10	8.74	4.0344E-04	1.8665E-04	2.9933E-06	5.5894E-01
SFD8	122.72	8.72	3.8433E-04	1.9493E-04	-3.2067E-06	5.5889E-01
SFD9	-	-	-	-	-	-
SFD10	169.48	8.63	4.1772E-04	2.1110E-04	-1.8559E-05	5.5892E-01
SFD11	191.23	8.57	4.1381E-04	1.7941E-04	1.0208E-05	5.5897E-01
SFD12	214.33	8.5	4.0687E-04	1.9237E-04	3.7089E-05	5.5911E-01
SFD13	237.98	8.44	4.1172E-04	2.0807E-04	1.1983E-05	5.5903E-01
SFD14	262.38	8.43	4.2312E-04	2.0493E-04	2.6865E-05	5.5912E-01
SFD15	1.42	8.51	4.9381E-04	2.0939E-04	7.7171E-06	5.5749E-01
SFD16	6.13	8.54	4.9760E-04	2.1621E-04	6.4034E-06	5.5750E-01
SFD17	24.62	8.52	5.3647E-04	2.0101E-04	1.7379E-06	5.5753E-01
SFD18	29.47	8.5	5.8227E-04	2.4387E-04	9.6559E-06	5.5774E-01
SFD19	47.97	8.6	5.7782E-04	2.4222E-04	2.3926E-05	5.5780E-01
SFD20	77.70	8.62	5.4562E-04	2.6355E-04	2.3517E-05	5.5777E-01
SFD21	-	-	-	-	-	-
SFD22	124.33	8.65	6.1322E-04	2.8053E-04	-2.4561E-05	5.5772E-01
SFD23	147.40	8.66	5.4264E-04	3.6320E-04	1.4655E-06	5.5787E-01
SFD24	170.55	8.59	5.5423E-04	2.7347E-04	3.9438E-05	5.5788E-01
SFD25	193.05	8.52	5.0964E-04	2.7035E-04	2.2214E-05	5.5771E-01
SFD26	218.05	8.51	5.3808E-04	2.6401E-04	4.8914E-05	5.5787E-01

SFD27	242.30	8.48	5.8343E-04	2.7828E-04	1.6738E-05	5.5785E-01
SFD28	263.28	8.4	5.2444E-04	2.8287E-04	3.5241E-05	5.5782E-01
SFD29	2.67	8.56	3.6027E-04	2.4102E-04	-1.6775E-06	5.5803E-01
SFD30	6.68	8.54	6.7055E-04	2.7711E-04	3.3944E-05	5.5889E-01
SFD31	24.38	8.52	7.0996E-04	2.9939E-04	1.5038E-06	5.5886E-01
SFD32	29.83	8.47	7.4364E-04	3.1354E-04	1.8087E-05	5.5903E-01
SFD33	52.88	8.54	7.7168E-04	3.4295E-04	-1.1160E-05	5.5902E-01
SFD34	76.98	8.55	7.6394E-04	3.1780E-04	2.5824E-05	5.5912E-01
SFD35	100.33	8.53	7.6824E-04	3.2362E-04	3.5287E-05	5.5918E-01
SFD36	124.60	8.53	7.5982E-04	3.4332E-04	1.4043E-05	5.5911E-01
SFD37	145.77	8.47	7.2795E-04	3.3218E-04	2.8020E-04	5.6022E-01
SFD38	169.55	8.45	7.2433E-04	3.3044E-04	4.2314E-05	5.5914E-01
SFD39	193.03	8.37	7.2739E-04	3.3653E-04	4.4195E-05	5.5916E-01
SFD40	217.30	8.31	7.1942E-04	3.4684E-04	1.8629E-05	5.5905E-01
SFD41	240.73	8.3	7.9662E-04	3.6657E-04	1.7296E-05	5.5924E-01
SFD42	264.68	8.28	7.2928E-04	3.5642E-04	4.8067E-05	5.5922E-01
SFE1	1.60	8.66	6.5482E-04	1.7593E-04	4.0946E-06	5.5831E-01
SFE2	4.53	8.61	4.1190E-04	1.3924E-04	1.6283E-05	5.5781E-01
SFE3	22.07	8.63	4.1812E-04	1.5437E-04	7.7017E-06	5.5781E-01
SFE4	30.07	8.53	3.9691E-04	1.5631E-04	-1.6375E-05	5.5766E-01
SFE5	51.27	8.46	4.1112E-04	1.6990E-04	1.2227E-05	5.5785E-01
SFE6	73.73	8.74	3.6298E-04	1.7255E-04	2.6018E-06	5.5771E-01
SFE7	93.10	8.74	3.7041E-04	1.8375E-04	2.2042E-05	5.5784E-01
SFE8	122.72	8.7	4.0676E-04	2.0196E-04	-2.2356E-05	5.5775E-01
SFE9	-	-	-	-	-	-
SFE10	169.47	8.68	4.1734E-04	2.1048E-04	-7.8458E-06	5.5785E-01
SFE11	191.23	8.58	4.5868E-04	2.0701E-04	4.3400E-06	5.5798E-01
SFE12	214.33	8.5	3.8069E-04	2.0390E-04	-2.2087E-05	5.5770E-01
SFE13	237.98	8.41	4.1979E-04	2.0453E-04	1.3496E-05	5.5794E-01
SFE14	262.38	8.38	4.0540E-04	2.1443E-04	3.3334E-05	5.5802E-01
SFE15	1.42	8.5	5.3996E-04	2.4016E-04	9.1852E-06	5.5898E-01
SFE16	6.13	8.57	5.1265E-04	2.2428E-04	2.5513E-05	5.5897E-01
SFE17	23.12	8.52	4.9970E-04	2.3019E-04	2.5355E-05	5.5895E-01
SFE18	29.47	8.47	5.2776E-04	2.5059E-04	7.3827E-06	5.5897E-01
SFE19	47.97	8.52	5.3472E-04	2.5880E-04	3.5372E-05	5.5912E-01
SFE20	77.70	8.61	5.2937E-04	2.6550E-04	-1.8241E-05	5.5889E-01
SFE21	-	-	-	-	-	-
SFE22	124.33	8.67	5.7036E-04	2.7693E-04	8.9479E-06	5.5911E-01
SFE23	147.40	8.67	5.4825E-04	2.8665E-04	-4.0313E-05	5.5887E-01
SFE24	172.72	8.6	5.4566E-04	2.7782E-04	-7.9314E-07	5.5902E-01

SFE25	193.05	8.55	5.3220E-04	2.7825E-04	2.1106E-05	5.5909E-01
SFE26	218.05	8.53	5.4334E-04	2.8509E-04	1.8996E-05	5.5912E-01
SFE27	242.30	8.5	5.6505E-04	2.8229E-04	1.4376E-06	5.5908E-01
SFE28	263.28	8.42	5.3359E-04	2.7756E-04	1.3854E-05	5.5906E-01
SFE29	2.67	8.56	3.7768E-04	2.6150E-04	1.7208E-05	5.5624E-01
SFE30	6.68	8.56	6.7293E-04	2.8962E-04	-3.7880E-05	5.5664E-01
SFE31	24.38	8.52	7.3193E-04	3.0541E-04	-1.4508E-05	5.5690E-01
SFE32	29.83	8.48	7.4227E-04	3.1604E-04	2.7349E-05	5.5713E-01
SFE33	52.88	8.55	7.5231E-04	3.2819E-04	3.1673E-05	5.5719E-01
SFE34	76.98	8.57	7.2958E-04	3.2825E-04	5.9111E-06	5.5703E-01
SFE35	100.33	8.56	7.1631E-04	3.4370E-04	3.7830E-07	5.5701E-01
SFE36	124.60	8.51	7.0470E-04	3.4810E-04	1.3448E-05	5.5705E-01
SFE37	145.77	8.48	7.3633E-04	3.4785E-04	1.6851E-05	5.5713E-01
SFE38	169.72	8.46	7.7230E-04	3.4875E-04	2.1058E-05	5.5722E-01
SFE39	193.03	8.39	7.4498E-04	3.5123E-04	3.3626E-05	5.5723E-01
SFE40	217.30	8.35	7.2208E-04	3.6403E-04	-4.3721E-04	5.5509E-01
SFE41	240.73	8.34	7.5617E-04	3.4595E-04	1.6841E-05	5.5717E-01
SFE42	264.68	8.32	7.6893E-04	3.6041E-04	-2.2791E-05	5.5704E-01
SFF1	1.62	8.63	4.1365E-04	1.5440E-04	1.5363E-05	5.5745E-01
SFF2	4.53	8.63	4.4105E-04	1.7021E-04	5.5293E-06	5.5749E-01
SFF3	22.08	8.6	4.1213E-04	1.6573E-04	9.7384E-06	5.5744E-01
SFF4	30.07	8.45	4.1328E-04	1.6167E-04	6.8766E-06	5.5742E-01
SFF5	51.27	8.42	4.5922E-04	1.8665E-04	1.5173E-05	5.5760E-01
SFF6	73.73	8.71	4.0633E-04	2.0688E-04	-9.8112E-07	5.5747E-01
SFF7	93.10	8.69	3.5367E-04	2.0878E-04	6.1064E-06	5.5740E-01
SFF8	122.73	8.69	4.0446E-04	1.9787E-04	3.0789E-05	5.5759E-01
SFF9	-	-	-	-	-	-
SFF10	169.47	8.62	4.0137E-04	2.1254E-04	1.5213E-05	5.5754E-01
SFF11	191.23	8.55	3.8916E-04	2.1590E-04	-1.9861E-05	5.5736E-01
SFF12	214.33	8.49	3.9552E-04	2.1691E-04	1.6431E-05	5.5754E-01
SFF13	237.98	8.38	3.9003E-04	2.2348E-04	3.9009E-05	5.5764E-01
SFF14	262.38	8.35	4.2248E-04	2.3522E-04	2.1782E-05	5.5766E-01
SFF15	1.42	8.49	5.3907E-04	2.3595E-04	1.2070E-05	5.5938E-01
SFF16	6.13	8.57	5.3400E-04	2.4148E-04	-1.0415E-05	5.5928E-01
SFF17	23.12	8.53	5.4532E-04	2.5273E-04	1.5448E-05	5.5944E-01
SFF18	29.47	8.53	5.7992E-04	2.4509E-04	1.6151E-05	5.5950E-01
SFF19	47.97	8.61	5.8465E-04	2.6184E-04	1.9376E-05	5.5956E-01
SFF20	77.68	8.62	5.6051E-04	2.9113E-04	-1.5440E-05	5.5941E-01
SFF21	-	-	-	-	-	-
SFF22	124.33	8.66	5.5795E-04	2.8589E-04	1.2277E-05	5.5952E-01

SFF23	147.40	8.66	5.8599E-04	2.9879E-04	-2.3015E-06	5.5954E-01
SFF24	170.72	8.61	5.7390E-04	2.8179E-04	1.4019E-05	5.5955E-01
SFF25	193.05	8.56	5.5287E-04	2.8165E-04	1.1745E-05	5.5950E-01
SFF26	218.05	8.55	5.4649E-04	2.8735E-04	2.5530E-06	5.5946E-01
SFF27	242.30	8.51	5.9152E-04	2.8597E-04	2.1012E-05	5.5963E-01
SFF28	263.28	8.45	5.5403E-04	2.7320E-04	2.2811E-05	5.5953E-01
SFF29	2.67	8.56	3.5018E-04	2.9716E-04	-2.7316E-05	5.5936E-01
SFF30	6.68	8.54	6.3123E-04	2.8169E-04	-1.4280E-05	5.5995E-01
SFF31	24.38	8.55	7.0300E-04	2.8091E-04	2.8138E-05	5.6029E-01
SFF32	29.83	8.52	7.0387E-04	2.9826E-04	2.5071E-05	5.6031E-01
SFF33	52.88	8.56	6.4730E-04	3.1451E-04	7.9473E-06	5.6015E-01
SFF34	76.97	8.56	6.5871E-04	3.1349E-04	1.0180E-05	5.6018E-01
SFF35	100.33	8.56	7.0536E-04	3.1700E-04	1.8260E-05	5.6032E-01
SFF36	124.60	8.51	7.2191E-04	3.2207E-04	3.1421E-05	5.6042E-01
SFF37	145.77	8.44	7.1643E-04	4.1878E-04	-5.6653E-05	5.6021E-01
SFF38	169.72	8.44	6.9911E-04	3.2107E-04	5.0294E-04	5.6250E-01
SFF39	193.03	8.36	6.6140E-04	3.3617E-04	4.7129E-05	5.6040E-01
SFF40	217.30	8.33	7.0009E-04	3.5066E-04	1.4718E-07	5.6029E-01
SFF41	240.73	8.3	6.8779E-04	3.3903E-04	3.8197E-05	5.6042E-01
SFF42	264.68	8.3	6.6718E-04	3.2216E-04	3.6108E-05	5.6033E-01

Table A.2. *Summary of GR(Cl) batch solubility experiment data. Triplicates A, B, and C were performed in pure water. Triplicates D, E, and F were performed in simulated seawater. Samples 1-14 correspond to 0 d old GR(Cl); 15-28 to 2 d old GR(Cl); and 29-42 to 7 d old GR(Cl).*

Sample ID	Sample Age (h)	pH	Cl^- (M)	Fe^{2+} (M)	Fe^{3+} (M)	Ionic Strength (M)
CFA1	1.62	8.78	1.2707E-03	6.8361E-04	2.1240E-04	2.9614E-03
CFA2	4.52	8.42	1.7834E-03	7.8126E-04	8.9174E-05	2.8568E-03
CFA3	22.18	8.19	1.9489E-03	9.4041E-04	1.3796E-04	3.4769E-03
CFA4	30.13	8.17	2.0880E-03	9.0029E-04	1.7252E-04	3.6217E-03
CFA5	51.33	8.2	2.2365E-03	8.8478E-04	2.4978E-04	4.0126E-03
CFA6	73.78	8.21	2.2666E-03	6.5901E-04	4.4183E-05	2.6510E-03
CFA7	93.15	8.28	2.2614E-03	8.6602E-04	6.6053E-05	3.1609E-03
CFA8	122.80	8.25	2.2577E-03	9.4745E-04	1.0966E-04	3.5181E-03
CFA10	169.53	8.24	2.1940E-03	9.1529E-04	1.2834E-04	3.5060E-03
CFA11	191.30	8.19	2.1587E-03	9.0437E-04	1.6292E-05	2.9622E-03
CFA12	214.42	7.8	2.1919E-03	7.8050E-04	1.7989E-04	3.4668E-03
CFA13	238.02	7.33	2.1868E-03	7.6128E-04	1.5084E-04	3.2949E-03
CFA14	262.47	7.17	2.2323E-03	8.3081E-04	-6.6486E-05	2.4787E-03
CFA15	1.50	8.75	1.6320E-03	6.6916E-04	1.8144E-05	2.2388E-03
CFA16	6.20	8.38	2.2185E-03	1.0196E-03	5.9031E-05	3.4153E-03
CFA17	23.18	8.15	2.5408E-03	1.1664E-03	-5.4322E-05	3.3595E-03
CFA18	29.58	8.14	2.5931E-03	1.0828E-03	4.8177E-05	3.6797E-03
CFA19	48.08	8.15	2.6514E-03	1.1522E-03	-5.9378E-05	3.3636E-03
CFA20	77.67	8.16	2.6475E-03	1.1843E-03	2.0874E-06	3.7025E-03
CFA22	124.43	8.19	2.5958E-03	1.1014E-03	1.0485E-04	3.9734E-03
CFA23	147.50	8.21	2.5478E-03	1.1427E-03	1.2101E-04	4.1046E-03
CFA24	170.85	8.19	2.6247E-03	1.0411E-03	1.0272E-04	3.8575E-03
CFA25	193.18	8.18	2.5713E-03	1.0827E-03	1.1881E-04	3.9865E-03
CFA26	218.18	8.2	2.6584E-03	1.1464E-03	1.4821E-04	4.2898E-03
CFA27	242.42	8.2	2.6631E-03	1.0540E-03	7.5021E-05	3.7779E-03
CFA28	263.50	8.18	2.6838E-03	1.1098E-03	-5.0595E-05	3.3346E-03
CFA29	2.75	8.42	2.0805E-03	9.5234E-04	2.3468E-05	3.0518E-03
CFA30	6.77	8.22	2.2582E-03	9.8125E-04	7.0463E-05	3.4095E-03
CFA31	24.45	8.18	2.3860E-03	1.0348E-03	1.4896E-05	3.3305E-03
CFA32	29.93	8.19	2.3558E-03	9.8119E-04	-2.3945E-05	3.0333E-03
CFA33	52.95	8.2	2.3503E-03	1.0249E-03	3.2877E-05	3.3737E-03
CFA34	77.00	8.19	2.3890E-03	9.9610E-04	1.8078E-04	4.0010E-03
CFA35	100.42	8.18	2.3812E-03	1.1390E-03	5.3140E-05	3.7084E-03
CFA36	124.62	8.19	2.3916E-03	9.8200E-04	5.0715E-06	3.1834E-03

CFA37	145.82	8.2	2.3600E-03	9.9438E-04	1.0696E-04	3.6509E-03
CFA38	169.82	8.18	2.4248E-03	9.9447E-04	3.8319E-05	3.3746E-03
CFA39	193.12	8.15	2.4507E-03	1.0078E-03	1.2019E-04	3.7825E-03
CFA40	217.35	8.02	2.4322E-03	9.4540E-04	9.4652E-05	3.5333E-03
CFA41	240.82	7.96	2.4359E-03	9.7217E-04	3.5132E-05	3.3209E-03
CFA42	264.77	7.94	2.4648E-03	9.8503E-04	1.0253E-04	3.6643E-03
CFB1	1.62	8.77	1.4668E-03	9.8957E-04	2.8626E-04	4.0037E-03
CFB2	4.52	8.38	2.0836E-03	1.0394E-03	5.1473E-04	5.4380E-03
CFB3	22.17	8.17	2.2279E-03	1.1389E-03	1.6404E-04	4.1307E-03
CFB4	30.13	8.17	2.2189E-03	9.5722E-04	5.2585E-05	3.2613E-03
CFB5	51.33	8.14	2.2547E-03	1.1051E-03	2.0352E-04	4.2541E-03
CFB6	73.78	8.22	2.3039E-03	1.0701E-03	7.9014E-06	3.3285E-03
CFB7	93.15	8.26	2.3556E-03	1.0427E-03	2.5237E-04	4.3998E-03
CFB8	122.80	8.22	2.3422E-03	1.1907E-03	2.6528E-04	4.7472E-03
CFB10	169.53	8.25	2.2030E-03	9.3361E-04	6.2482E-05	3.2508E-03
CFB11	191.30	8.24	2.2308E-03	9.2753E-04	1.1748E-04	3.5000E-03
CFB12	214.42	8.2	2.2870E-03	9.3731E-04	5.7143E-05	3.2760E-03
CFB13	238.02	7.42	2.1962E-03	7.3616E-04	1.1161E-04	3.0728E-03
CFB14	262.47	7.32	2.2323E-03	9.3717E-04	3.7758E-05	3.1605E-03
CFB15	1.50	8.74	1.8201E-03	6.4600E-04	2.7926E-05	2.3304E-03
CFB16	6.20	8.29	2.2456E-03	9.8330E-04	6.0840E-05	3.3642E-03
CFB17	23.18	8.14	2.6250E-03	1.0834E-03	1.8904E-05	3.5651E-03
CFB18	29.58	8.18	2.6791E-03	1.0842E-03	7.0448E-05	3.8257E-03
CFB19	48.08	8.18	2.7618E-03	1.1411E-03	1.0524E-05	3.7112E-03
CFB20	77.83	8.18	2.7132E-03	1.1455E-03	5.5115E-05	3.8963E-03
CFB22	124.43	8.22	2.6934E-03	1.1234E-03	2.1836E-04	4.5768E-03
CFB23	147.50	8.22	2.6763E-03	1.1750E-03	1.6620E-04	4.4370E-03
CFB24	170.85	8.2	2.7154E-03	1.2174E-03	1.6559E-04	4.5386E-03
CFB25	193.18	8.18	2.6492E-03	1.1983E-03	1.6771E-04	4.4767E-03
CFB26	218.18	8.19	2.7617E-03	1.0864E-03	6.2376E-05	3.8352E-03
CFB27	242.42	8.21	2.7922E-03	1.0520E-03	1.8303E-04	4.3246E-03
CFB28	263.50	8.18	2.6838E-03	1.1068E-03	2.3642E-06	3.5670E-03
CFB29	2.75	8.45	2.2124E-03	9.2917E-04	5.3423E-05	3.2063E-03
CFB30	6.77	8.29	2.4112E-03	1.0367E-03	8.6303E-05	3.6683E-03
CFB31	24.45	8.18	2.5583E-03	1.0818E-03	6.3221E-05	3.7279E-03
CFB32	29.93	8.22	2.4975E-03	9.9577E-04	1.5344E-04	3.9316E-03
CFB33	52.95	8.19	2.4837E-03	1.0781E-03	3.2339E-05	3.5444E-03
CFB34	77.00	8.2	2.5212E-03	1.1087E-03	1.4128E-04	4.1146E-03
CFB35	100.42	8.21	2.5374E-03	1.1323E-03	2.3175E-04	4.5770E-03
CFB36	124.62	8.21	2.5400E-03	1.0204E-03	7.5912E-05	3.6533E-03

CFB37	145.82	8.2	2.5059E-03	9.7029E-04	9.1770E-05	3.6073E-03
CFB38	169.82	8.19	2.5743E-03	1.1065E-03	7.6276E-05	3.8442E-03
CFB39	193.12	8.19	2.5713E-03	1.0277E-03	1.5883E-04	4.0565E-03
CFB40	217.35	8.16	2.5402E-03	1.0198E-03	8.0361E-05	3.6720E-03
CFB41	240.82	8.05	2.5010E-03	9.6938E-04	9.2479E-05	3.6060E-03
CFB42	264.77	7.93	2.5309E-03	1.0195E-03	4.3842E-05	3.5022E-03
CFC1	1.62	8.77	1.4610E-03	6.7088E-04	4.7716E-05	2.2899E-03
CFC2	4.52	8.41	2.0836E-03	1.0219E-03	1.6266E-04	3.8189E-03
CFC3	22.17	8.16	2.2369E-03	9.2323E-04	1.3611E-04	3.5781E-03
CFC4	30.13	8.15	2.2643E-03	9.5934E-04	6.5634E-05	3.3469E-03
CFC5	51.33	8.17	2.2638E-03	1.0105E-03	1.3917E-04	3.7799E-03
CFC6	73.78	8.24	2.2759E-03	9.2339E-04	5.4287E-05	3.2299E-03
CFC7	93.15	8.26	2.3269E-03	9.1485E-04	4.8174E-05	3.2108E-03
CFC8	122.78	8.25	2.3232E-03	1.0071E-03	1.4666E-04	3.8367E-03
CFC10	169.52	8.27	2.1673E-03	1.0297E-03	1.5600E-04	3.8459E-03
CFC11	191.30	8.27	2.1323E-03	9.8448E-04	1.2918E-04	3.6174E-03
CFC12	214.42	8.23	2.2200E-03	9.4672E-04	2.6137E-04	4.1805E-03
CFC13	238.02	8.22	2.2435E-03	9.2883E-04	1.0970E-04	3.4739E-03
CFC14	262.47	8.16	2.2515E-03	9.1499E-04	1.4834E-04	3.6240E-03
CFC15	1.48	8.72	2.1567E-03	1.0154E-03	-1.9514E-04	2.2336E-03
CFC16	6.18	8.28	2.2638E-03	1.0223E-03	8.5791E-05	3.5636E-03
CFC17	23.17	8.16	2.6682E-03	1.1144E-03	4.3241E-05	3.7582E-03
CFC18	29.57	8.17	2.7343E-03	1.1653E-03	3.0343E-05	3.8350E-03
CFC19	48.05	8.18	2.8418E-03	1.2063E-03	2.2973E-05	3.9375E-03
CFC20	77.80	8.18	2.8034E-03	1.2259E-03	4.5439E-05	4.0588E-03
CFC22	124.42	8.19	2.8061E-03	1.1926E-03	7.1429E-05	4.1104E-03
CFC23	147.48	8.19	2.8113E-03	1.2472E-03	1.5582E-04	4.6020E-03
CFC24	170.82	8.19	2.8453E-03	1.2482E-03	6.6503E-05	4.2192E-03
CFC25	193.17	8.18	2.7764E-03	1.2513E-03	1.4773E-04	4.5563E-03
CFC26	218.17	8.18	2.8569E-03	1.1946E-03	2.0645E-05	3.9114E-03
CFC27	242.40	8.21	2.9149E-03	1.2115E-03	9.2416E-05	4.2971E-03
CFC28	263.50	8.2	2.8744E-03	1.1589E-03	1.4468E-04	4.4069E-03
CFC29	2.75	8.51	2.2397E-03	9.8356E-04	1.1702E-04	3.6152E-03
CFC30	6.77	8.29	2.5328E-03	1.1271E-03	2.2829E-05	3.6242E-03
CFC31	24.43	8.19	2.7318E-03	1.1408E-03	1.9012E-04	4.5038E-03
CFC32	29.93	8.21	2.6812E-03	1.1312E-03	1.1540E-04	4.1231E-03
CFC33	52.95	8.18	2.6584E-03	1.1447E-03	7.5568E-06	3.6534E-03
CFC34	77.00	8.18	2.6940E-03	1.1687E-03	7.4768E-05	4.0216E-03
CFC35	100.42	8.21	2.7039E-03	1.1154E-03	4.8192E-05	3.8004E-03
CFC36	124.62	8.19	2.7328E-03	1.1699E-03	8.7744E-05	4.1017E-03

CFC37	145.82	8.19	2.6609E-03	1.1407E-03	9.4690E-05	4.0387E-03
CFC38	169.82	8.19	2.7330E-03	1.1870E-03	8.9241E-05	4.1430E-03
CFC39	193.12	8.16	2.7695E-03	1.1600E-03	1.5183E-04	4.3887E-03
CFC40	217.35	8.12	2.6996E-03	1.1456E-03	8.9451E-07	3.6456E-03
CFC41	240.82	8.13	2.6831E-03	1.0779E-03	1.0486E-04	3.9699E-03
CFC42	264.77	8.12	2.7158E-03	1.1007E-03	1.8314E-04	4.3842E-03
CFD1	1.58	8.73	5.5610E-01	1.1674E-04	9.6357E-05	5.5677E-01
CFD2	4.48	8.72	5.5610E-01	1.2700E-04	7.2574E-06	5.5639E-01
CFD3	22.13	8.73	5.5610E-01	1.4208E-04	1.9830E-05	5.5648E-01
CFD4	30.10	8.7	5.5610E-01	1.5746E-04	7.7243E-06	5.5646E-01
CFD5	51.30	8.71	5.5610E-01	1.7690E-04	1.3997E-05	5.5652E-01
CFD6	73.77	8.66	5.5610E-01	1.9183E-04	3.5219E-05	5.5665E-01
CFD7	93.12	8.63	5.5610E-01	2.3659E-04	1.2265E-07	5.5658E-01
CFD8	122.75	8.71	5.5610E-01	2.3076E-04	1.3713E-05	5.5663E-01
CFD10	169.48	8.68	5.5610E-01	2.4516E-04	6.6536E-06	5.5663E-01
CFD11	191.27	8.66	5.5610E-01	2.6401E-04	6.5453E-06	5.5666E-01
CFD12	214.38	8.68	5.5610E-01	2.6743E-04	1.3813E-05	5.5670E-01
CFD13	237.98	8.63	5.5610E-01	2.7671E-04	-1.1487E-05	5.5661E-01
CFD14	262.43	8.63	5.5610E-01	2.5624E-04	1.5509E-05	5.5669E-01
CFD15	1.50	8.63	5.5674E-01	2.8674E-04	9.0045E-06	5.5736E-01
CFD16	6.18	8.54	5.5674E-01	2.9844E-04	1.1310E-04	5.5785E-01
CFD17	23.17	8.54	5.5674E-01	3.3456E-04	2.3715E-05	5.5752E-01
CFD18	29.57	8.52	5.5674E-01	4.4209E-04	1.5168E-05	5.5770E-01
CFD19	48.05	8.48	5.5674E-01	3.8321E-04	-1.3830E-05	5.5745E-01
CFD20	77.80	8.45	5.5674E-01	3.7293E-04	7.2346E-05	5.5781E-01
CFD22	124.40	8.5	5.5674E-01	4.4664E-04	2.2557E-05	5.5774E-01
CFD23	147.48	8.47	5.5674E-01	4.7028E-04	-2.3426E-05	5.5758E-01
CFD24	170.82	8.46	5.5674E-01	4.9880E-04	2.1108E-05	5.5784E-01
CFD25	193.17	8.46	5.5674E-01	4.8912E-04	6.8333E-05	5.5803E-01
CFD26	218.17	8.48	5.5674E-01	4.9533E-04	-2.4349E-05	5.5762E-01
CFD27	242.40	8.48	5.5674E-01	5.2143E-04	3.0119E-05	5.5792E-01
CFD28	263.50	8.45	5.5674E-01	4.7559E-04	8.0821E-05	5.5806E-01
CFD29	2.72	8.55	5.5641E-01	5.0286E-04	2.6495E-05	5.5754E-01
CFD30	6.73	8.53	5.5641E-01	4.8484E-04	5.2620E-05	5.5762E-01
CFD31	24.42	8.47	5.5641E-01	5.6653E-04	1.2466E-05	5.5760E-01
CFD32	29.92	8.36	5.5641E-01	5.5024E-04	6.6515E-05	5.5781E-01
CFD33	52.93	8.42	5.5641E-01	5.5923E-04	7.5244E-05	5.5787E-01
CFD34	76.98	8.42	5.5641E-01	6.2125E-04	1.2823E-05	5.5771E-01
CFD35	100.40	8.41	5.5641E-01	6.2969E-04	-1.1150E-06	5.5767E-01
CFD36	124.60	8.4	5.5641E-01	6.5722E-04	2.9810E-05	5.5786E-01

CFD37	145.80	8.39	5.5641E-01	5.6918E-04	8.8771E-05	5.5795E-01
CFD38	169.78	8.39	5.5641E-01	6.7825E-04	1.4551E-05	5.5783E-01
CFD39	193.10	8.39	5.5641E-01	6.9556E-04	1.6111E-05	5.5788E-01
CFD40	217.33	8.39	5.5641E-01	7.1068E-04	2.9395E-05	5.5797E-01
CFD41	240.80	8.39	5.5641E-01	6.8979E-04	3.0736E-05	5.5793E-01
CFD42	264.75	8.4	5.5641E-01	7.2149E-04	2.3772E-05	5.5796E-01
CFE1	1.58	8.82	5.5744E-01	1.6201E-04	-2.0095E-05	5.5768E-01
CFE2	4.48	8.73	5.5744E-01	1.3714E-04	5.2500E-06	5.5774E-01
CFE3	22.13	8.66	5.5744E-01	1.4767E-04	6.1396E-07	5.5774E-01
CFE4	30.10	8.75	5.5744E-01	1.6782E-04	4.2250E-07	5.5778E-01
CFE5	51.30	8.59	5.5744E-01	1.7157E-04	-1.4271E-05	5.5772E-01
CFE6	73.77	8.65	5.5744E-01	1.8668E-04	7.4157E-06	5.5785E-01
CFE7	93.12	8.65	5.5744E-01	1.9341E-04	2.2302E-05	5.5793E-01
CFE8	122.75	8.69	5.5744E-01	2.0514E-04	4.0613E-05	5.5804E-01
CFE10	169.48	8.68	5.5744E-01	2.4692E-04	2.1280E-05	5.5803E-01
CFE11	191.27	8.66	5.5744E-01	2.5458E-04	3.1020E-05	5.5809E-01
CFE12	214.38	8.68	5.5744E-01	2.6596E-04	2.0500E-05	5.5807E-01
CFE13	237.98	8.63	5.5744E-01	2.7240E-04	1.8424E-05	5.5807E-01
CFE14	262.42	8.62	5.5744E-01	3.4492E-04	-4.6051E-05	5.5793E-01
CFE15	1.50	8.64	5.5622E-01	3.0235E-04	1.2494E-05	5.5688E-01
CFE16	6.18	8.57	5.5622E-01	4.3809E-04	-1.1998E-04	5.5655E-01
CFE17	23.17	8.51	5.5622E-01	4.1053E-04	1.7537E-05	5.5712E-01
CFE18	29.55	8.55	5.5622E-01	2.9900E-04	6.9975E-05	5.5713E-01
CFE19	48.05	8.45	5.5622E-01	3.5288E-04	3.6469E-05	5.5709E-01
CFE20	77.80	8.29	5.5622E-01	4.2035E-04	1.5375E-05	5.5713E-01
CFE22	124.40	8.48	5.5622E-01	4.5296E-04	2.8715E-05	5.5725E-01
CFE23	147.48	8.43	5.5622E-01	4.7124E-04	5.6539E-06	5.5718E-01
CFE24	170.82	8.31	5.5622E-01	4.9355E-04	8.8764E-06	5.5724E-01
CFE25	193.17	8.45	5.5622E-01	5.1425E-04	5.3637E-06	5.5727E-01
CFE26	218.17	8.44	5.5622E-01	5.2187E-04	-9.2027E-06	5.5722E-01
CFE27	244.40	8.46	5.5622E-01	5.3604E-04	-2.7834E-05	5.5716E-01
CFE28	263.50	8.47	5.5622E-01	5.0685E-04	3.6512E-05	5.5739E-01
CFE29	2.72	8.58	5.5588E-01	5.2454E-04	-1.5885E-06	5.5692E-01
CFE30	6.73	8.5	5.5588E-01	4.9784E-04	4.3832E-05	5.5707E-01
CFE31	24.42	8.5	5.5588E-01	5.9682E-04	-7.7461E-06	5.5704E-01
CFE32	29.90	8.46	5.5588E-01	6.0617E-04	2.4967E-05	5.5720E-01
CFE33	52.93	8.44	5.5588E-01	5.4111E-04	8.7698E-05	5.5735E-01
CFE34	76.97	8.42	5.5588E-01	6.2220E-04	6.4988E-05	5.5741E-01
CFE35	100.40	8.42	5.5588E-01	6.7464E-04	-2.4574E-05	5.5712E-01
CFE36	124.60	8.4	5.5588E-01	6.1638E-04	-5.7695E-05	5.5685E-01

CFE37	145.80	8.39	5.5588E-01	6.8181E-04	2.4593E-05	5.5735E-01
CFE38	169.78	8.4	5.5588E-01	6.5087E-04	6.4825E-04	5.6010E-01
CFE39	193.10	8.4	5.5588E-01	7.2711E-04	1.0274E-04	5.5779E-01
CFE40	217.33	8.4	5.5588E-01	7.2977E-04	-1.1172E-05	5.5729E-01
CFE41	240.80	8.41	5.5588E-01	7.3320E-04	5.9799E-04	5.6003E-01
CFE42	264.75	8.41	5.5588E-01	7.5194E-04	3.9730E-05	5.5756E-01
CFF1	1.58	8.77	5.5701E-01	1.6543E-04	2.2908E-05	5.5745E-01
CFF2	4.48	8.78	5.5701E-01	1.4659E-04	7.6947E-06	5.5735E-01
CFF3	22.12	8.77	5.5701E-01	1.4379E-04	1.4544E-05	5.5737E-01
CFF4	30.10	8.8	5.5701E-01	1.7256E-04	-2.6655E-06	5.5735E-01
CFF5	51.30	8.61	5.5701E-01	1.9715E-04	7.0418E-06	5.5744E-01
CFF6	73.77	8.71	5.5701E-01	2.4265E-04	-1.2173E-05	5.5745E-01
CFF7	93.12	8.69	5.5701E-01	2.2126E-04	1.4199E-06	5.5747E-01
CFF8	122.75	8.7	5.5701E-01	2.3869E-04	1.3097E-05	5.5755E-01
CFF10	169.48	8.67	5.5701E-01	2.6432E-04	1.5187E-05	5.5761E-01
CFF11	191.27	8.66	5.5701E-01	2.4403E-04	4.9095E-05	5.5773E-01
CFF12	214.38	8.67	5.5701E-01	2.6241E-04	2.2566E-05	5.5764E-01
CFF13	237.98	8.66	5.5701E-01	2.8525E-04	3.1787E-05	5.5773E-01
CFF14	262.42	8.65	5.5701E-01	2.9419E-04	-1.1868E-06	5.5760E-01
CFF15	1.48	8.65	5.5729E-01	2.9942E-04	2.0508E-05	5.5798E-01
CFF16	6.17	8.59	5.5729E-01	3.0201E-04	1.9706E-05	5.5798E-01
CFF17	23.15	8.55	5.5729E-01	3.4116E-04	-6.1977E-06	5.5794E-01
CFF18	29.53	8.57	5.5729E-01	3.0894E-04	4.0499E-05	5.5809E-01
CFF19	48.03	8.48	5.5729E-01	3.8438E-04	5.5452E-06	5.5808E-01
CFF20	77.78	8.4	5.5729E-01	4.0770E-04	4.3386E-05	5.5830E-01
CFF22	124.38	8.52	5.5729E-01	4.1160E-04	5.3533E-05	5.5835E-01
CFF23	147.47	8.47	5.5729E-01	3.8209E-04	1.3545E-04	5.5866E-01
CFF24	170.80	8.39	5.5729E-01	4.6226E-04	2.2857E-05	5.5832E-01
CFF25	193.15	8.43	5.5729E-01	4.7455E-04	1.9994E-05	5.5833E-01
CFF26	218.15	8.47	5.5729E-01	4.2307E-04	4.5504E-05	5.5834E-01
CFF27	242.38	8.47	5.5729E-01	4.6487E-04	3.1667E-06	5.5823E-01
CFF28	263.47	8.49	5.5729E-01	5.0037E-04	-5.6337E-06	5.5826E-01
CFF29	2.72	8.6	5.5546E-01	5.0616E-04	2.8148E-05	5.5660E-01
CFF30	6.73	8.48	5.5546E-01	4.9413E-04	4.2999E-05	5.5664E-01
CFF31	24.42	8.5	5.5546E-01	5.4345E-04	9.1986E-07	5.5655E-01
CFF32	29.90	8.44	5.5546E-01	5.1905E-04	7.2065E-05	5.5682E-01
CFF33	52.93	8.44	5.5546E-01	5.2924E-04	3.5627E-05	5.5668E-01
CFF34	76.97	8.41	5.5546E-01	5.9196E-04	-9.4785E-06	5.5660E-01
CFF35	100.38	8.42	5.5546E-01	4.4734E-04	9.8016E-05	5.5679E-01
CFF36	124.60	8.41	5.5546E-01	5.7994E-04	4.6322E-05	5.5683E-01

CFF37	145.80	8.39	5.5546E-01	6.3208E-04	3.5367E-05	5.5688E-01
CFF38	169.78	8.42	5.5546E-01	6.8330E-04	5.7838E-05	5.5708E-01
CFF39	193.10	8.41	5.5546E-01	6.4734E-04	5.0445E-05	5.5698E-01
CFF40	217.33	8.43	5.5546E-01	6.6736E-04	6.6434E-05	5.5709E-01
CFF41	240.80	8.43	5.5546E-01	7.4023E-04	-2.8127E-06	5.5693E-01
CFF42	264.75	8.42	5.5546E-01	6.4888E-04	3.3865E-06	5.5677E-01

Appendix B

Appendix B.1. *PHREEQC model of GR(Cl) dissolution. GR(Cl) log k from Refait and Génin (1993).*

```
   Input file: C:\Users\Neil\Desktop\Phreeqc Files\Dec 11, 2018 - Test 3.pqi
  Output file: C:\Users\Neil\Desktop\Phreeqc Files\Dec 11, 2018 - Test 3.pqo
Database file: C:\Program Files (x86)\USGS\Phreeqc Interactive 3.4.0-
12927\database\minteq.dat

------------------
Reading data base.
------------------

        SOLUTION_MASTER_SPECIES
        SOLUTION_SPECIES
        SOLUTION_SPECIES
        PHASES
        SURFACE_MASTER_SPECIES
        SURFACE_SPECIES
        END
-----------------------------------
Reading input data for simulation 1.
-----------------------------------

        DATABASE C:\Program Files (x86)\USGS\Phreeqc Interactive 3.4.0-
12927\database\minteq.dat
        PHASES
        GR1
          Fe3Fe(OH)8Cl = Fe+3 + 3 Fe+2 + 8 OH- + Cl-
          log_k          -81.922
        END
------------------
End of simulation.
------------------

-----------------------------------
Reading input data for simulation 2.
-----------------------------------

        SOLUTION
        EQUILIBRIUM_PHASES 1
           GR1       0 10
        END
-------------------------------------------
Beginning of initial solution calculations.
-------------------------------------------
```

Initial solution 1.

----------Solution composition----------

Elements	Molality	Moles
Pure water		

----------Description of solution----------

pH = 7.000
pe = 4.000
Activity of water = 1.000
Ionic strength (mol/kgw) = 1.003e-07
Mass of water (kg) = 1.000e+00
Total alkalinity (eq/kg) = 4.619e-10
Total carbon (mol/kg) = 0.000e+00
Total CO2 (mol/kg) = 0.000e+00
Temperature (°C) = 25.00
Electrical balance (eq) = -4.619e-10
Percent error, 100*(Cat-|An|)/(Cat+|An|) = -0.23
Iterations = 0
Total H = 1.110124e+02
Total O = 5.550622e+01

----------Distribution of species----------

Species	Molality	Log Activity	Log Molality	Log Activity	Gamma	mole V cm³/mol
OH-	1.005e-07	1.005e-07	-6.998	-6.998	-0.000	(0)
H+	1.001e-07	1.000e-07	-7.000	-7.000	-0.000	0.00
H2O	5.551e+01	1.000e+00	1.744	0.000	0.000	18.07
H(0)	1.416e-25					
H2	7.079e-26	7.079e-26	-25.150	-25.150	0.000	(0)
O(0)	0.000e+00					
O2	0.000e+00	0.000e+00	-42.080	-42.080	0.000	(0)

----------Saturation indices----------

Phase	SI**	log IAP	log K(298 K, 1 atm)	
O2(g)	-39.12	44.00	83.12	O2

**For a gas, SI = log10(fugacity). Fugacity = pressure * phi / 1 atm.
For ideal gases, phi = 1.

Beginning of batch-reaction calculations.

Reaction step 1.

Using solution 1.
Using pure phase assemblage 1.

----------Phase assemblage----------

Phase	SI	log IAP	log K(T, P)	Moles in assemblage Initial	Final	Delta
GR1	0.00	-81.92	-81.92	1.000e+01	1.000e+01	-2.288e-06

----------Solution composition----------

Elements	Molality	Moles
Cl	2.288e-06	2.288e-06
Fe	9.151e-06	9.151e-06

----------Description of solution----------

pH = 8.903 Charge balance
pe = -1.409 Adjusted to redox equilibrium
Activity of water = 1.000
Ionic strength (mol/kgw) = 1.786e-05
Mass of water (kg) = 1.000e+00
Total alkalinity (eq/kg) = 1.373e-05
Total carbon (mol/kg) = 0.000e+00
Total CO2 (mol/kg) = 0.000e+00
Temperature (°C) = 25.00
Electrical balance (eq) = -4.619e-10
Percent error, 100*(Cat-|An|)/(Cat+|An|) = -0.00
Iterations = 11
Total H = 1.110125e+02
Total O = 5.550624e+01

----------Distribution of species----------

Species	Molality	Log Activity	Log Molality	Log Activity	Gamma	mole V cm³/mol
OH-	8.071e-06	8.031e-06	-5.093	-5.095	-0.002	(0)
H+	1.257e-09	1.251e-09	-8.901	-8.903	-0.002	0.00
H2O	5.551e+01	1.000e+00	1.744	-0.000	0.000	18.07

```
Cl          2.288e-06
  Cl-           2.288e-06   2.277e-06    -5.641    -5.643    -0.002     (0)
  FeCl+2        1.368e-24   1.341e-24   -23.864   -23.873    -0.009     (0)
  FeCl2+        1.370e-29   1.364e-29   -28.863   -28.865    -0.002     (0)
  FeCl3         3.104e-36   3.104e-36   -35.508   -35.508     0.000     (0)
Fe(2)       6.864e-06
  Fe+2          5.487e-06   5.380e-06    -5.261    -5.269    -0.009     (0)
  FeOH+         1.367e-06   1.360e-06    -5.864    -5.866    -0.002     (0)
  Fe(OH)2       9.254e-09   9.254e-09    -8.034    -8.034     0.000     (0)
  Fe(OH)3-      2.762e-10   2.749e-10    -9.559    -9.561    -0.002     (0)
Fe(3)       2.288e-06
  Fe(OH)4-      2.011e-06   2.001e-06    -5.697    -5.699    -0.002     (0)
  Fe(OH)3       2.503e-07   2.503e-07    -6.602    -6.602     0.000     (0)
  Fe(OH)2+      2.678e-08   2.665e-08    -7.572    -7.574    -0.002     (0)
  FeOH+2        1.027e-13   1.007e-13   -12.989   -12.997    -0.009     (0)
  Fe+3          2.038e-20   1.950e-20   -19.691   -19.710    -0.019     (0)
  FeCl+2        1.368e-24   1.341e-24   -23.864   -23.873    -0.009     (0)
  Fe2(OH)2+4    2.952e-25   2.728e-25   -24.530   -24.564    -0.034     (0)
  FeCl2+        1.370e-29   1.364e-29   -28.863   -28.865    -0.002     (0)
  Fe3(OH)4+5    1.718e-30   1.519e-30   -29.765   -29.819    -0.054     (0)
  FeCl3         3.104e-36   3.104e-36   -35.508   -35.508     0.000     (0)
H(0)        1.455e-18
  H2            7.274e-19   7.274e-19   -18.138   -18.138     0.000     (0)
O(0)        0.000e+00
  O2            0.000e+00   0.000e+00   -56.104   -56.104     0.000     (0)

-----------------------------Saturation indices-------------------------------

  Phase               SI** log IAP   log K(298 K,   1 atm)

  Fe(OH)2.7Cl0.3    5.67      2.63   -3.04  Fe(OH)2.7Cl0.3
  Fe3(OH)8          6.31     26.53   20.22  Fe3(OH)8
  Ferrihydrite      2.11      7.00    4.89  Fe(OH)3
  Goethite          6.50      7.00    0.50  FeOOH
  GR1               0.00    -81.92  -81.92  Fe3Fe(OH)8Cl
  Hematite         18.00     14.00   -4.01  Fe2O3
  Lepidocrocite     5.63      7.00    1.37  FeOOH
  Maghemite         7.61     14.00    6.39  Fe2O3
  Magnetite        22.80     26.53    3.74  Fe3O4
  O2(g)           -53.14     29.98   83.12  O2

**For a gas, SI = log10(fugacity). Fugacity = pressure * phi / 1 atm.
  For ideal gases, phi = 1.

------------------
End of simulation.
------------------
```

```
-----------------------------------
Reading input data for simulation 3.
-----------------------------------

-------------------------------
End of Run after 0.176 Seconds.
-------------------------------
```

Appendix B.2. *PHREEQC model of GR(SO_4) dissolution. GR(SO_4) log k from Ayala-Luis et al. (2008).*

```
  Input file: C:\Users\Neil\Desktop\Phreeqc Files\Dec 11, 2018 - Test 1.pqi
 Output file: C:\Users\Neil\Desktop\Phreeqc Files\Dec 11, 2018 - Test 1.pqo
Database file: C:\Program Files (x86)\USGS\Phreeqc Interactive 3.4.0-
12927\database\minteq.dat

------------------
Reading data base.
------------------

        SOLUTION_MASTER_SPECIES
        SOLUTION_SPECIES
        SOLUTION_SPECIES
        PHASES
        SURFACE_MASTER_SPECIES
        SURFACE_SPECIES
        END
-----------------------------------
Reading input data for simulation 1.
-----------------------------------

        DATABASE C:\Program Files (x86)\USGS\Phreeqc Interactive 3.4.0-
12927\database\minteq.dat
        PHASES
        GR2
          Fe4Fe2(OH)12SO4 = 2 Fe+3 + 4 Fe+2 + 12 OH- + SO4-2
          log_k          -139.2
        END
------------------
End of simulation.
------------------

-----------------------------------
Reading input data for simulation 2.
-----------------------------------

        SOLUTION
        EQUILIBRIUM_PHASES 1
           GR2       0 10
        END
-------------------------------------------
Beginning of initial solution calculations.
-------------------------------------------

Initial solution 1.
```

----------Solution composition----------

Elements Molality Moles

Pure water

----------Description of solution----------

pH = 7.000
pe = 4.000
Activity of water = 1.000
Ionic strength (mol/kgw) = 1.003e-07
Mass of water (kg) = 1.000e+00
Total alkalinity (eq/kg) = 4.619e-10
Total carbon (mol/kg) = 0.000e+00
Total CO2 (mol/kg) = 0.000e+00
Temperature (°C) = 25.00
Electrical balance (eq) = -4.619e-10
Percent error, 100*(Cat-|An|)/(Cat+|An|) = -0.23
Iterations = 0
Total H = 1.110124e+02
Total O = 5.550622e+01

----------Distribution of species----------

Species	Molality	Log Activity	Log Molality	Log Activity	Gamma	mole V cm³/mol
OH-	1.005e-07	1.005e-07	-6.998	-6.998	-0.000	(0)
H+	1.001e-07	1.000e-07	-7.000	-7.000	-0.000	0.00
H2O	5.551e+01	1.000e+00	1.744	0.000	0.000	18.07
H(0)	1.416e-25					
H2	7.079e-26	7.079e-26	-25.150	-25.150	0.000	(0)
O(0)	0.000e+00					
O2	0.000e+00	0.000e+00	-42.080	-42.080	0.000	(0)

----------Saturation indices----------

Phase	SI**	log IAP	log K(298 K, 1 atm)	
O2(g)	-39.12	44.00	83.12	O2

**For a gas, SI = log10(fugacity). Fugacity = pressure * phi / 1 atm.
For ideal gases, phi = 1.

Beginning of batch-reaction calculations.

Reaction step 1.

Using solution 1.
Using pure phase assemblage 1.

----------Phase assemblage----------

Phase	SI	log IAP	log K(T, P)	Moles in assemblage: Initial	Final	Delta
GR2	0.00	-139.20	-139.20	1.000e+01	1.000e+01	-1.385e-07

----------Solution composition----------

Elements	Molality	Moles
Fe	8.309e-07	8.309e-07
S	1.385e-07	1.385e-07

----------Description of solution----------

pH = 7.925 Charge balance
pe = 2.116 Adjusted to redox equilibrium
Activity of water = 1.000
Ionic strength (mol/kgw) = 1.882e-06
Mass of water (kg) = 1.000e+00
Total alkalinity (eq/kg) = 1.108e-06
Total carbon (mol/kg) = 0.000e+00
Total CO2 (mol/kg) = 0.000e+00
Temperature (°C) = 25.00
Electrical balance (eq) = -4.619e-10
Percent error, 100*(Cat-|An|)/(Cat+|An|) = -0.02
Iterations = 11
Total H = 1.110124e+02
Total O = 5.550622e+01

----------Distribution of species----------

Species	Molality	Log Activity	Log Molality	Log Activity	Gamma	mole V cm³/mol
OH-	8.457e-07	8.443e-07	-6.073	-6.073	-0.001	(0)
H+	1.192e-08	1.190e-08	-7.924	-7.925	-0.001	0.00
H2O	5.551e+01	1.000e+00	1.744	-0.000	0.000	18.07
Fe(2)	5.539e-07					
Fe+2	5.396e-07	5.362e-07	-6.268	-6.271	-0.003	(0)
FeOH+	1.427e-08	1.425e-08	-7.846	-7.846	-0.001	(0)

```
  FeSO4          1.312e-11   1.312e-11   -10.882   -10.882     0.000     (0)
  Fe(OH)2        1.019e-11   1.019e-11   -10.992   -10.992     0.000     (0)
  Fe(OH)3-       3.188e-14   3.183e-14   -13.496   -13.497    -0.001     (0)
  Fe(HS)2        0.000e+00   0.000e+00  -120.218  -120.218     0.000     (0)
  Fe(HS)3-       0.000e+00   0.000e+00  -179.628  -179.629    -0.001     (0)
Fe(3)         2.770e-07
  Fe(OH)2+       9.836e-08   9.820e-08    -7.007    -7.008    -0.001     (0)
  Fe(OH)3        9.697e-08   9.697e-08    -7.013    -7.013     0.000     (0)
  Fe(OH)4-       8.163e-08   8.149e-08    -7.088    -7.089    -0.001     (0)
  FeOH+2         3.551e-12   3.529e-12   -11.450   -11.452    -0.003     (0)
  Fe+3           6.597e-18   6.503e-18   -17.181   -17.187    -0.006     (0)
  FeSO4+         7.453e-21   7.441e-21   -20.128   -20.128    -0.001     (0)
  Fe2(OH)2+4     3.439e-22   3.351e-22   -21.464   -21.475    -0.011     (0)
  Fe(SO4)2-      3.242e-26   3.237e-26   -25.489   -25.490    -0.001     (0)
  Fe3(OH)4+5     7.158e-27   6.876e-27   -26.145   -26.163    -0.017     (0)
H(0)          1.176e-23
  H2             5.880e-24   5.880e-24   -23.231   -23.231     0.000     (0)
O(0)          0.000e+00
  O2             0.000e+00   0.000e+00   -45.919   -45.919     0.000     (0)
S(-2)         0.000e+00
  HS-            0.000e+00   0.000e+00   -61.448   -61.448    -0.001     (0)
  H2S            0.000e+00   0.000e+00   -62.431   -62.431     0.000     (0)
  S5-2           0.000e+00   0.000e+00   -63.116   -63.119    -0.003     (0)
  S4-2           0.000e+00   0.000e+00   -63.350   -63.353    -0.003     (0)
  S6-2           0.000e+00   0.000e+00   -63.402   -63.405    -0.003     (0)
  S-2            0.000e+00   0.000e+00   -66.439   -66.442    -0.003     (0)
  S3-2           0.000e+00   0.000e+00   -66.803   -66.806    -0.003     (0)
  S2-2           0.000e+00   0.000e+00   -68.049   -68.052    -0.003     (0)
  Fe(HS)2        0.000e+00   0.000e+00  -120.218  -120.218     0.000     (0)
  Fe(HS)3-       0.000e+00   0.000e+00  -179.628  -179.629    -0.001     (0)
S(6)          1.385e-07
  SO4-2          1.385e-07   1.376e-07    -6.859    -6.861    -0.003     (0)
  FeSO4          1.312e-11   1.312e-11   -10.882   -10.882     0.000     (0)
  HSO4-          1.591e-13   1.588e-13   -12.798   -12.799    -0.001     (0)
  FeSO4+         7.453e-21   7.441e-21   -20.128   -20.128    -0.001     (0)
  Fe(SO4)2-      3.242e-26   3.237e-26   -25.489   -25.490    -0.001     (0)

-----------------------------Saturation indices-------------------------------

  Phase               SI** log IAP   log K(298 K,   1 atm)

  Fe2(SO4)3       -58.54    -54.96    3.58  Fe2(SO4)3
  Fe3(OH)8          2.53     22.75   20.22  Fe3(OH)8
  Ferrihydrite      1.70      6.59    4.89  Fe(OH)3
  FeS(ppt)        -55.88    -59.79   -3.92  FeS
  Goethite          6.09      6.59    0.50  FeOOH
  GR2               0.00   -139.20 -139.20  Fe4Fe2(OH)12SO4
  Greigite       -209.71   -254.74  -45.03  Fe3S4
```

Hematite	17.18	13.17	-4.01	Fe2O3
Jarosite-H	-13.56	-25.66	-12.10	(H3O)Fe3(SO4)2(OH)6
Lepidocrocite	5.22	6.59	1.37	FeOOH
Mackinawite	-55.15	-59.79	-4.65	FeS
Maghemite	6.79	13.17	6.39	Fe2O3
Magnetite	19.01	22.75	3.74	Fe3O4
Melanterite	-10.66	-13.13	-2.47	FeSO4:7H2O
O2(g)	-42.96	40.16	83.12	O2
Pyrite	-90.61	-109.09	-18.48	FeS2
Sulfur	-47.18	-49.29	-2.11	S

**For a gas, SI = log10(fugacity). Fugacity = pressure * phi / 1 atm.
For ideal gases, phi = 1.

End of simulation.

Reading input data for simulation 3.

End of Run after 0.465 Seconds.

Appendix B.3. *PHREEQC model of magnetite dissolution. Magnetite log k from MINTEQ 2016 database.*

```
   Input file: C:\Users\Neil\Desktop\Phreeqc Files\Dec 11, 2018 - Test 2.pqi
  Output file: C:\Users\Neil\Desktop\Phreeqc Files\Dec 11, 2018 - Test 2.pqo
Database file: C:\Program Files (x86)\USGS\Phreeqc Interactive 3.4.0-
12927\database\minteq.dat

------------------
Reading data base.
------------------

        SOLUTION_MASTER_SPECIES
        SOLUTION_SPECIES
        SOLUTION_SPECIES
        PHASES
        SURFACE_MASTER_SPECIES
        SURFACE_SPECIES
        END
-----------------------------------
Reading input data for simulation 1.
-----------------------------------

        DATABASE C:\Program Files (x86)\USGS\Phreeqc Interactive 3.4.0-
12927\database\minteq.dat
        SOLUTION
        EQUILIBRIUM_PHASES 1
           Magnetite 0 10
        END
-------------------------------------------
Beginning of initial solution calculations.
-------------------------------------------

Initial solution 1.

-----------------------------Solution composition------------------------------

        Elements           Molality       Moles

        Pure water

----------------------------Description of solution----------------------------

                                pH  =   7.000
                                pe  =   4.000
                      Activity of water  =   1.000
                Ionic strength (mol/kgw)  =   1.003e-07
                     Mass of water (kg)  =   1.000e+00
                Total alkalinity (eq/kg)  =   4.619e-10
```

Total carbon (mol/kg) = 0.000e+00
Total CO2 (mol/kg) = 0.000e+00
Temperature (°C) = 25.00
Electrical balance (eq) = -4.619e-10
Percent error, 100*(Cat-|An|)/(Cat+|An|) = -0.23
Iterations = 0
Total H = 1.110124e+02
Total O = 5.550622e+01

----------Distribution of species----------

Species	Molality	Log Activity	Log Molality	Log Activity	Gamma	mole V cm³/mol
OH-	1.005e-07	1.005e-07	-6.998	-6.998	-0.000	(0)
H+	1.001e-07	1.000e-07	-7.000	-7.000	-0.000	0.00
H2O	5.551e+01	1.000e+00	1.744	0.000	0.000	18.07
H(0)	1.416e-25					
H2	7.079e-26	7.079e-26	-25.150	-25.150	0.000	(0)
O(0)	0.000e+00					
O2	0.000e+00	0.000e+00	-42.080	-42.080	0.000	(0)

----------Saturation indices----------

Phase	SI**	log IAP	log K(298 K, 1 atm)	
O2(g)	-39.12	44.00	83.12	O2

**For a gas, SI = log10(fugacity). Fugacity = pressure * phi / 1 atm.
For ideal gases, phi = 1.

Beginning of batch-reaction calculations.

Reaction step 1.

Using solution 1.
Using pure phase assemblage 1.

----------Phase assemblage----------

Phase	SI	log IAP	log K(T, P)	Moles in assemblage Initial	Final	Delta
Magnetite	0.00	3.74	3.74	1.000e+01	1.000e+01	-9.273e-13

----------Solution composition----------

Elements	Molality	Moles
Fe	2.785e-12	2.785e-12

----------Description of solution----------

pH = 7.000 Charge balance
pe = 4.954 Adjusted to redox equilibrium
Activity of water = 1.000
Ionic strength (mol/kgw) = 1.003e-07
Mass of water (kg) = 1.000e+00
Total alkalinity (eq/kg) = 4.656e-10
Total carbon (mol/kg) = 0.000e+00
Total CO2 (mol/kg) = 0.000e+00
Temperature (°C) = 25.00
Electrical balance (eq) = -4.619e-10
Percent error, 100*(Cat-|An|)/(Cat+|An|) = -0.23
Iterations = 8
Total H = 1.110124e+02
Total O = 5.550622e+01

----------Distribution of species----------

Species	Molality	Log Activity	Log Molality	Log Activity	Gamma	mole V cm³/mol
OH-	1.005e-07	1.005e-07	-6.998	-6.998	-0.000	(0)
H+	1.000e-07	1.000e-07	-7.000	-7.000	-0.000	0.00
H2O	5.551e+01	1.000e+00	1.744	-0.000	0.000	18.07
Fe(2)	9.250e-13					
Fe+2	9.221e-13	9.207e-13	-12.035	-12.036	-0.001	(0)
FeOH+	2.913e-15	2.912e-15	-14.536	-14.536	-0.000	(0)
Fe(OH)2	2.478e-19	2.478e-19	-18.606	-18.606	0.000	(0)
Fe(OH)3-	9.211e-23	9.208e-23	-22.036	-22.036	-0.000	(0)
Fe(3)	1.860e-12					
Fe(OH)2+	1.647e-12	1.646e-12	-11.783	-11.784	-0.000	(0)
Fe(OH)3	1.934e-13	1.934e-13	-12.714	-12.714	0.000	(0)
Fe(OH)4-	1.935e-14	1.934e-14	-13.713	-13.714	-0.000	(0)
FeOH+2	4.978e-16	4.971e-16	-15.303	-15.304	-0.001	(0)
Fe+3	7.724e-21	7.698e-21	-20.112	-20.114	-0.001	(0)
Fe2(OH)2+4	6.690e-30	6.650e-30	-29.175	-29.177	-0.003	(0)
Fe3(OH)4+5	2.308e-39	2.287e-39	-38.637	-38.641	-0.004	(0)
H(0)	1.748e-27					
H2	8.739e-28	8.739e-28	-27.059	-27.059	0.000	(0)
O(0)	1.092e-38					
O2	5.459e-39	5.459e-39	-38.263	-38.263	0.000	(0)

-----Saturation indices-----

Phase	SI**	log IAP	log K(298 K, 1 atm)	
Fe3(OH)8	-16.49	3.74	20.22	Fe3(OH)8
Ferrihydrite	-4.00	0.89	4.89	Fe(OH)3
Goethite	0.39	0.89	0.50	FeOOH
Hematite	5.78	1.77	-4.01	Fe2O3
Lepidocrocite	-0.48	0.89	1.37	FeOOH
Maghemite	-4.61	1.77	6.39	Fe2O3
Magnetite	0.00	3.74	3.74	Fe3O4
O2(g)	-35.30	47.82	83.12	O2

**For a gas, SI = log10(fugacity). Fugacity = pressure * phi / 1 atm.
For ideal gases, phi = 1.

End of simulation.

Reading input data for simulation 2.

End of Run after 0.187 Seconds.

Appendix C

Appendix C.1. *^{57}Fe Mössbauer Spectrometry Report.*

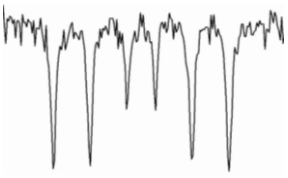

^{57}Fe Mössbauer Spectrometry Report

Full name:	Neil Macpherson
Group:	Environmental Geochemistry, University of Alberta, Canada
Identification of Transformation of Green Rust into Magnetite, pt. 2	
Analysis by:	Manuel Schad, James M. Byrne, Andreas Kappler, University of Tuebingen

Introduction:

^{57}Fe Moessbauer spectroscopy was performed in order to determine the extent of transformation of chloride and sulfate green rust to magnetite over time.

Materials and Methods:

Mineral suspensions were prepared by filtration in an anoxic glovebox (100% N_2) and kept anoxic until they were transferred to the instrument and loaded inside a closed-cycle exchange gas cryostat (Janis cryogenics). Measurements were collected at 140 K with a constant acceleration drive system (WissEL) in transmission mode with a ^{57}Co/Rh source and calibrated against a 7µm thick α-^{57}Fe foil measured at room temperature. All spectra were analysed using Recoil (University of Ottawa) by applying the Voigt Based Fitting (VBF) routine [1]. The half width at half maximum (HWHM) was fixed to a value of 0.138 mm/s for all samples.

Results:

Spectra collected at 140 K and copied directly from the fitting software are shown in Figure 1 while the fitting parameters are summarized in Table 1. Raw asci files will be provided for better figure presentation. All spectra consist of a combination of twin doublets, which are characteristic for green rust (GR) and twin sextets, which is characteristic for magnetite [2, 3].

The fitting of GR required two doublets: A narrow doublet, which represents the Fe(III) component of the mineral and a wide doublet which represents the Fe(II) component of the mineral.
For the chloride GR the narrow doublet had a center shift of between 0.41 - 0.43 mm s^{-1} and a quadrupole splitting of between 0.42 - 0.45 mm s^{-1}. The wide doublet had a center shift of 1.22 mm s^{-1} and quadrupole splitting values between 2.67 - 2.77 mm s^{-1}. These values are in good agreement with reported literature values for green rust [4-6].
The narrow doublet of the sulphate GR had center shift values between 0.40 - 0.43 mm s^{-1} and quadrupole splitting values between 0.45 - 0.52 mm s^{-1}. The wider Fe(II) double center shift values between 1.22 - 1.23 mm s^{-1} and quadrupole splitting values between 2.81 - 2.87 mm s^{-1}. All values are within the range of reported literature values for sulphate GR [5, 7].

Magnetite requires two sextets for fitting, representing the tetrahedral and octahedral components of the mineral. The tetrahedral site generally had center shift values between 0.35 – 0.39 mm s^{-1}, quadrupole shift values between -0.01 - 0.03 mm s^{-1} and a hyperfine field parameter between 48.7 - 50.1 T. The octahedral site on the other hand is characterized by center shift values between 0.72 - 0.82 mm s^{-1},

quadrupole shift values between -0.04 - 0.07 mm s^{-1} and 45.7 - 47.7 T. In general, these values are well in line with reported literature values [8-11]. However, it should be noted that center shift ≥ 0.8 mm s^{-1} is high but still within acceptable range.

Using the equation

$$\frac{Fe(II)}{Fe(III)} = \frac{0.5B}{0.5B + A}$$

the stoichiometry of magnetite can be calculated using the relative abundance (R.A.) of the tetrahedral (low δ, high B_{hf}, site A) and octahedral site (high δ, low B_{hf}, site B).

22.5% of the spectral area of the initial chloride GR corresponds to magnetite. With a Fe(II)/Fe(III) ratio = 0.5 the magnetite has ideal stoichiometry. However, the stoichiometry of the GR deviates slightly from the expected Fe(II)/Fe(III) ratio = 0.67 (0.69 instead of 0.67). Sample C-24 shows an increase in magnetite abundance by 2.5% to a total of 25% of the spectral area. A Fe(II)/Fe(III) ratio of 0.41 suggests that the magnetite is slightly oxidized while at the same time the GR is more reduced (Fe(II)/Fe(III) = 0.71). The final sample (C-26) shows a further increase in magnetite abundance to 31.2% of the total spectral area with a Fe(II)/Fe(III) ratio = 0.43. The stoichiometry of the GR developed further to a more reduced state with 76.2% of the Fe in the GR being present as Fe(II).

Unlike the starting point sample of the chloride GR, the sulphate GR sample (S-23) shows the presence of GR. Additionally, there is indications for a sextet in the spectrum which cannot be properly resolved, indicating that it is at the lower limit of the detection range. Therefore, the presence of low amounts of magnetite cannot be excluded but would require independent confirmation by e.g. XRD. The starting material appears to be slightly oxidized with a Fe(II)/Fe(III) ratio = 0.63 instead of the expected value of 0.67. Sample S-24 shows a transformation of 17.3% of the GR into magnetite. With a Fe(II)/Fe(III) ratio = 0.35 this magnetite shows a significant degree of oxidation. Similarly, the GR became slightly more oxidized (Fe(II)/Fe(III) = 0.62). The final sample (S-26) shows a further increase in magnetite abundance to 24.4% of the spectral area. Interestingly, both minerals became more reduced again: The Fe(II)/Fe(III) ratio of the magnetite is 0.43 (compared to 0.35 for S-24) while the Fe(II) content in the GR increased to 0.64 (S-24, Fe(II)/Fe(III) = 0.62).

Ultimately however, a full Fe mass balance ($Fe_{total} = Fe_{solid} + Fe_{sorbed} + Fe_{dissolved}$) would be required to fully understand the GR to magnetite transformation pathways.

Table 7: Hyperfine parameters. Results of the fitting spectra. δ – center shift, ΔE_Q – quadrupole splitting, ε – quadrupole shift (for sextets only), B_{hf} – hyperfine magnetic field, R.A. – relative abundance of the mineral phase at the given temperature, ± - error in the relative abundance, χ^2 indicates the goodness of fit.

Sample	Site	Phase	δ (mm s^{-1})	ΔE_Q (mm s^{-1})	ε (mm s^{-1})	B_{hf} (T)	R. A. (%)	±	χ^2
Cl^- GR, C-23	QSD 1	GR (Fe(II))	1.22	2.67	-	-	53.7	2.2	0.63
	QSD 2	GR (FeIII)	0.41	0.43	-	-	23.8	1.2	
	HFD 1	Magnetite	0.35	-	0.02	48.7	7.6	1.9	
	HFD 2	Magnetite	0.82	-	0.07	45.7	14.9	2.8	
Cl^- GR, C-24	QSD 1	GR (Fe(II))	1.22	2.70	-	-	53.4	1.2	0.88
	QSD 2	GR (FeIII)	0.43	0.42	-	-	21.6	6.3	
	HFD 1	Magnetite	0.38	-	0.02	49.1	10.4	1.3	
	HFD 2	Magnetite	0.74	-	0	46.5	14.6	1.5	
Cl^- GR, C-26	QSD 1	GR (Fe(II))	1.22	2.77	-	-	52.4	1.5	0.73
	QSD 2	GR (FeIII)	0.41	0.45	-	-	16.4	0.8	
	HFD 1	Magnetite	0.36	-	0.03	49.7	12.5	1.5	
	HFD 2	Magnetite	0.72	-	-0.02	47.5	18.7	1.8	
SO_4^{2-} GR, S-23	QSD 1	GR (Fe(II))	1.23	2.87	-	-	62.8	1.1	0.81
	QSD 2	GR (FeIII)	0.40	0.52	-	-	37.2	1.1	
SO_4^{2-} GR, S-24	QSD 1	GR (Fe(II))	1.22	2.85	-	-	51.2	1.7	0.66
	QSD 2	GR (Fe(III))	0.40	0.50	-	-	31.5	1.2	
	HFD 1	Magnetite	0.39	-	0.02	49.7	8.3	1.8	
	HFD 2	Magnetite	0.80	-	-0.04	47.3	9.0	2.2	
SO_4^{2-} GR, S-26	QSD 1	GR (Fe(II))	1.23	2.81	-	-	48.8	1.0	0.76
	QSD 2	GR (Fe(III))	0.43	0.45	-	-	26.8	0.7	
	HFD 1	Magnetite	0.36	-	-0.01	50.1	9.7	1.0	
	HFD 2	Magnetite	0.75	-	0.01	47.7	14.7	1.3	

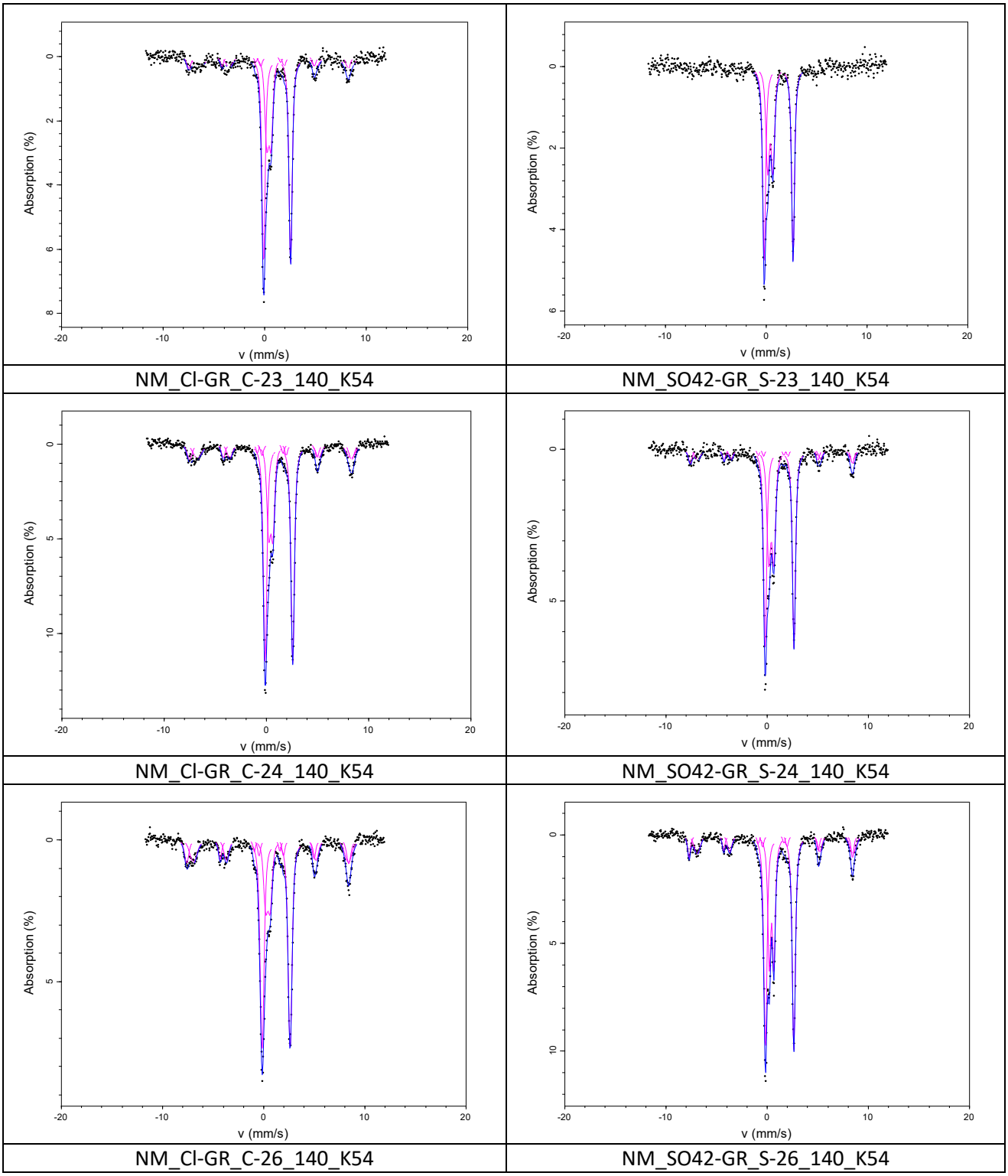

Figure 1: Mössbauer spectra obtained at 140 K.

References:

1. Rancourt, D. and J. Ping, *Voigt-based methods for arbitrary-shape static hyperfine parameter distributions in Mössbauer spectroscopy.* Nuclear Instruments and Methods in Physics Research Section B: Beam Interactions with Materials and Atoms, 1991. **58**(1): p. 85-97.
2. Schwertmann, U. and R.M. Cornell, *Iron oxides in the laboratory*. 2008: John Wiley & Sons.
3. Murad, E. and J. Cashion, in *Mössbauer Spectroscopy of Environmental Materials and Their Industrial Utilization*. 2004, Springer.
4. Refait, P. and J. Génin, *The mechanisms of oxidation of ferrous hydroxychloride β-Fe2 (OH) 3Cl in aqueous solution: the formation of akaganeite vs goethite.* Corrosion Science, 1997. **39**(3): p. 539-553.
5. Génin, J.-M.R., et al., *Thermodynamic equilibria in aqueous suspensions of synthetic and natural Fe (II)− Fe (III) green rusts: Occurrences of the mineral in hydromorphic soils.* Environmental Science & Technology, 1998. **32**(8): p. 1058-1068.
6. Emmerich, M., et al., *Abundance, distribution, and activity of Fe (II)-oxidizing and Fe (III)-reducing microorganisms in hypersaline sediments of Lake Kasin, southern Russia.* Applied and environmental microbiology, 2012: p. AEM. 07637-11.
7. Simon, L., et al., *Structure of the Fe (II-III) layered double hydroxysulphate green rust two from Rietveld analysis.* Solid State Sciences, 2003. **5**(2): p. 327-334.
8. Posth, N.R., et al., *Simulating Precambrian banded iron formation diagenesis.* Chemical Geology, 2013. **362**: p. 66-73.
9. Byrne, J.M., et al., *Redox cycling of Fe (II) and Fe (III) in magnetite by Fe-metabolizing bacteria.* Science, 2015. **347**(6229): p. 1473-1476.
10. Byrne, J.M., et al., *Size dependent microbial oxidation and reduction of magnetite nano-and micro-particles.* Scientific reports, 2016. **6**: p. 30969.
11. Sundman, A., et al., *Interactions between magnetite and humic substances: redox reactions and dissolution processes.* Geochemical transactions, 2017. **18**(1): p. 6.